The Role and Behavior of *Arabidopsis thaliana* Lipid Transfer Proteins During Cuticular Wax Deposition

by

Allan DeBono

B.S., The University of Toronto, 2003

M.S., The University of Guelph, 2005

A THESIS SUBMITTED IN PARTIAL FULFILLMENT OF

THE REQUIREMENTS FOR THE DEGREE OF

DOCTOR OF PHILOSOPHY

in

The Faculty of Graduate Studies

(Botany)

THE UNIVERSITY OF BRITISH COLUMBIA

(Vancouver)

November 2011

© Allan DeBono, 2011

Abstract

The primary aerial surfaces of terrestrial plants are coated with a protective hydrophobic layer comprising insoluble and soluble lipids. The lipids are known collectively as cuticular wax. To generate the waxy cuticle during elongative growth, plants dedicate half of the fatty acid metabolism of their epidermal cells. It is unknown how cuticular wax is exported from the plasma membrane into the cell wall, and eventually, to the cuticle at the cell surface. I hypothesized that lipid transfer proteins (LTPs) were responsible for plasma membrane to cell wall transport of cuticular lipids. Using an epidermis-specific microarray, I identified five candidate Arabidopsis LTPs. I discovered that mutations in gene *At1g27950* result in a stem wax phenotype: reduced cuticular lipid nonacosane resulting in reduced total wax compared to wild-type. This gene encodes a glycosylphosphatidylinositol (GPI)-linked LTP and thus was named *LTPG*.

In contrast, to LTPG, no detectable wax phenotype was found in mutants for classical LTPs. In phylogenetic analyses, these LTPs clustered into a weakly related group that I named LTPAs. In an attempt to overcome genetic redundancy I made double and triple mutants from the candidate LTPAs. None of these mutants displayed detectable changes in wax compared with wildtype.

Using live cell imaging, I showed that LTPG is localized to the epidermal cell plasma membrane and the cell wall and accumulates non-uniformly on the plant surface. I employed fluorescence recovery after photobleaching to demonstrate that, in the plasma membrane, LTPG is relatively immobile and exhibits a complicated recovery, the latter appears linked to the flux of cuticular lipids through the plasma membrane. LTPG accumulates over the long cell walls of stem epidermal cells and this protein moves when observed over 1 min intervals. I created a GPI-linked LTPA and demonstrated that it can rescue the *ltpg-1* mutation.

I demonstrate that LTPG is required for wax export by associating with the plant cell wall. This is the first experimental evidence linking the lipid transfer function of a plant LTP to a biological role, which in this case is lipid movement through the cell wall to the cuticle.

Preface

In chapter 2, the protocol used for plant tissue preparation in confocal microscopy (Section 2.7) has been published.

Yonghua Li-Beisson, Basil Shorrosh, Fred Beisson, Mats X. Andersson, Vincent Arondel,Philip D. Bates, Sésbastien Baud, David Bird, [Allan DeBono], Timothy P. Durrett, Rochus B. Franke, Ian A. Graham, Kenta Katayama, Amélie A. Kelly, Tony Larson, Jonathan E. Markham, Martine Miquel, Isabel Molina, Ikuo Nishida, Owen Rowland, Lacey Samuels, Katherine M. Schmid, Hajime Wada, Ruth Welti, Changcheng Xu, Réémi Zallot, and John Ohlrogge. (2010) The Arabidopsis Book.

URL: http://www.bioone.org/doi/full/10.1199/tab.0133

I developed the plant tissue preparation and staining regimen for confocal microscopy.

Chapter 3 has been published except for the work presented in Figures 3-6 and 3-8.

[Allan DeBono], Trevor H. Yeats, Jocelyn K.C. Rose, David Bird, Reinhard Jetter, Ljerka Kunst and Lacey Samuels. (2009) Arabidopsis LTPG Is a Glycosylphosphatidylinositol-Anchored Lipid Transfer Protein Required for Export of Lipids to the Plant Surface. The Plant Cell 21:1230-1238.

I was responsible for all experiments with the exception for purification of recombinant LTPG from *E. coli* and the TNS assay. The purification of recombinant LTPG and the TNS assays were performed by Dr. Trevor Yeats.

In chapter 4, the isolation of double and triple mutants was assisted by Angel Shan and Colin MacLeod. The GC-FID protocol used for wax analyses described in chapter 4 was developed collaboratively with Scott Liang using standards generated by members of the Kunst Lab.

In chapter 5, the molecular cloning of secreted-YFP and cytoplasmic-YFP was assisted by Angel Shan. The selection of transgenic plants described was assisted by Andre Fallavollita.

Table of contents

List of tables

List of figures

List of abbreviations

ACP – acyl carrier protein

BSFTA – N, O-Bis (trimethylsilyl)trifluoroacetamide

CER5 – eceriferum5

CER6 – eceriferum6

CETP – cholesterol ester transfer protein

Col-0 – Columbia – 0

DEX – dexamethasone

DIR1 – defective in induced resistance1

DMSO – dimethyl sulfoxide

DPI – dots per inch

ECR – enoyl-CoA reductase

EDTA - Ethylenediaminetetraacetic acid

ER – endoplasmic reticulum

FABP – fatty acid binding protein

FAE – fatty acid elongase

FAR – fatty acyl-CoA reductase

FP – fluorescent protein

FRAP – fluorescence recovery after photobleaching

FRET – fluorescence resonance energy transfer

GC-FID – gas chromatography with flame ionization detection

GFP – green fluorescent protein

GPI – glycosylphosphatidylinositol

GPI-PLD – GPI phospholipase D

KCR – beta-keto-acyl-CoA reductase

LACS – long chain acyl CoA synthetase

LTI6b- lower temperature induced6b

LTP – lipid transfer protein

LTPG- lipid transfer protein glycosylphosphatidylinositol anchored

MAH1 – mid chain alkane hydroxylase1

PLTP – phospholipid transfer protein

SDS-PAGE – sodium dodecyl sulfate-polyacrylamide gel electrophoresis

rLTPG – recombinant LTPG

RNAi – ribonucleic acid interference

TNS – 2-(p-toluidinyl) naphthalene-6 sulfonic acid

VLCFA – very long chain fatty acid

YFP- yellow fluorescent protein

Acknowledgements

I thank my supervisor and mentor, Dr. Lacey Samuels for her optimism, quirky humor and seeing the potential in me. I wish to thank my committee member Dr. Ljerka Kunst for her helpful advice and suggestions during my studies. I thank my other committee member, Dr. Reinhard Jetter, for teaching me wax analysis, analytical chemistry and the opportunity to train in his lab. I thank Dr. Jocelyn Rose of Cornell University for allowing me to train in his lab and Dr. Trevor Yeats for helping me with protein expression and biochemistry. I am thankful for the team of undergraduate students that contributed to my thesis, for their dedication, hard work and the happiness they brought to my project: Andre Fallavollita, Colin MacCleod, Angel Shan, and John Shin. I thank the Bioimaging staff for the help they provided: Brad, Derrick, Garnet, and Kevin.

Thanks to Dr. Geoff Wasteneys who provided encouragement, good humor, and the tools to do research. I am also indebted to Dr. Loren Rieseberg for giving me an opportunity to practice molecular biology in his lab.

I am deeply indebted to the many good people I have met and the friends I've made in the Department of Botany: Amanda Catching, Yuan Ruan, Ryan Eng, Gabriel Levesque-Tremblay, Elahe Esfandiari, Zorica Kotur, Scott Liang, Dr. Matt King, Dr. Miki Fujita, Dr. Chris Ambrose and Eric Johnson. Each of you inspired me by making science joyful with your kind acts and generosity.

Finally, I thank my loving family for all of their support. Thank you Louise and Tony for being the siblings I needed. Thank you Mom and Dad for your love, support, encouragement, and the immigrant work ethic; I love you both very much. Thanks for buying me my first computer Dad. We didn't know it then, but I became a scientist that day. Finally, thank you to my Megan. None of this was possible without your love, strength, support and encouragement. I am built on you.

1. Introduction

1.1 Ecophysiology and evolutionary perspective of the cuticle

The development of a waxy cuticle covering the aerial surfaces of plants represents a critical evolutionary adaptation (Post-Beittenmiller, 1996). A key ecophysiological function leading to terrestrial plant existence is the water-proofing or creation of a barrier to non-stomatal water loss (Raven, 1984). The hydrophobic property promotes a clean and dry surface that prevents the accumulation of surface debris, known as the Lotus-Effect (Barthlott and Neinhuis, 1997). Reduced surface debris results in higher photosynthetic potential and efficient gas exchange (Raven, 1984). The altered wettability conferred by the waxy cuticle provides protection from bacterial and fungal pathogens by limiting the ability of water to pool on flat surfaces (Barthlott and Neinhuis, 1997). In addition, the cuticle provides protection against ultraviolet radiation (Riederer and Muller, 2006). The ontogeny of the plant cuticle dates to the late Silurian to early Devonian period and coincided with or followed a period of extinction during which early plants without cuticles were outcompeted by cuticularized plants (Raven, 1984). The emergence of the cuticle before stomata and tracheids indicates the importance of the cuticle and its ubiquity (Wellman and Gray, 2000). This adaptation is more intriguing given that cuticular wax deposition and transport has evolved in parallel, in both plants and arthropods (Hadley, 1981).

1.2 Composition and structure of the plant cuticle

The structure and development of the cuticle is not completely understood. Analytical chemistry shows that the cuticle is comprised of cutin, cutan and an organic solvent-soluble wax component that is predominantly composed of aliphatic very long chain fatty acid (VLCFA) and VLCFA derivatives with chain lengths greater than 20 carbons such as alkanes, aldehydes, primary alcohols and alkyl esters. The above are considered ubiquitous wax constituents (Jetter et al., 2006; Pollard et al., 2008). The diversity of waxes and their constituents increases when taxon-specificity and subsequently, organ-specificity are considered (Jetter et al., 2006).

The structure of cutin is poorly understood, although what is proposed, based on chemistry and reasonable estimates of inter- and/or intramolecular associations suggests a covalently cross-linked polyester structure (Pollard et al., 2008). Understanding cutin is made difficult by the inertness of some of the cutin components and subsequent necessity for harsh chemical methods (BF_3-CH_3OH, $LiAlH_4$, or methanolic KOH) involved in its depolymerization and chemical analysis (Stark and Tian, 2006).

In Arabidopsis, the most abundant monomers of cutin are α,ω-dicarboxylic acids, representing greater than 50% of Arabidopsis cutin, followed by ω-hydroxy fatty acids at up to 32% and unsubstituted fatty acids (Franke et al., 2005). These compounds are likely esterified to form polymers and/or linked together as ethers through alcohol functional groups (Kolattukudy, 1980; Graca et al., 2002; Pollard et al., 2008). The discovery of glycerol as a component of depolymerized cutin introduces further possibilities of esterification or ether formation between polymers of cutin through a glycerol bridge (Graca et al., 2002). Ohlrogge's group showed that glycerol-3-phosphate-acyl transferases (GPAT) 4 and 8 are involved in the assembly of cutin (Li et al., 2007). Double mutants, *gpat4 gpat8* display lower desiccation tolerance and increased susceptibility to fungal pathogens (Li et al., 2007).

These findings helped generate hypotheses as to the possible configuration of cutin *in vivo* yet experimental evidence is lacking (Pollard et al., 2008).

Cutan represents the fraction of aliphatic compounds that remain after cutin depolymerization (Kolattukudy, 2001; Pollard et al., 2008). Kolattukudy showed that linoleic and linolenic acids were preferentially incorporated into cutan from apple peel and hydrogen iodide hydrolysis suggested the presence of ether bonds (Kolattukudy et al., 1973).

Waxes are embedded in and overlaid upon the cutin layer, and are in direct contact with the environment. Wax compositions show abundant chemical species diversity, containing

predominately aliphatics but including phenolics and triterpenoids (Jetter et al., 2006; Kunst and Samuels, 2009). The soluble cuticular wax of Arabidopsis stems is dominated by nonacosane, nonacosan-15-one, and noncosan-15-ol.

1.3 Cuticular wax biogenesis

The biosynthesis of VLCFA backbone precursors of aliphatic wax components is a two stage process requiring: (1) Fatty acids synthesized in the plastid (*de novo* synthesis of C16 and C18 fatty acids) and (2) Elongation of fatty acids to C20, and up to C34, in the endoplasmic reticulum (ER) (Kunst et al., 2006).

The first stage of wax biosynthesis involves of the production of C16 and C18 fatty acids by stromal enzymes. Ketoacyl-ACP synthases condense acetyl-CoA to malonyl-ACP or malonyl-ACP to a growing acyl chain to yield β-ketoacyl-ACP. Reduction by ketoacyl-ACP reductases yields β-hydroxyacyl-ACP, followed by dehydration by β-hydroxyacyl-ACP dehydratase to yield transΔ2-enoyl-ACP and finally, reduction by 2,3-trans-enoyl-ACP reductase to yield a saturated acyl chain (Somerville et al., 2000). This cycle of condensation, reduction, dehydration, and reduction yields an acyl chain that is two carbons longer than the starting acyl chain. It continues until C16 and C18 acyl-ACPs are generated.

The second stage involves the elongation of plastid synthesized C16 and C18 to C20 through C34. Fatty acids are first cleaved from ACP by thioesterases and exported from the plastid by an unknown mechanism (Bonaventure et al., 2003; Kunst et al., 2006). During or immediately after export from the plastid, the C16 and C18 acids are esterified to coenzyme A (CoA) by a long chain acyl CoA synthetase (LACS) (Shockey et al., 2002; Schnurr et al., 2004; Lu et al., 2009). Esterification to CoA is believed to improve solubility in the cytoplasm and prevent reabsorption into the plastid (Kunst et al., 2006). The extension of C16 acyl-CoAs and C18 acyl-CoAs is analogous to the process described for *de novo* biosynthesis, requiring a four-enzyme fatty acid

elongase (FAE) complex that catalyzes condensation, reduction, dehydration and reduction to yield VLCFAs (Samuels et al., 2008; Kunst and Samuels, 2009). The four catalytic domains of the FAE include 1. β-keto-acyl-CoA synthase (KCS), 2. β-keto-acyl-CoA reductase (KCR), 3. β-hydroxyacyl-CoA dehydratase (HCD) and 4. enoyl-CoA reductase (ECR) (Kunst et al., 2006; Samuels et al., 2008; Kunst and Samuels, 2009). KCS activity determines the chain length specificity of the condensation reaction (Millar et al., 1999). There are 21 KCS enzymes annotated in the Arabidopsis genome and the role of some KCSs in wax synthesis, such as the epidermis-specific CER6 (Millar et al., 1999; Fiebig et al., 2000; Kunst and Samuels, 2009), KCS2/DAISY and KCS20 (Lee et al., 2009), was demonstrated by mutant analysis. The genetic impairment of the CER6 enzyme resulted in decreased C26-C30 VLCFAs and their derivatives. The use of this mutant is described in chapter 5, testing localization and dynamics of an LTP as this mutant provides a genetic background with reduced wax flux and reduced VLCFA content in the membranes.

After addition of two-carbon units by the condensing KCS, the elongase complex reduces and dehydrates the elongating fatty acid. Recently, the Arabidopsis KCR was identified (Beaudoin et al., 2009). RNA interference (RNAi) of the KCR transcript resulted in, in some lines, large reductions in wax attributed to decreases in the VLCFA derivatives. Furthermore, heterologous expression in yeast demonstrated complementation of the yeast KCR mutant *ybr159Δ* (Beaudoin et al., 2009). Like GLOSSY8, the KCR of maize, AtKCR is located in the ER (Xu et al., 2002). AtPAS2 was recently identified as the HCD of the FAE complex (Bach et al., 2008). Mutants in Arabidopsis *pas2* displayed reduced VLCFAs, developmental defects and functional equivalence to the yeast HCD, *phs1*. The enoyl-CoA reductase (ECR/CER10) of Arabidopsis was cloned and localized to the ER, as well as shown to fully complement the yeast ECR mutant, *tsc13*, temperature sensitive phenotype (Zheng et al., 2005). Acyl chains are the substrates that enter

the downstream wax biosynthesis pathways of acyl reduction or decarbonylation to generate primary alcohols and wax esters or alkanes, secondary alcohols, and ketones, respectively.

1.3.1 Biosynthesis of primary alcohols and wax esters

Primary alcohol biosynthesis is carried out by fatty acyl-CoA reductases (FAR) (Pollard et al., 1979; Rowland et al., 2006). These enzymes reduce acyl-CoA carbonyl group to yield primary alcohols without producing an aldehyde intermediate. CER4 in Arabidopsis carries out fatty acyl reduction activities; *cer4* mutants show reductions in the products of the acyl reduction pathway, primary alcohols and alkyl esters. They have greater than 80% reductions in both leaf and stem primary alcohols and stem alkyl esters compared with wild type plants (Jenks et al., 1995). CER4 is highly homologous to the FAR of jojoba, is localized to the ER in yeast and is capable of generating C24 and C26 primary alcohols in a heterologous yeast system (Rowland et al., 2006).

Wax esters are formed by the acylation of primary alcohols catalyzed by wax synthase (Lardizabal et al., 2000; Metz et al., 2000). Twelve wax synthases exist in Arabidopsis, annotated on the basis of their sequence similarity to the jojoba wax synthase. Eleven other related acyl transferases are annotated according to sequence similarity with bacterial [*Acinetobacter calcoaceticus*] wax synthase/diacylglycerol acyl transferases (Li et al., 2008), one of which, WSD1, displayed reduced wax esters upon mutation and displayed wax synthase activity in heterologous *E. coli* and yeast expression systems (Li et al., 2008).

1.3.2 Biosynthesis of alkanes, secondary alcohols and ketones

The enzymes catalyzing the production of alkanes are not known. Overall a VLCFA is reduced to an aldehyde and decarbonylated, but the chemical mechanism of the one carbon loss is not known (Kunst et al., 2006; Kunst and Samuels, 2009). Mutants of the decarbonylation pathway show reductions in alkanes, secondary alcohols and ketones. Putative decarbonylation pathway

mutants include *cer1* (Aarts et al., 1995), *cer2*, *cer22* (Rashotte et al., 2004) and *cer3/yre/flp1/wax2* (Chen et al., 2003; Rowland et al., 2007), none of the gene products has been verified biochemically as *de facto* decarbonylases (Samuels et al., 2008; Kunst and Samuels, 2009). Although none of these proteins have been identified as proper decarbonylases, mutant phenotypes suggest they act at the top of the decarbonylation pathway in unexpected ways. The mutant *cer1* has greater than 90% reduction in stem wax alkanes, secondary alcohols and ketones; there is also decrease in primary alcohols (Jenks et al., 1995). The *cer22* mutant displays a considerable decrease in all decarbonylation pathway products, a decrease in primary alcohols and an increase in wax esters (Rashotte et al., 2004). The phenotype displayed by *cer3* is a decrease in all decarbonylation pathway products with no increase in acyl reduction pathway products (Chen et al., 2003), and confirmed by Rowland et al. (2007). The biosynthesis of ketones and secondary alcohols is thought to occur by oxidation of alkanes to secondary alcohols with further oxidation to yield ketones (Kunst et al., 2006; Kunst and Samuels, 2009). Reverse genetic analysis in Arabidopsis identified a cytochrome P450, MIDCHAIN ALKANE HYDROXYLASE1 (MAH1), required for normal secondary alcohol and ketone production in stem wax (Greer et al., 2007).

1.4 Cuticular lipid transport

The transport of aliphatic cuticular lipids from the plasma membrane to the cuticle is poorly understood. Some of the components thought to be involved in cuticular lipid transport and their relationships are only now being deciphered (Pighin et al., 2004; Bird et al., 2007; DeBono et al., 2009; McFarlane et al., 2010). Presumably, the transport process begins at the ER where waxes are biosynthesized. At this time no information is available about this portion of the transport process. What is known of transport is confined to the plasma membrane. ATP binding cassette (ABC) transporters are large, energy-dependent membrane-bound proteins defined by their ability to export chemicals and cuticular lipids (Verrier et al., 2008). In Arabidopsis, ABC

transporters such as ABCG12/CER5 and ABCG11/WBC11 are required to transport cuticular lipids across the plasma membrane of epidermal cells to the cuticle (Pighin et al., 2004; Bird et al., 2007; Panikashvili et al., 2007). In *abcg11/wbc11* and *abcg12/cer5* mutants, the stems of Arabidopsis have decreased surface wax levels as a result of impaired cuticular lipid transport. Unlike *abcg12*, *abcg11* shows severe developmental difficulties, including stunted growth and cuticular fusions thought to cause tearing at the plant surface (Bird et al., 2007; Panikashvili et al., 2007). Recently, homodimers of ABCG11 as well as heterodimers of ABCG11 and ABCG12 have been shown to interact in a protoplast system (McFarlane et al., 2010). Different combinations of ABCG proteins are presumed necessary for cutin and wax transport.

Although the discoveries of these important transport proteins are critical first steps in understanding cuticular lipid transport, little is known about the mechanism of transport from the plasma membrane through the outer periclinal cell wall (the cell wall that is immediately proximal to the environment), to the cuticle. The cell wall is linked to the protoplast through membrane adhesion sites (discussed in Chapter 5) and plasmodesmal connections to neighboring cells (Staehelin and Newcomb, 2000). Once a cuticular lipid is extruded from an epidermal cell, it must traverse a hydrophilic, charged, and aqueous environment. The cuticular layer, the layer subtended by the primary cell wall is embedded with pectin (Jeffree, 2006) and may represent a physical impediment to cuticular wax transport. It is unlikely then that ABC transporters eject cuticular lipids from plant epidermal cells directly to the hydrophilic cell wall. Once across the cell wall, cuticular lipids would, next partition from the hydrophilic, charged environment of the wall into the hydrophobic environment of the cuticle and can self organize at the plant surface (Jetter et al., 2006).

1.4.1 Lipid transfer proteins: structure and ligand binding

Lipid transfer proteins (LTP) have long been suspected as lipidic cargo shuttles *in planta* (Douady et al., 1982; Kader et al., 1984; Breu et al., 1989; Sterk et al., 1991). LTPs are excellent

candidates as proteins that may move cuticular lipids from the plasma membrane of epidermal cells to the cuticle. However, when *in vitro* lipid binding or lipid shuttling data is considered, it is difficult to reconcile extremely low single protein lipid binding (Douady et al., 1982; Kader et al., 1984; Breu et al., 1989) with the *in vivo* cuticular lipid/wax transport requirements. It is more likely that a group of specialized LTPs engages in cuticular lipid trafficking instead of a scenario in which each of the 70 annotated LTPs based on the presence of eight cysteine residues and propensity to form α-helices in the Arabidopsis genome makes a small contribution to wax transport. The idea of specialized LTPs is given some strength when LTP sequence analyses are performed. Structurally, LTPs have low sequence similarity (Yeats and Rose, 2008; Edstam et al., 2011). The signature characteristic of LTP primary structure is 8 conserved cysteine residues (Takishima et al., 1986) and has been used to define this as a protein 'family' (Kader, 1996; Jose-Estanyol et al., 2004). In addition, the primary structure typically contains small hydrophobic amino acid residues (glycine, alanine), acidic residues arranged such that they protrude away from the core protein structure that does not contain phenylalanine (Kader, 1996; Yeats and Rose, 2008). LTPs are better described as a family based on structural similarity (*i.e.* secondary and tertiary) and not on primary amino acid sequence. The available X-ray crystal data suggest that LTPs are cup-shaped molecules, comprised of four α-helices (Shin et al., 1995; Kader, 1996; Lee et al., 1998; Charvolin et al., 1999). The α-helices are held in proximity to one another with four disulfide bridges required for the formation of the putative lipid-binding cavity (Kader, 1996; Charvolin et al., 1999; Landon et al., 2001; Lascombe et al., 2008). Experiments show that binding of fluorescent lipid analogues in a dose dependent fashion does not occur in a reducing environment. This suggests that disulfide bonding is required for function (Zachowski et al., 1998; Buhot et al., 2004; Sawano et al., 2008; DeBono et al., 2009). It is possible then that different combinations of α-helices and α-helix flexibility may impart substrate specificity similar to enzyme cavity depth of yeast KCS (Denic and Weissman, 2007). The crystal structure of rice LTP provides evidence that the carboxy-terminal loop may be responsible for binding

with some lipid substrates and additional expansive properties may be imparted by glycine- or proline-induced α -helix flexibility (Yeats and Rose, 2008).

Despite protein crystal or structural studies showing a hydrophobic core region in LTPs, little experimental evidence exists demonstrating that they bind biologically relevant lipid molecules. There is an inherent chemical and subsequent technical difficulty with solubilizing lipidic substrates in hydrophilic buffers that are suitable for protein storage. There is also a recurring problem of biological significance in LTP-ligand studies: ligands are lipidic but seldom biologically relevant. Fluorescently labeled C12, C16 and C18 fatty acid derivatives were used to characterize binding by maize LTP (Zachowski et al., 1998). Such fluorescent fatty acids are representative of fatty acids, not cuticular wax components; at best, they are similar to cutin monomers. Similarly, several structures of LTPs are reportedly complexed with one or more molecules of lysomyristylphophatidylcholine (Charvolin et al., 1999), lysolecithin (Gomar et al., 1996), and prostaglandin B_2 (Tassin Moindrot et al., 2000). While it is acknowledged that such ligands were used to facilitate technical problems involved while solving protein structure (Gomar et al., 1996) they fail to address the binding of the likely biological ligands and thus functions of LTPs.

Despite the described limitations, these experiments show convincingly that LTPs bind lipidic compounds *in vitro* (Gomar et al., 1996; Zachowski et al., 1998; Charvolin et al., 1999; Tassin Moindrot et al., 2000). Two interesting results exist: 1. The binding capacity of an LTP may exceed one hydrophobic molecule (Zachowski et al., 1998; Cheng et al., 2004). 2. LTPs are capable of binding substrates up to C20 in length (Tassin Moindrot et al., 2000). These findings lend support to the hypothesis that LTPs are capable of binding large hydrophobic molecules similar to cuticular waxes, the VLCFAs and their derivatives. Maize and rice LTPs bind up to two fatty acid analogues *in vitro* (Zachowski et al., 1998; Cheng et al., 2004). It is unfortunate that the exact stoichiometry was not calculated but it is clear that maize LTP can bind the volume

of two C12 acid molecules. These data suggest that the volume of the hydrophobic cavity of this LTP is sufficiently large to accommodate at least a C24 fatty acid. Lending further support to this idea, the work of Tassin Moindrot et al., (2000) showed that a wheat LTP was capable of binding prostaglandin B_2. LTPs have been demonstrated to bind to methyl jasmonate (Girault et al 2008). Taken together, these results show that LTPs can bind both linear and bulky molecules that contain functional groups such as carbonyl groups and hydroxyl groups and moieties such as planar rings. Subsequently, this shows that the hydrophobic core is not fixed and LTPs have an ability to expand considerably. Expansion of the LTP core is possible; early X-ray crystallography studies noted that the first and fourth α-helices of maize LTP were bent by proline residues (Shin et al., 1995; Cheng et al., 2004). The single sp^3-hybridized carbon-carbon bonds are approximately 1.54Å (Karplus, 1963). If stretched end-to-end the length of a typical carbon chain found in cuticular lipid nonacosane is approximately 43Å. Although it remains to be determined whether LTPs bind cuticular lipids, this information is consistent with such a role considering the hydrophobic pocket depth found for maize and rice LTPs is 37Å and 34Å, respectively (Shin et al., 1995; Cheng et al., 2004). Given the flexibility of the LTP structure, these results are exciting since Arabidopsis LTPs may, by analogy to other LTPs, have the capacity to bind the VLCFA components and derivatives of cuticular waxes, which are greater than twenty carbons in length and contain various functional groups.

1.4.2 Comparison of plant LTPs with metazoan lipid transfer proteins

LTP research started when Wirtz and Zilversmit (1968) discovered that rat liver homogenates were able to transfer phosphotidylcholine and to a lesser extent phosphatidylethanolamine, between microsomal membranes and mitrochondria. Later it was shown that the active component in a beef liver homogenate was a protein of approximately 20 kD that became known as a phospholipid exchange protein (Demel et al., 1973), and later phospholipid transfer protein (PLTP). Using potato tuber homogenates, it was shown that such activity was also demonstrable

in plants (Abdelkader and Mazliak, 1970). Whereas metazoans have many lipid exchanging or transferring proteins moving phospholipids, oxylipins, oxysterols, sterols, cholesterol-esters, plants appeared to have proteins that largely showed no specificity for one lipid type earning the designation 'non-specific (ns)' lipid transfer proteins which was then reduced to LTP. This is not to imply that specific lipid transfer proteins do not exist in plants; phophatidylinositol, glycerolipid, and sterol transfer proteins have been reported based on demonstrated function or similarity with human or yeast homologues (Böhme et al., 2004; Edqvist et al., 2004; West et al., 2008). Metazoan LTPs/lipid binding proteins show few structural similarities with plant LTPs. Metazoan lipid transfer proteins are a large and diverse family of proteins represented by cholesterol ester transfer proteins (CETP), phospholipid transfer proteins (PLTP) (Bruce et al., 1998), and fatty acid binding proteins (FABP) (Storch and Thumser, 2000). These proteins are not structurally related but are grouped together for this discussion. CETP and PLTP are soluble blood serum proteins that associate with and sometimes modify high density lipoproteins (Tall, 1986; Bruce et al., 1998). CETPs and PLTPs are boomerang-shaped and composed of two β-barrels bound by β-sheets (Bruce et al., 1998; Qiu et al., 2007). FABPs are globular proteins owing to ten anti-parallel β-strands oriented to form a barrel, capped by two α-helices (Storch and Thumser, 2000). These shapes are in contrast to plant LTPs, which are extremely compact, containing predominantly α-helical structures linked by unstructured loops (Shin et al., 1995).

In both plant and metazoan LTPs, disulfide bonds appear to be used analogously to stabilize protein structure and protect the hydrophobic portion of the protein from the aqueous environment. Similar to plant LTPs, metazoan LTPs contain one to three disulfide bridges which may assist to envelope lipidic cargo (Huuskonen et al., 1999; Beamer et al., 1997; Huuskonen et al., 1999).

Whereas plant LTPs appear to be 9-20 kD in mass prior to processing (Kader, 1996), FABP are approximately 14-15 kD (Storch and Thumser, 2000) and PLTPs 50-80 kD (Van Tol, 2002).

The lower size and mass of LTPs may reflect a need to remain within the size exclusion limit of the cell wall, which is reported to be 17 to 67 kD (Tepeer and Taylor, 1981; Baron-Epel et al., 1988).

1.5 LTP localization: a role in cuticular wax deposition?

Cuticular wax components must leave epidermal cells where they are synthesized and traverse the apoplast to reach the cuticle. Several lines of evidence suggest that processed LTPs are destined for secretion, contrary to claims of interorganellar lipid transfer (Kader et al., 1984; Arondel et al., 1990). Carrot suspension cells were found to secrete an LTP to the growth medium (Sterk et al., 1991). These results, in addition to the detection of an amino-terminal signal sequence in a LTP of spinach, suggest that LTPs are secreted proteins (Bernhard et al., 1991). Indeed, inspection of Arabidopsis LTPs with the PrediSi (Hiller et al., 2004) signal peptide prediction tool shows that 65 of 72 annotated LTPs bear signal peptides (Table 1-1). Studies of maize LTP suggested that this protein localized to the epidermis (Sossountzov et al., 1991). It was the seminal work of Kolattukudy that finally clarified the localization of LTPs. In broccoli, the LTP WAX9 was present in the organic solvent-soluble waxes of leaves (Pyee et al., 1994). Detection of WAX9 by immunocytochemistry showed cell wall localization (Pyee et al., 1994) similar to other reports in maize and Arabidopsis (Sossountzov et al., 1991; Thoma et al., 1994). Unlike the other LTPs studied, notably Arabidopsis LTP1 (Thoma et al., 1993) and maize LTP (Sossountzov et al., 1991), WAX9 displays localization to epidermal cell anticlinal walls as well as periclinal cell walls (Pyee et al., 1994). DIR1 is also thought to be localized to the cell wall (Champigny et al., 2011). However the localization of DIR1 as presented, showed localization to transvacuolar ER strands and perinuclear ER, suggesting some mislocalization (Champigny et al., 2011). Localization to all sides of the epidermal cell wall may reflect a more complicated movement of lipidic cargo than envisioned, where cuticular lipids are deposited to the outer periclinal cell surface facing the cuticle. Such deposition could be influenced by the

membrane environment and/or glycosylation status of the LTP(s) involved. These experiments were critical because they assigned non-cytoplasmic localization, in contrast to cytoplasmic roles initially hypothesized by Kader (1984), and lent support to a proposed role of these proteins in cuticular lipid trafficking; however they failed to demonstrate function.

The tops of rapidly elongating inflorescence stems and young, expanding leaves of Arabidopsis have been found to be areas of greatest deposition of soluble cuticular wax (Suh et al., 2005). For LTPs to have a role in cuticular lipid deposition, their expression should be coordinated with times of known wax deposition during development. In broccoli, LTPs were detected during times of leaf expansion when predicted bulk transfer of cuticular lipids to the surface of broccoli leaves occurs. WAX9 expression was highest in expanding leaves and decreased with leaf age. The protein was 25 times more abundant on young leaves (Pyee et al., 1994). These results match very closely the gene expression and wax expression data acquired for expanding Arabidopsis stems (Suh et al., 2005) because they indicate wax deposition is maximal during tissue expansion. Unfortunately, Kolattukudy (Pyee et al., 1994) reported the amount of WAX9 (mg) per approximate mass of broccoli leaf (kg) without stating soluble wax amounts extracted, forgoing the possibility of stoichiometric calculations at different developmental stages.

1.6 Putative biological functions of LTPs

LTPs represent a large and diverse group of proteins, especially in Arabidopsis where more than 70 genes are annotated (Beisson et al., 2003; Figure 1-1). This diversity is responsible for many reports of putative functions and/or correlations with stress responses and development. These correlative reports include salt stress (Sottosanto et al., 2004); upregulation during enzyme-mediated cutin degradation (Chassot et al., 2007); cell expansion (Nieuwland et al., 2005); induction by drought stress (Cameron et al., 2006b); upregulation in auxin transport-impaired backgrounds (Wenzel et al., 2008); and induction by ABA (Nemhauser et al., 2006). A report

suggests that *Brassica campestris* non-specific LTP may have therapeutic properties as a suppressor of HIV reverse transcriptase (Lin et al., 2007). In assessing biological function using genetic approaches, the possibility that observed mutant phenotypes result from pleiotropic effects from a modified cuticle must be considered.

Certain LTPs have been implicated in disease resistance. The best characterized such LTP is DEFECTIVE IN INDUCED RESISTANCE 1 (DIR1), involved in systemic acquired resistance (SAR; Maldonado et al., 2002). Disruption of DIR1 by T-DNA insertional mutagenesis results in Arabidopsis being unable to develop SAR, leading the authors to conclude that DIR1 may transport a lipidic signal involved with establishing acquired resistance. The colonization by the arbuscular mycorrhizal fungus, *Glommus mossae*, is known to cause a salicylic acid-dependent induction of rice LTP (Blilou et al., 2000). Although mycorrhizal fungi are beneficial, this suggests that LTP induction occurs during infection of plant tissues.

LTP antimicrobial properties have been long known. Overexpression of barley LTP2 in both tobacco and Arabidopsis conferred enhanced resistance to *Pseudomonas syringae* (Molina and Garcia-Olmedo, 1997). The antimicrobial activity of LTPs is not limited to protection from bacteria. In sugar beet intercellular washing fluid, two proteins that had strong homology to LTPs were able to delay fungal growth and caused reduced mycelia size of developing fungi (Nielsen et al., 1996). Antifungal properties are known for wheat LTP, (Isaac Kirubakaran et al., 2008), wheat LTP expressed in carrot (Jayaraj and Punja, 2007), barley and maize (Molina et al., 1993). The absence of LTPG in Arabidopsis is thought to enhance susceptibility to *Alternaria brassicicola* (Lee et al., 2009). Together these results suggest that some LTPs are involved in defense to pathogens.

The LTP/pathogen link became more complicated to interpret when it was shown that an overexpressed, cell wall-targeted cutinase in Arabidopsis results in resistance to infection by

Botrytis cinerea although three LTP genes (*At4g12470*, *At4g12480*, and *At4g12490*) were strongly upregulated in the cutinase-overexpressing plants (Chassot et al., 2007). The resistance displayed was independent of pathways for the hormones salicylic acid, jasmonic acid and ethylene. The postulated mechanism behind this counter-intuitive result is that the disorganized cuticle allows plants to release a fungitoxic substance although the release of elicitor compounds that induce defense responses cannot be ruled out. These results do not implicate LTPs as the mechanism for the observed resistance response. It is more likely, that in some cases, this response may occur through modifications of the cuticle by way of LTPs.

1.7 A microarray used to choose candidate LTP candidates

Since *Arabidopsis thaliana* has over 70 LTPs annotated by sequence analysis (Beisson et al., 2003; Suh et al., 2005), a brute force approach for detecting candidate LTPs would be highly inefficient. The size of the putative LTP family made choosing promising candidates difficult. Microarray data derived from Arabidopsis stem epidermal peels made it feasible to assess transcript expression levels in the epidermis as compared with the whole stem (Suh et al., 2005). This microarray allowed me to determine which, if any, LTP transcripts were enriched in the epidermal peels compared to the remainder of the stem. LTP transcripts enriched in the epidermal peels are hypothesized to be involved in cuticle biosynthesis/deposition. Subsequently, a correlation analysis was also used to gauge LTP expression versus the expression of known cuticular lipid metabolic genes (Paige and Bird, unpublished; Table 1-2). In this way, each Arabidopsis gene could be assigned a numerical coefficient that describes its expression relative to known cuticular lipid genes such as *CER5, CER6* and *CER1*. Transcripts that were found to be enriched in the epidermis with respect to the remainder of the stem and well correlated with the pre-determined cuticular lipid genes proved very useful. This approach pointed to candidate genes in cuticular lipid transport and biosynthesis, which were validated using reverse genetic studies of T-DNA insertional mutants. Some mutants with cuticular lipid phenotypes identified

using this approach included *WBC11*, an ABC transporter (Bird et al., 2007); *MAH1* (Greer et al., 2007), a cytochrome P450; and *WSD1*, a wax synthase (Li et al., 2008).

1.7.1 Nomenclature system for Arabidopsis LTPs

Due to the large number of annotated LTP or LTP-like genes and their implication in different biological phenomena (DIR1; Maldonado et al., 2002) nomenclature has been awkward and problematic. A tentative system of nomenclature was developed that grouped the Arabidopsis LTPs into eight groups based on the number of amino acids between the fourth and fifth conserved cysteine residues in the core motif of the LTP tertiary structure (Beisson et al., 2003). This does not allow for the nomenclature of LTPs to expand as more become discovered and implicated in biological processes as discussed below. I have modified Beisson's nomenclature such that groups numbered 1 through 8 are designated A through H. The first Arabidopsis LTP to be characterized (Thoma et al., 1993), *AtLTP1* (At2g38540), is *LTPA5* by my system of nomenclature. Alleles of this gene would be named *LTPA5-1*, *LTPA5-2* and so on. By Beisson's nomenclature *LTPA5* would be *LTP5-1* and its alleles would be *LTP5-1-1, LTP5-1-2, LTP5-1-3 etc.* My system of nomenclature creates a simple framework for naming yet to be characterized LTP genes and their alleles and parallels closely the system of nomenclature recently adopted for ABC transporters (Verrier et al., 2008).

1.8 Glycosylphosphatidylinositol proteins

Prior to this work, studies of wax transport have primarily involved plasma membrane localized ABC transporters (Pighin et al., 2004; Bird et al., 2007; Luo et al., 2007 Panikashvili et al., 2007). Since the journey of a given wax molecule does not terminate at the plasma membrane, the logical, next component of a putative wax export mechanism would be a protein that can interact with the plasma membrane and cell wall. Glycosylphosphatidylinositol (GPI) proteins are a class of proteins found at the plasma membrane and display exoplasmic topology, that is, they face the extracellular environment (Sedbrook et al., 2002; Roudier et al., 2005; Ellis et al., 2010).

Fungal, parasitic, and mammalian cell line GPI proteins also display exoplasm-facing topology (Kinoshita et al., 2008; Fujita and Kinoshita, 2010). GPI linkage confers exoplasmic topology to proteins and is evolutionarily conserved among diverse organisms; GPI linkage is a structural feature of many plant proteins, including some LTPs (Borner et al., 2002; Elortza et al., 2003; Borner et al., 2005; Elortza et al., 2006). Plant GPI LTPs, localized at the plasma membrane, have the potential to interact with the cell wall/exoplasm as described for other biological systems.

GPI proteins are secreted proteins that are post-translationally modified such that they become covalently linked to a glycolipid. GPI proteins have three critical elements: 1. An amino terminal signal sequence to enter the ER and the secretory pathway; 2. A hydrophobic carboxy-terminal signal sequence 15-20 amino acids in length; and 3. The ω-site or the specific amino acid to which a GPI is added (Figure 1-2). The latter two are known as the GPI domain. These proteins are synthesized at the ER such that they are extruded into the ER lumen and, following secretion, topologically, face the outside of the cell. When the hydrophobic GPI domain enters the ER membrane, translocation is stopped. This signal is recognized by a three-component transamidase complex, consisting of Gaa1p, Gpi8p, and Gpi16p subunits in yeast (Gerber et al., 1992; Fraering et al., 2001; Mayor and Riezman, 2004; Orlean and Menon, 2007; Kinoshita and Fujita, 2009; Signorell and Menon, 2009). The transamidase covalently links the proprotein at the ω-site to a pre-assembled GPI in the ER membrane (Orlean and Menon, 2007; Kinoshita and Fujita, 2009; Signorell and Menon, 2009; Fujita and Kinoshita, 2010). There are approximately eleven enzymatic reactions that are coordinated in order to synthesize a GPI moiety and attach it to the ω-site (These steps are reviewed in Orlean and Menon, 2007; Fujita and Kinoshita, 2010). Moreover, current understanding implicates at least 23 gene products in GPI biosynthesis (Kinoshita and Fujita, 2009). The biosynthesis of the GPI moiety is outside the scope of this thesis chapter. For the most comprehensive recent reviews, the reader is directed elsewhere

(Orlean and Menon, 2007; Signorell and Menon, 2009; Kinoshita and Fujita, 2009). I will use Kliss' nomenclature of "GPI protein" in place of "GPI-anchored protein," indicating that proteins modified with a GPI moiety can exist as bound to the plasma membrane or covalently cross-linked to, and only associated with, the cell wall (Caro et al., 1997).

The biological importance of GPI proteins is underscored by their abundance at the plasma membrane; approximately 10-20% of all membrane proteins are GPI proteins (Orlean and Menon, 2007). In plants, the best known GPI proteins are the cell wall proteins SKU5, COBRA (Sedbrook et al., 2002; Roudier et al., 2005) and the AGPs (Ellis et al., 2010). All known GPI proteins in plants are localized to the extracellular face of the plasma membrane and/or cell wall. Indeed, COBRA was found to be enriched in the outer periclinal cell wall of root cells (Roudier et al., 2005). GPI protein LTPs at the plasma membrane could facilitate transport of biomolecules to the cell wall or cuticle. Indeed, Borner and colleagues (2003) showed by phospholipase C cleavage and protein sequence analysis that over 200 genes encode GPI proteins in Arabidopsis; two GPI proteins identified in this thesis work, LTP-GPI (LTPG) and LTPE23 were encoded by these genes.

1.9 Overall research goal

Cuticular wax transport has been understood primarily through the lens of ABC-transporter studies. These studies have revealed that ABC transporters are required for cuticular wax and cutin export from epidermal cells. The path of a cuticular wax from the plasma membrane to the cell surface is not known. The focus of my thesis work is to examine the role of LTPs in cuticular wax transport from the plasma membrane to the cell surface.

My thesis objectives can be expressed in these questions:

1. Are highly expressed, epidermal LTPs required for wax export?

2. Is LTPG responsible for wax transport?
3. Is LTPG capable of lipid binding *in vitro*?
4. What features of LTPG are conferred by the GPI domain?
5. Does the LTPG GPI domain influence its behavior in the lipid bilayer?
6. Are LTP domains functionally interchangeable?
7. Is cell wall or plasma membrane localization of LTPG required for wax trafficking?

I used analytical chemistry, molecular genetics and confocal microscopy to address these questions.

1.9.1 Which of the LTPs, expressed strongly during cuticle deposition, are required for wax export?

The objective of this work was to test if LTPs are required for wax export using Arabidopsis mutants. To choose the candidate genes for reverse genetic analysis, an Arabidopsis stem epidermal-peel microarray was used to identify genes highly expressed in this tissue (Bird et al., 2007; Greer et al., 2007; Li et al., 2008). LTPs with high expression during cuticle secretion were hypothesized to have some involvement in cuticular wax deposition. Five candidate LTPs, including LTPG, were chosen for further analyses. *Ltpg* mutants show a decrease in wax stem accumulation (Chapter 3). Mutations in the other four candidate LTPs do not show wax reductions compared to wild type (Chapter 4). Since it was probable that functional redundancy may have contributed to muting observable phenotypes, double and triple mutants were generated for the possible combinations of the LTPA type candidates. They too displayed no wax deficiencies when compared to wild type (Chapter 4).

1.9.2 Is LTPG responsible for wax transport?

The objective of these experiments was to test if a wildtype copy of LTPG could restore wax in the *ltpg-1* mutant. Only one allele for *ltpg* was available, but independent RNAi lines also supported the observation that wax reduction phenotype was caused by a defect at this locus. To confirm that mutation at this locus was responsible for the observed phenotype, I demonstrated that introduction of *LTPG* expressed from its native promoter restored the wax deficiency in the *ltpg-1* plants. With the same objective, in a parallel experiment, I transformed a native promoter-driven copy of *LTPG* internally fused with YFP. In both experiments, I used gas chromatography with flame ionization detection (GC-FID) to quantify the wax amount of wildtype; *ltpg; proLTPG::LTPG* in *ltpg* and *proLTPG::YFP-LTPG* in *ltpg-1*plants. Transgenic plants expressing LTPG and YFP-LTPG had wax levels that were indistinguishable from that found in WT.

1.9.3 Is LTPG capable of lipid binding *in vitro*?

The objective of these experiments was to test the hypothesis that the predicted hydrophobic pocket of LTPG can bind lipids. I probed the structure of LTPG by using the fluorescent lipid reporter 2-(p-toluidinyl) naphthalene-6-sulfonic acid (TNS). To perform this experiment, I expressed recombinant LTPG in the yeast *Pichia pastoris* and in *E. coli.* This work is described in Chapter 3.

1.9.4 What features of LTPG are conferred by the GPI domain?

The goal for this set of experiments was to test whether LTPG requires the GPI domain or can function without a GPI domain like an “A-type LTP”. The GPI domain is an energetically expensive post-translational modification requiring the coordinated effort of many proteins. I reasoned that the presence of a GPI linkage on LTPG conferred properties that assist with or are required for wax trafficking. To this end, I attempted to express a version of LTPG that lacked

the predicted omega site (the exact amino acid sequence alteration KGG**S**→K~~GGS~~PQ) with amino acids PQ, resulting in a protein tethered to the plasma membrane through the hydrophobic transmembrane anchor of the GPI domain. In a complementary experiment, I deleted the GPI domain in its entirety. LTPAs are soluble proteins, unlinked to the membrane. I wanted to determine if adding a synthetic GPI domain to a LTPA, the mutant for which displays no measurable wax phenotype, can rescue the *ltpg-1* mutant. These experiments are described in Chapter 5.

1.9.5 Does the LTPG GPI domain influence its behavior in the lipid bilayer?

The previous objective addressed the nature of the GPI domain as it pertains to the function of LTPG. Next I asked how the GPI domain of LTPG influences the interaction of LTPG with its environment. To this end, I used fluorescence recovery after photobleaching (FRAP) in order to study the dynamics of LTPG in the plasma membrane. Once I established the dynamics of LTPG, I studied the behavior of the non-wax related protein GFP-LTI6b (GFP fused to LOWTEMPERATUREINDUCED6b) to create a membrane protein measure of mobility. To demonstrate that my microscope system, imaging parameters, and method were able to capture a complete recovery, I engineered and used cytoplasmic-YFP. In order to separate the effect of the GPI domain from the LTP domain, I engineered a construct such that the GPI domain and amino terminal signal sequence were fused to YFP. To study the effect of an altered lipid flux through the plasma membrane I used *cer6* and *mah1* mutants; I introduced YFP-LTPG by crossing into each mutant background. These results are described in Chapter 5.

Table 1-1: Amino terminal secretion signal sequence predictions for all annotated Arabidopsis LTPs.

LTP	Cleavage position	Is cleaved?	Score	LTP	Cleavage position	Is cleaved?	Score
At2g15050	25	Y	0.65	At3g22580	26	Y	0.83
At2g18370	24	N	0.33	At4g22490	22	Y	0.67
At2g38530	25	Y	0.55	At4g22520	27	Y	0.69
At2g38540	25	Y	0.67	At4g28395	60	Y	0.71
At3g08770	19	Y	1.00	At1g18280.1	22	Y	0.74
At3g51590	24	Y	0.58	At1g62795.1	25	Y	0.72
At3g51600	25	Y	0.67	At1g62790.2	25	Y	0.72
At4g08530	28	N	0.42	At4g12360.1	23	Y	0.97
At4g33355.2	28	Y	0.69	* At1g27950.1	32	Y	0.65
At4g33355.1	28	Y	0.69	At1g36150.1	21	Y	0.93
At5g59310	23	Y	0.73	At1g73890.1	24	Y	0.79
At5g59320	23	Y	0.81	At2g27130	20	Y	1.00
At2g15325	27	N	0.25	At2g44290	24	Y	0.60
At5g01870	22	Y	0.90	At2g44300	24	Y	0.67
At1g48750	26	Y	0.94	At2g48130.1	24	Y	0.87
At1g66850	19	Y	0.62	At2g48140.1	20	Y	0.63
At1g73780	29	Y	0.51	At3g22600	24	Y	0.77
At3g18280	28	Y	0.96	At3g22620	21	Y	0.71
At3g57310	24	Y	0.52	At3g43720.1	22	Y	0.69
At5g38160	24	Y	0.54	At3g43720.2	22	Y	0.69
At5g38170	17	Y	0.57	At4g08670.1	20	Y	0.84
At5g38180	17	N	0.40	At4g14815.1	22	Y	0.67
At1g32280	23	N	0.49	At4g22630	29	Y	0.68
At3g07450	29	Y	0.63	At4g22640	27	Y	0.72
At3g52130	26	Y	0.70	At5g09370.1	24	Y	0.96
At4g30880	22	Y	0.60	At5g09370.2	24	Y	0.96
At4g33550	21	N	0.48	At3g58550.1	29	Y	0.66
At5g07230	24	Y	0.85				
At5g48485	26	Y	0.69				
At5g48490	25	Y	0.50				
At5g52160	32	Y	1.00				
At5g55410.1	30	Y	0.52				
At5g55410.2	30	Y	0.52				
At5g55450	30	Y	0.58				
At5g55460	24	Y	0.60				
At5g56480	23	Y	0.67				
At5g62080	30	Y	0.72				
At5g05960	25	Y	0.56				
At3g53980.1	23	Y	0.78				
At3g53980.2	23	Y	0.78				
At1g70240/ At1g70250	19	Y	0.71				
At1g73550	25	N	0.00				
At1g73560	21	Y	0.71				
At2g37870	23	Y	0.83				
At2g48140	20	Y	0.63				
At3g22570	24	Y	0.90				

Secretion signal sequences were detected with Predsi (www.predisi.de, Hiller et al., 2004). **LTP** indicates the accession or Arabidopsis identifier. **Cleavage position** indicates amino acid after which cleavage occurs. **Cleavage** indicates whether cleavage occurs (Y) or not (N). LTPAs appear upon yellow background. LTPs that do not contain a detectable signal sequence appear on grey backgrounds. LTPG is marked with *.

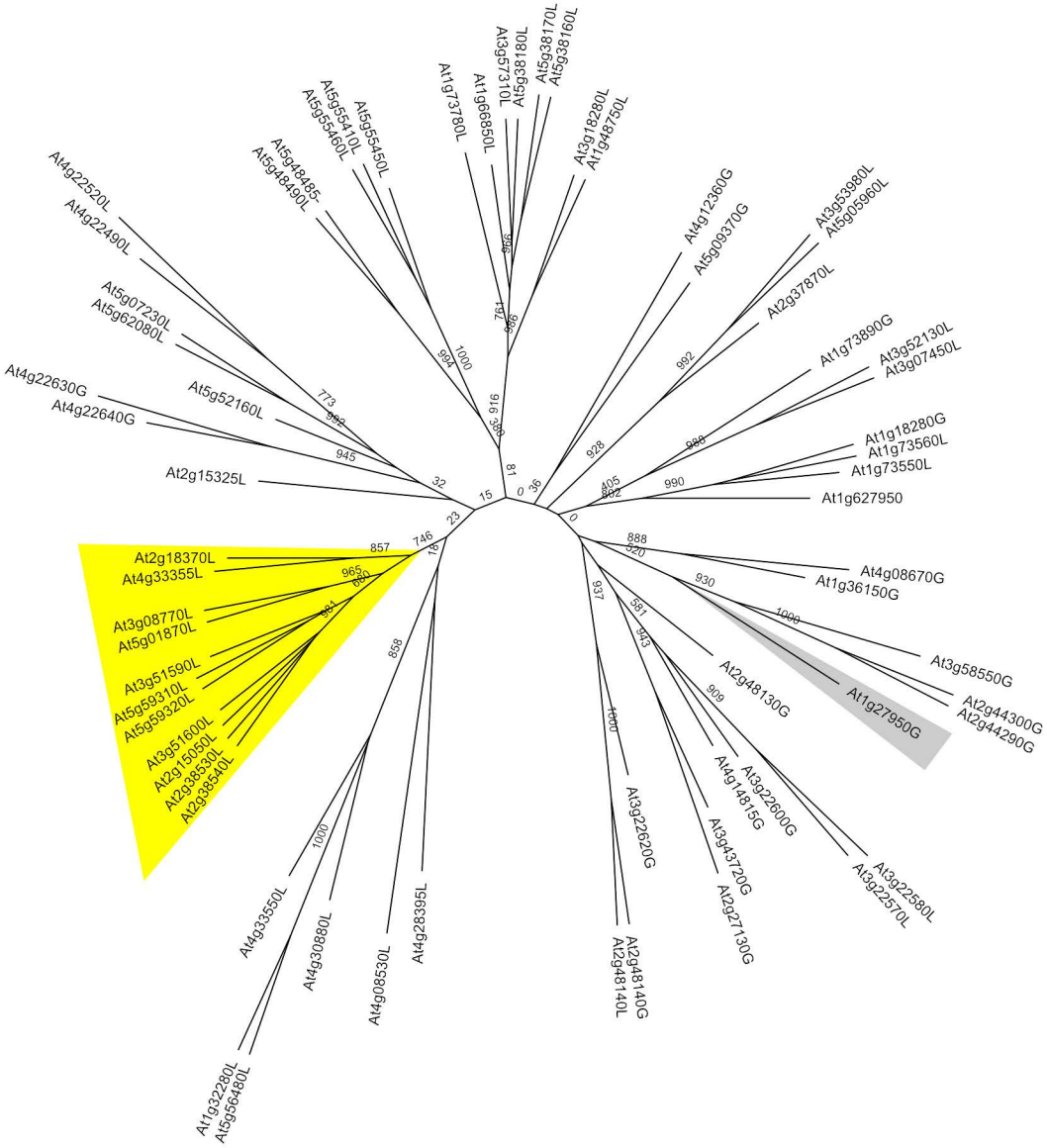

Figure 1-1: Phylogenetic tree of all lipid transfer proteins (LTPs) annotated in the Arabidopsis genome. Tree is based on amino acid sequences available at TAIR and assembled in PhyML. Numbers indicate bootstrap values out of 1000 replicates. The LTPA subtype (yellow) and LTPG/At1g27950 (grey) are shown.

Table 1-2: Correlation ranking of LTPs with cuticular lipid genes.

	Correlation Rank of LTPs with cuticular lipid genes							Ratio of expression[a]	
LTP	*CER6*	*ABCG12/ CER5*	*FATB1*	*CER4*	*CER1*	*CER1b*	*LACS2*	Top epidermis: stem	Bottom epidermis: stem
A1	1405	330	21195	18677	23137	21118	10783	4.29	3.37
A8	242	329	2377	17300	10629	10067	4189	2.75	3.64
A13	5322	24876	18799	4675	263	344	19068	1.61	1.50
G	899	294	3938	11665	1424	1480	66	3.79	8.73
E23	1396	306	3794	10479	5238	4301	155	3.22	4.75

LTP genes studied in this thesis are shown correlated with known cuticular lipid genes. Small rank number indicates strong correlation. Large numbers indicate weaker correlation. *LTPG* is strongly correlated with *LACS2* and *ABCG12/CER5*. [a]Correlation values are compared with transcript abundance reported in Suh et al. 2005.

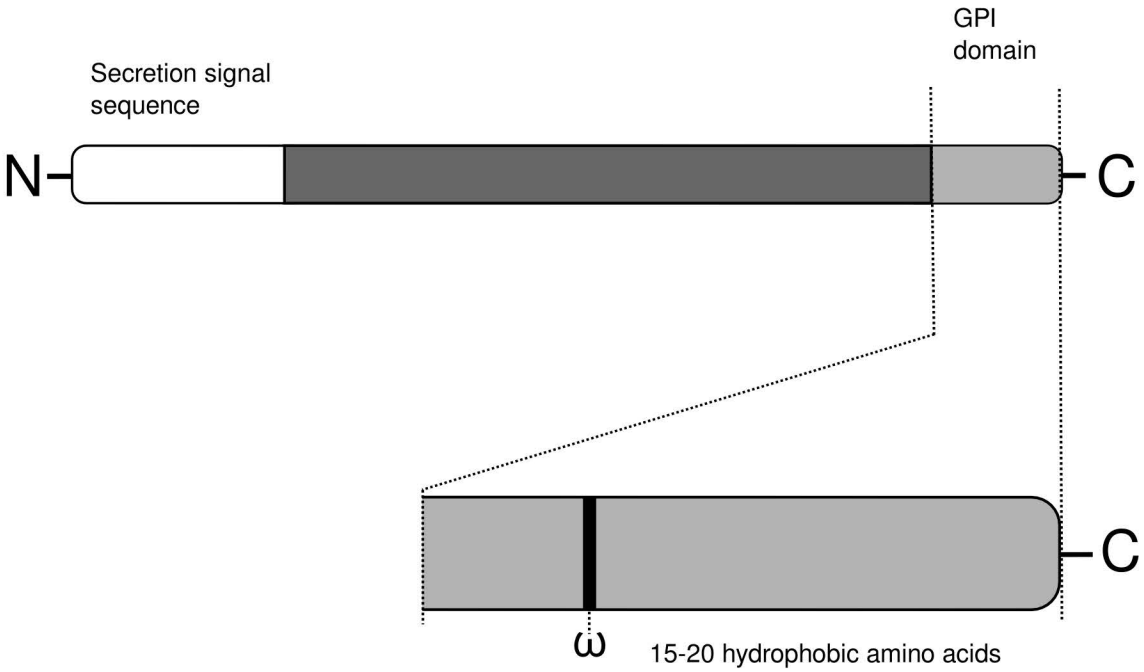

Figure 1-2: Domains of a generic GPI protein. (Top) The amino-terminus contains a secretion signal sequence and the carboxy terminus contains the GPI domain. (Bottom) The GPI domain contains the ω-site or the region to which the pre-made GPI anchor is added. Downstream from the ω is a hydrophobic domain that transiently anchors the protein to the ER prior to GPI linkage.

2. Materials and methods

2.1 Plant materials and growth conditions

All plants used for this study were *Arabidopsis thaliana*, ecotype Columbia-0 (Col-0). Seeds bearing T-DNAs and Arabidopsis BACs were obtained from the Arabidopsis stock center (ABRC; Columbus, Ohio). Seeds bearing RNAi constructs were obtained from the European Arabidopsis Stock Centre (NASC; Nottingham, England). Seeds were imbibed and seedlings were grown for 7-10 days on sterile ½ X MS (2.2 g/L) medium (Sigma-Aldrich) and 0.8-1% agar (Fisher Scientific) supplemented with 1X Gamborg vitamins (Sigma-Aldrich) in 90 mm petri plates. When required for transgenic and/or genotype selection, antibiotics or herbicides were added to the medium as described in Table 2-1. Transgenic plants used for experimentation were from generations T1, T2, and T3. In all cases at least 10 independent lines were examined for transgenics, except for YFP-GPI/line 675. Only 1 transgenic line was recovered for YFP-GPI.

Seedlings were transferred to soil after 7-10 days on medium and fertilized with 20-20-20 mixture (Scotts' Miracle-Gro) according to the manufacturer's recommendation. Plants were grown in Sunshine mix #4 (Sungro) in environmentally controlled chambers under 24 hour fluorescent light with 90-115 $\mu E/m^2$ intensity and 21^oC. Mutant plants and RNAi lines used in this study are listed in Table 2-2. When parasitic insects (Western flower thrips, aphids) were detected in growth chambers, 500 pieces of *Orius* (BioBest n.v.) were added to the affected growth chamber.

2.2 Wax analysis and gas chromatography

Wax was extracted from the surfaces of primary stems when they were 10 to 15 cm in length. All instruments and glassware used to handle, excise, and extract wax from stems were washed in pure chloroform. Buds, flowers and siliques were excised from the main stem. To measure surface area, stems were scanned on a flatbed scanner (8800F; Canon) as color photographs at

300 dpi. Two-dimensional stem areas were then extracted using the color threshold function of ImageJ (Abramoff et al., 2004). To obtain cylindrical surface area, square stem areas were multiplied by π. Next, the stems were immersed for 30 s in beakers containing approximately 20 mL chloroform to which exactly 5 or 10 µg of internal standard, tetracosane (Sigma-Aldrich), had been added. The chloroform-wax solution was allowed to dry in the beakers at room temperature, resuspended in 400 µL of pure chloroform, and transferred to GC vials (Agilent). The 400 µL wax solution was dried under a gentle stream of nitrogen gas with heat (not exceeding 50^{o}C). The dry mixture was derivatized in 10 µL of N, O-bis (trimethylsilyl)trifluoroacetamide (BSTFA) and 10 µL pyridine (Sigma-Aldrich) for 60 to 90 min at 70^{o}C. After this time, each sample was dried under a stream of nitrogen exactly as above. Two different gas chromatographs with flame ionization detectors (GC-FID) were used. The wax analyses of single mutants *ltpg-1*, *At2g15050*, *At3g51600*, *At3g43720* and *At5g59320* were performed with a Hewlett-Packard 6890 GC-FID, with on column injection (Agilent) following the exact parameters described by Greer et al. (2007). One replication of *ltpa* double mutants was performed with an HP6890. All subsequent wax analyses were performed on an Agilent 7890A GC-FID with splitless injection, using an HP-1 column (Agilent, 30 m, 320 µm bore, 0.10 µm film). GC parameters were empirically developed in collaboration with Scott Liang, to achieve an equivalent level of sensitivity and resolution to acquisitions produced on the 6890 system. The injection method was splitless at 300 ^{o}C for GC-FID. At the start of the program, the temperature was 50 ^{o}C for 2 min and then increased at a rate of 40 ^{o}C/min to 200 ^{o}C, held constant at 200 ^{o}C for 1 min, then increased again at a rate of 3 ^{o}C/min to 320 ^{o}C, and finally, held at 320 ^{o}C for 15 min. The carrier gas used for GC-FID was hydrogen. The pressure program used was constant flow at 2 mL/min. The FID detector program was heating at 300 ^{O}C, with hydrogen flow at 30 mL/min, compressed air at 350 mL/min, and helium at 23 mL/min. The initial column pressure was 4.9 psi with H_2 carrier gas flow of 2 mL/min for the first 30 min. After 30 min, the flow was raised to 100 mL/min and over a span of 31.75 min was dropped to 4

mL/min. Total run time was 61.75 min. After automatic peak integration, the amount of each component was determined by comparing the area under its peak compared with the area under the standard, tetracosane peak. To ensure that peaks did not change between the HP6890 and HP7890A, WT Arabidopsis stem wax was processed 10 times during the development of the reported 7890A parameters to ensure consistent analysis. To further verify the protocol, wax standards extracted and obtained from the Kunst lab (Dept. of Botany, UBC) were processed through the 7890A system with the protocol described above to confirm the identity of the peaks. The method described, confirmed the identity of hexacosanol, nonacosan-15-ol, nonacosan-15-one, nonacosane and tricontanal. Wax esters were verified by their characteristic doublet peaks after GC parameters (Jetter et al., 2006). For all GC data, at least 5 individual plants per genotype per biological replicate are shown. One-way Welch ANOVA was performed with JMP versions 7 through 9 to account for values from a given population that deviated from normality. Post-hoc tests were performed with SPSS 16 (SPSS) in order to compare *ltpg-1*, *ltpg-i1*, *ltpg-i2*, and *YFP-LTPG* with the wild type (Col-0). When data displayed significant deviations from normality, Kruskal-Wallis, non-parametric, post-hoc statistical analyses were performed.

2.3 Isolation of mutants

2.3.1 DNA extraction

DNA for genotyping was harvested with Whatman FTA cards (Whatman). All solutions are listed in Appendix A. Young, healthy (not wilted, green, no trauma detectable by eye) rosette leaves from less than 20 day old plants were pressed to FTA cards, overlaid with parafilm and pushed into the FTA card with the conical end of a mini centrifuge tube. FTA-leaf imprints were allowed to dry for a minimum of 60 min prior to processing. The processing of FTA-leaf imprints included cutting a single piece of the FTA-leaf imprint with a single-hole puncher, producing a 5 mm disc that was transferred to a 0.2 mL PCR tube. The disc was washed in FTA

wash solution two times. The disc was then washed in Tris-EDTA (TE-1) solution two times and then dried in a PCR machine, with lid open for 25 min at 60^{o}C.

In order to genotype double and triple *ltp* mutants, a homemade silica column based DNA clean up system was employed. Young leaf samples (approximately 1 cm^{2} square cutting from a healthy leaf), less than 100 mg total mass, were transferred to mini centrifuge tubes in 450 µL of Lysis buffer and 3 steel beads. The tissue was macerated in a TissueLyser (Qiagen) with parameters set to 30 Hz for 1.5 min. Samples yielded inconsistent maceration making it necessary to reorient the mini centrifuge tubes part way through the process to achieve complete maceration. Samples were kept on ice from this point in the protocol onward. Next, samples were heated at 65^{o}C for 10 min and the solution was mixed 2-3 times until the viscosity of the mixture increased (indication of complete lysis). 130 µL of protein precipitation buffer was then added to this mixture. Samples were centrifuged and the supernatant was transferred to clean tubes. All centrifugations from this point were performed for 1 minute at 8000 rpm. The mixture was neutralized by the addition of 1.5 volumes of binding buffer. The DNA was bound to the silica column (Epoch life science) by centrifuging binding buffer/ DNA mixture through the column. This process was repeated until the entire volume of the binding buffer/ DNA mixture was passed through the column. The columns were then washed of residual binding buffer with 500 µL ethanol wash solution. Washing was repeated followed by centrifugation for 2 min at 14000 rpm (~20, 000 k). Columns were dried by centrifugation for 2 min. Samples were eluted in 2 x 55 µL aliquots of Tris-EDTA solution by incubating for 5 min at room temperature followed by centrifugation at 14000 rpm. DNA generated by this method seldom failed when used for genotyping PCRs.

2.3.2 Genotyping PCR

Genotyping PCR was performed using two programs, one using DNA from FTA cards and one using DNA from mutants. As with many PCR parameters, they are highly flexible and can be

altered with changing experimental needs. PCR conditions used in this study are listed in Tables 2-3 and 2-4.

2.4 Electrophoresis

All electrophoresis of nucleic acids was performed in sodium borate buffer (Appendix A; Brody and Kern, 2004). Typical electrophoresis voltages were 180 V for gels smaller than 10 cm; 300 V for gels larger than 10 cm.

2.5 Molecular cloning

All cloning PCRs were performed with Finnzymes Phusion (Finnzymes Oy). Each primer pair described can be found in Appendix C. Cloning PCRs typically followed the recipe of dH_2O, 5X HF, 0.5 µM of sense and antisense primer, 300-500 ng of DNA, 0.2 M dNTPs. Cycling conditions were typically 98^{o}C 60 s; 98^{o}C 15 s; 72^{o}C 30-60 s per kb template.

Plasmid preparation was performed by following a modified protocol of Ebeneezer and Gargamel (1972). *E. coli* clones were grown in 2-5 mL of Luria-Bertani broth and after 16-24 hrs of growth, pelleted by centrifugation for 1 min at 20000 g. The pellet was resuspended by vortexing in 250 µL of cell resuspension solution. The mixture was lysed in 250 µL alkaline lysis solution and mixed gently. Finally the solution was neutralized with 350 µL neutralization solution and placed on ice for 5 min. The mixture was centrifuged for 10 min at 20000 g and the resulting supernatant was passed through a pre-made silica column (Epochlifescience) to adsorb plasmid DNA. The column was washed three times in column wash solution. Finally the column was centrifuged for 2 min at 20000 g to remove residual ethanol contamination. DNA was eluted with 100 µL dH_2O.

Amplicons required for the production of genomic copies of *LTPG* were synthesized from BAC F13K9 (ABRC). The untagged, genomic copy of *LTPG* including 1800 basepairs (bp) upstream of the start translation site and 800 bp downstream of the stop translation site was

produced with primers P3 and P4 and cloned into pUC19. This construct was subcloned into the EcoRI and PstI restriction sites of pCambia1300 (Cambia). In order to create a fluorescent chimera for localization studies, citrine yellow fluorescent protein (YFP) was chosen for acid stability in the cell wall (Griesbeck et al., 2001). YFP-LTPG was created in two fragments (F1 and F2) which resulted in an internal YFP chimera where YFP was fused in frame and downstream of the amino terminal signal sequence. The position to where I cloned YFP was determined with *in silico* tools iPSORT and PrediSi (Bannai et al., 2002; Hiller et al., 2004). These tools were used to predict that the most downstream signal sequence cleavage site was at the carboxy-terminus of amino acid 32, alanine in between sequences ALA | DEC. Fragment one (F1) was amplified from BAC F13K9 with primer P3 and P5, yielding a KpnI-XhoI amplicon containing the promoter (as above) as well as the sequence coding the amino-terminal signal sequence, and introduced into pSTBlue1 (EMD), yielding pF1. Fragment two (F2) was amplified using primers P6 and P7 as an XbaI-PstI amplicon and introduced into pGem3z (Promega), yielding pF2. Citrine YFP was amplified with P8 and P9 as an XhoI-XbaI amplicon and subcloned into pF1 to yield pF1-YFP. F1-YFP was removed as a KpnI-XbaI cassette and subcloned into pF2 to yield the full length YFP-LTPG in pGem3z. The complete construct was subcloned into pCambia1300 (www.cambia.org). Each construct was maintained and propagated from *E. coli* JM109 (Promega) or Top'10 (Invitrogen).

2.5.1 Cloning with pGreen based vectors

The vector pGreenII0229 (Hellens et al., 2000) was used to generate the following constructs where all genes were driven by the 1800 bp *LTPG* promoter described above: secreted citrineYFP (sec-YFP), cytoplasmic citrine YFP (cyto-YFP), YFPLTPA1-omega (YFPLTPAω), YFP-GPI-omega (YFP-GPI). Schematic diagrams of these constructs can be found in Appendix D. These constructs were employed in fluorescence recovery after photobleaching (FRAP) experiments, localization studies and complementation analysis.

2.5.2 Design of pGreen based vectors

2.5.2.1 YFP-GPI

The YFP-GPI construct contained YFP with a GPI domain. It was designed such that the LTPG amino terminal signal sequence was fused in frame with both YFP and the *LTPG* GPI domain. To make YFP-GPI, YFP-LTPG in pCambia1300 was digested with the EcoRI and XbaI to release a cassette at the 5' end, containing the *LTPG* promoter and the 3' end YFP (named Fy). Next, YFP-LTPG in pCambia1300 was used to amplify the LTPG GPI domain with P35 and P4. The *in silico* tool Bigπ was used to determine the position of the ω site (Eisenhaber et al., 2003). Next, employing amino acid sequence alignments with LTPA type LTPs, the sequence was examined for a region upstream from the ω site that did not correspond to the fourth LTPG alpha helix. The amino acid sequence that was downstream of the fourth alpha helix and upstream of the ω site was taken to be unstructured region of the GPI domain (Orlean and Menon, 2007). The analysis showed that the region from amino acid P151 to the stop translation site was required. This region was amplified from YFP-LTPG plasmid with primers P35 and P7. These primers also conferred the native transcription termination sequence. The P35-P7 amplicon was digested with XbaI and PstI and doubly ligated to Fy and EcoRI and PstI digested pGreenII0229 yielding proLTPG::YFP-GPI.

2.5.2.2 Secreted YFP

Secreted YFP (sec-YFP) was designed to yield free YFP secreted by the *LTPG* amino terminal signal sequence. The construct sec-YFP was generated with two independent PCRs that were simultaneously ligated to pNOS. Using the YFP-LTPG plasmid as template, the sequences corresponding to the *LTPG* promoter, amino terminal signal sequence and YFP were cloned using P41 and P44. These oligonucleotides introduced EcoRI and SpeI restriction sites. This amplicon was cloned into the EcoRI and XbaI restriction sites of pNOS. The construct pNOS bears the nopaline synthase transcription terminator from pMDC32, provided by Dr. Ben

Blackman (Curtis and Grossniklaus, 2003) cloned into the restriction sites XbaI and SacI (DeBono & Rieseberg, unpublished).

2.5.2.3 Cytoplasmic YFP

Cytoplasmic YFP (cyto-YFP), whose expression was driven by the *LTPG* promoter, was designed as a control protein in the cytoplasm lacking LTPG or the GPI domain. The construct cyto-YFP was generated using two independent PCRs followed by simultaneous ligation of two amplicons into the pNOS vector. The *LTPG* promoter was amplified from the plasmid YFP-LTPG using P41 and P37 (the latter was phosphorylated). *YFP* was amplified from the same template using primers with P45 and P44. The primers introduced start and stop translation sites. The *LTPG* promoter and *YFP* amplicons were ligated to one another and to the pNOS vector in the EcoRI and XbaI sites in a single step ligation yielding *proLTPG::YFP*

2.5.2.4 YFP-LTPA1ω

YFP-LTPA1ω bears the promoter and GPI domain of *LTPG* cloned in frame with YFPLTPA1/ At2g15050. Using genomic DNA as template, the promoter of LTPG was amplified with P25 and P36 and cloned into pGreenII0229. The LTPG GPI domain was amplified from YFP-LTPG template using P31 and P32, introducing restriction sites BamHI and SpeI. This amplicon was cloned into pGreenII0229, yielding p3'GPI-domain. LTPA1 containing the region just downstream of the amino terminal signal sequence, up to the stop translation site, was amplified with P29 and P30, bearing PstI and BamHI. This amplicon was cloned into p3'GPI-domain. YFP was amplified with P27 and P28 and subcloned into sites EcoRI and PstI site in p3'GPI-domain. The LTPG promoter was amplified with P41 and P37, yielding an EcoRI, blunt-ended amplicon. The 5' portion of LTPA1 containing the amino terminal signal sequence was amplified with P38 and P26 and ligated with the latter and p3'GPI-domain to yield the *proLTPG::YFP-LTPAω.*

2.5.3 Introduction of constructs into Arabidopsis

Plasmids based on the Cambia vectors were transformed into *Agrobacterium tumefaciens* GV3101 bearing helper plasmid pMP90. Plasmids based on pGreenII were introduced into GV3101 bearing mutually compatible plasmids pMP90 and pSOUP (Hellens et al., 2000). The constructs sec-YFP, cyto-YFP and YFP-GPI were introduced into WT Col-0. All other constructs were introduced into the *ltpg-1* mutant background. The floral dip technique was used to introduce all constructs described above into Arabidopsis (Clough and Bent, 1998).

2.6 Tissue handling and staining for confocal microscopy

Arabidopsis inflorescence stem tissues were excised from plants with a single sided razor and transferred to a sheet of dental wax (Ted Pella) for further processing. Transverse cuts were used to remove non target growth such as siliques, flowers, and buds. The cut/razor damaged end was hydrated with a drop of water placed on the dental wax while further cutting was performed. Less than or equal to 1 cm of tissue was imaged at a given time. Typically the area within 1 cm of the floral apex was imaged unless otherwise indicated.

Stains and / or chemicals were often unable to penetrate fresh stem tissue. This is likely due to two plant properties: 1. the hydrophobicity of the cuticle and 2. air spaces in the photosynthetic cortex. To avoid penetration problems I devised a centrifugation method to stain tissue with dyes and / or inhibitors. Cut pieces of stems were placed in 0.2 mL centrifuge tubes and centrifuged at less than 100 g in order to overcome the airspaces in tissues. Stem tissue that required staining and/or incubation in an inhibitor was incubated for 15 to 20 min and imaged immediately.

Tissues were stained with the following working dye concentrations and time durations: 10 µM FM4-64 (Invitrogen) for 15 to 30 min; 1.5 µM propidium iodide (Sigma) for 15 to 30 min;

and 1.6 µM hexyl rhodamine B (Sigma) for 10 min. All stock solutions were made up in dH_2O except for FM4-64 which was dissolved in HPLC grade DMSO (Sigma).

2.7 Confocal microscopy

Fluorescent proteins and dyes were imaged with laser scanning and spinning disk confocal systems. The laser scanning systems used were the Pascal LSM5 and Meta LSM510 (Zeiss). The spinning disk systems used were the Quorum WaveFX spinning disk system (Quorum technologies) and a Perkin Elmer UltraViewVox (Perkin Elmer). Both spinning disk systems were attached to DMI6000B inverted microscopes (Leica Microsystems). All light paths and typical settings are described in Appendix B.

2.7.1 Fluorescence recovery after photobleaching

Fluorescence recovery data was acquired with an UltraviewVox spinning disk confocal system (Perkin Elmer) using Volocity 5.2-5.5 software (Improvision). The light paths and filters used were identical to those presented in Appendix B, except the imaging parameters were modified in order to reduce photobleaching and minimize saturated pixels. The laser output for this system was determined in the summer of 2010, after 18 months of laser usage, using a standard low digital light meter (model PM100 – Thorlabs) through a 10X air objective (Leica). The following values of irradiation used during acquisitions represent the maxima needed to excite the dimmest fluorescent protein tagged individuals. The amount of irradiation, during the acquisitions for the 'GFP' or 488 nm laser diode line was less than or equal to 0.2 mW or approximately 10% using the laser intensity slider in the Volocity software. For 'YFP,' or the 514 nm laser diode line, the irradiation was less than or equal to 0.1 mW or less than 10% using the Volocity slider software.

FRAP acquisition parameters were as follows: The objective used was 63X (Leica) with numerical aperture 1.2, water immersion optics. The camera exposure settings were 240 ms with

pixel sensitivity set to 255 or maximum. The laser intensity was 6% to acquire pre and post bleach images. Fluorescent proteins were bleached with 70% laser intensity, repeated for 30-50 cycles, each lasting 10 ms. This paradigm produced a laser bleaching duration of 0.4 – 0.5 sec. Using the settings shown above, pre-bleach images were acquired for 10 s in real time. Images were captured for 60 – 80 sec at a rate of 1 image per sec. Pre-bleach images were captured for 10 sec at a rate of 5 sec per timepoint. Photobleaching was performed using an UltraVIEW PhotoKinesis module. Recovery images were captured for 60 sec at a rate of 1 sec per time point. A single bleaching event was performed in a given field of cells.

During the acquisition process expansion or flexion of the specimen may cause undesired shifts in the plane of focus. In order to maintain stability of tissue specimens during image acquisition, coverslips were affixed to the slide with molten wax (Fisher Scientific).

2.8 Heterologous expression of LTPG

In order to assay the *in vitro* function of LTPG, a recombinant protein engineering approach was taken. Recombinant LTPG (rLTPG) was expressed in both *Pichia pastoris* (Invitrogen) and in an *E. coli* BL21DE3 derivative, Rosetta-gami (EMD). Since LTPG contains alpha helix structure that is bridged by disulfide bonding, I judged that a eukaryotic expression system would be most appropriate to express this protein. I also used a modern, protein folding optimized, *E. coli* to express the protein.

2.8.1 Design and expression of recombinant LTPG in *Pichia pastoris* X-33

Two versions of rLTPG were created. The versions of LTPG were produced such that one lacked the GPI-domain and the other lacked the amino terminal signal sequence and carboxy-terminal GPI-domain. To achieve this, WT (Col-0) RNA (Lai et al., 2006) was used as template to generate two cDNAs with the described domain deletions. Primers P51 and P52 were used to create the former and primers P53 and P52 were used for the creation of the latter. The

P51-52 and P53-52 amplicons were cloned into the EcoRI and XbaI sites of the pPICZ vectors (Invitrogen). The P51-52 amplicon was cloned into pPICZB. The P53-P52 amplicon was cloned in to pPICZαC. These commercially available vectors have a multiple cloning site in frame with c-myc and hexa-Histidine (Invitrogen). Approximately 20 µg of each plasmid, pPICZB-delta-omega and pPICZB-deltaNTSS-delta-omega were harvested from *E. coli* and linearized overnight with restriction enzyme BstXI. Once complete vector linearization was achieved, the vectors were transformed into electro-competent *P. pastoris* for homologous recombination into the *P. pastoris* AOX1 locus. The production of electro-competent *P. pastoris* and subsequent transformation of vectors was carried out exactly as described by Cregg (Cregg, 2007). Recombinant *P. pastoris* cells were selected with antibiotic zeocin (100 mg/mL; Invitrogen).

Twelve zeocin resistant clones (six expressing each construct) were selected for small pilot expression studies. These clones were grown in rich YPD media (Ausubel et al., 1987) for 24 hrs, separated from media by centrifugation and washed with sterile dH_2O. The pellets resulting from centrifugation were cultured in 20 mL of BMMY (Invitrogen) containing 0.5% methanol to induce protein expression. Recombinant protein levels, recovered from clones after 113 hours of culture, were estimated and compared using 10% SDS PAGE (Ausubel et al., 1987). Gels were soaked in dH_2O for 15 min to remove SDS and stained with Coomassie brilliant blue (Ausubel et al., 1987). Gels were typically destained for 2 to 4 hours. Proteins were transferred to nitrocellulose membranes (Hybond; GE Healthcare), soaked with Western transfer buffer, using a semi-dry transfer apparatus (Biorad) at 130 mA for 1.5 hours. After protein transfer, membranes were blocked with TBST with 5% powdered milk (Carnation) for 30 min at room temperature inside a sealed sandwich bag. The membrane was washed three times in TBST in the same way. Primary α-c-MYC antibody (9E10, Santa Cruz Biotechnology) at a concentration of 1:20,000 for 60 min was used to detect tagged rLTPG. The membrane was washed three

times, as above, and incubated with secondary α-mouse IGG-alkaline phosphatase (Sigma Aldrich) diluted to 1:5,000 for 60 min. After washing the membrane, as above, the alkaline phosphatase was incubated with 1:1600 NBT/BCIP (Sigma Aldrich) in alkaline phosphatase buffer.

2.8.2 Expression of recombinant LTPG in *E. coli*

The biosynthesis of rLTPG in *E. coli* was the joint effort between myself and Dr. Trevor Yeats of the Rose lab at Cornell University. To express rLTPG in *E. coli,* an *LTPG* cDNA lacking both signal peptide and C-terminal GPI domain was produced by PCR with primers P10 and P11. The resulting amplicon was cloned into EcoRI and XhoI restriction sites of pGEX5-1 (GE Healthcare) and transformed into *E. coli* (Rosetta-gami; EMD). The cells were started in a 50 mL overnight culture. Next, the cells were transferred to 1 L of LB medium supplemented with 0.5% glucose and ampicillin (resistance conferred by pGEX5-1). The culture was grown to OD600 of 0.5 and induced with 0.1 mM isopropylthio-b-galactoside (IPTG) for four hours. The cells were then passed through a chilled french press to ensure lysis. The resulting lysate was harvested using GSTtrap columns (GE Health care) and polished to homogeneity as described (DeBono et al., 2009).

Table 2-1: Selective agents used to select transgenic plants generated for this study

Selective agent used in planta	Concentration (mg/mL or mM*)
Kanamycin (Kan)	30
Hygromycin (Hyg)	25
Phosphinothricin (PPT, crystalline)	7.5 - 10
Basta/Finale® (liquid suspension)	200- 300*

*200 mM was the preferred concentration when Ti vectors were smaller than 6000 bp to avoid selecting multi-insertion transgenics.

Table 2-2: T-DNA and RNAi lines used in this work

Gene	Locus identifier	Polymorphism
ltpg-1	At1g27950	SALK_072495
ltpgi-1	CATMA1a26130*	N290585
ltpgi-2	CATMA1a26130*	N290585
ltpa1	At2g15050	SALK_139292
ltpa8	At3g51600	SALK_03906, SALK_104674
ltpa13	At5g59320	SALK_038887, SALK_09524
ltpe23	At3g43720	SALK_100010, SALK_06947

© DEBONO ET AL., 2009 THE PLANT CELL

Table 2-3: Genotyping PCR conditions Salk T-DNA and AGRIKOLA lines

Step	Temperature (^{o}C)	Time (sec)/Repeat
1	94	120
2	94	45
3	55	45
4	72	120
5	-	Go to step 2, 39 times
6	72	300

Table 2-4: Touch Down PCR conditions for double and triple mutant genotyping.

Step	Temperature (°C)	Time (sec)/Repeat
1	94	120
2	94	30
3	62	20/1°C per cycle
4	72	120
5	-	Go to step 2, 14 times
6	94	30
7	50	20
8	72	120
9	-	Go to step 6, 26 times
10	72	300

3. Arabidopsis LTPG is a glycosylphosphatidylinositol-anchored lipid transfer protein required for export of lipids to the plant surface

3.1 Synopsis

The objective of the work described this chapter was to isolate Arabidopsis *LTP* genes whose mutants showed differences in total stem wax load and/or composition. Of seven candidates, mutation in a single LTP, *LTP Glycosylphosphatidylinositol anchored, LTPG,* had altered stem wax composition and reduced total load. The *ltpg* mutant had a 30% reduction in stem cuticular wax load, due to a 40-50% reduction in nonacosane (29 carbon) content. This phenotype was reproduced using RNAi lines directed against the LTPG transcript. Expression of fluorescent protein tagged and non-tagged LTPGs, driven by the native promoter, the *ltpg* mutant phenotype was rescued. The YFP-tagged LTPG was used for localization studies. YFP-LTPG has two localizations, one at the plasma membrane and one in the cell wall. This was determined by making comparisons with markers of the plasma membrane, cell wall and an engineered, cell wall directed, acid stable, YFP. Examining the localization over the course of development revealed that YFP-LTPG was found in expanding, cuticle depositing areas of the stem. Finally, using a heterologous expression system, it was shown that LTPG possesses a hydrophobic binding cavity.

3.2 Identification of candidate *LTP* genes highly expressed in the epidermis

Approximately 70 LTPs or LTP-like proteins are annotated in the Arabidopsis genome (Beisson et al., 2003). As described in Chapter 1, sequence analysis reveals that the genes encoding 70 LTPs within this gene family lack primary sequence homology (Figure 1-1). This family size made it unfeasible to screen the entire family of LTPs. Instead, a cuticular lipid gene microarray was used to search for LTPs whose expression was higher in the epidermis than the whole stem (Suh et al., 2005). This microarray narrowed the number of candidates by identifying transcripts enriched in expanding, cuticle depositing regions of the stem.

To reduce the list of candidate LTPs to under ten, I chose LTPs whose level of transcript in the epidermis peeled from the stem top was enriched by greater than or equal to 1.5 times compared to the remainder of the stem. This criterion yielded the LTPs At1g27950 (LTPG), At2g15050 (LTPA1), At3g51600 (LTPA8), and At3g43720 (LTPE23). At3g59320 (LTPA13) was chosen despite displaying a lower level of enrichment but displayed very high expression, 25% higher than the next, best expressed LTP mRNA. The expression of the LTPs studied in this work is listed in Table 3-1.

3.3 Isolation of epidermis-enriched *ltp* mutants

Homozygous T-DNA insertional mutants were obtained for each gene of interest. In the case of *ltpg-1/At1g27950*, only a single T-DNA insertion line existed in the Col-0 ecotype at the time of characterization. The *ltpg-1* T-DNA was detected 889 base pairs downstream from the start translation site, in the single intron of *LTPG*. To make up for the lack of alleles available, I chose to characterize RNA interference (RNAi) expressing plants from the AGRIKOLA consortium (Hilson et al., 2004). These plants are engineered to impair *LTPG* by using the constitutive cauliflower mosaic virus promoter, *35S*, to drive the expression of sense and antisense 100-400 bp DNAs that span intron-exon junctions called 'gene-specific tags' (GSTs). GSTs were designed to form a stable hairpin loop that is processed by the post-transcriptional gene silencing machinery resulting in RNAi (Allen and Howell, 2010). The 3' ends of the GSTs are fused to the *Flaveria PDK* intron (sense GST) and the castor bean *CAT* intron (anti-sense GST) (Hilson et al., 2004).

3.4 *ltpg-1* mutant has reduced cuticular wax

A goal of this chapter was to determine the chemical phenotype of *ltpg-1* mutants in detail. Gas chromatography with flame ionization detection (GC-FID) analyses was performed. Specifically I wanted to know whether cuticular wax was reduced compared with WT and whether this reduction was due to the absence of a specific compound. Using standard PCR methods,

homozygous *ltpg-1* T-DNA insertional mutants were detected and isolated. Similarly, RNAi or *ltpgi* lines were isolated after herbicide selection (Basta) and PCR. GC-FID was used to compare the wax composition of *ltpg-1*, *ltpg-i1* and *ltpg-i2* mutants with WT (Col-0) stems (Figure 3-1). When *LTPG* is disrupted by a T-DNA insertion or by RNAi, the stems of such mutants display 40-50% lower alkane content, resulting in an overall decrease of 30% wax when compared to WT plants grown in parallel (Figure 3-1). This decrease in alkanes is a result of reduced nonacosane levels (29 carbon alkane; Figure 3-2). The single T-DNA insertion, *ltpg* was almost perfectly phenocopied by RNAi lines *ltpg-i1* and *ltpg-i2* providing good evidence that impairment of the *LTPG* locus was responsible for the observed phenotype.

3.5 The wax of *ltpg-1* is restored by transgene complementation

Since the phenotype of *ltpg* was phenocopied by the *ltpgi* transgenics, I tested whether the expression of a cloned, genomic copy of *LTPG* could complement the observed phenotype. To achieve this, I generated two constructs for complementation testing (restoration of alkanes and total wax). Both constructs were driven by the native *LTPG* promoter cloned using the sequence 1800 base pairs upstream of the start translation site. One construct was an exact genomic copy (including the intron) of LTPG (proLTPG::LTPG) and the other was a genomic copy of LTPG with YFP fused internally (proLTPG::YFP-LTPG), downstream of the nucleotide sequences corresponding to the amino-terminal secretion signal (NTSS; shown in Appendix D). Both constructs were introduced into the *ltpg-1* genetic background.

Of the twelve proLTPG::YFP-LTPG individuals screened (T1), individual 30 appeared to produce fluorescence that was easily imaged and had restored wax levels. Individual 30 was used to breed homozygous seed stocks 507 through 510 (T3). Examination of the stem cuticular wax of proLTPG::YFP-LTPG; *ltpg-1* plants showed that the construct restored the wax load and alkane to 100% of wild-type levels (Figure 3-3). Twelve independent lines displayed similar, statistically significant levels of complementation. Furthermore, all twelve individuals displayed

identical localization: strong fluorescence was associated with the periphery of stem epidermal cells (described in Section 3.6).

Chemical analysis of the stem wax showed that transgenics expressing the exact genomic copy of LTPG, proLTPG::LTPG, were fully complemented. The amount of wax and alkane was restored to the stem surfaces in six independent transformants expressing *proLTPG::LTPG* in the *ltpg-1* background (Figure 3-4). Most individuals expressing *proLTPG::LTPG* were able to restore more than 100% of the alkane to the surface. This result was expected since the original *ltpg-1* T-DNA mutant was a partial loss of function and the effect of having the endogenous and introduced copy in the plant genome may have caused some over-expression.

3.6 YFP-LTPG is localized to the plasma membrane and cell wall

Using laser scanning and spinning disk confocal microscopy, proLTPG::YFP-LTPG appeared to localize to the periphery of epidermal cells, possibly the plasma membrane. Counter-staining stem epidermal cells with the plasma membrane and endocytic vesicle stain FM4-64 showed coincident localization between this dye and YFP-LTPG (Figure 3-5 A-F). Observation of secant planes through the midline of epidermal cells showed colocalization with FM4-64 and not the cell wall stain propidium iodide (Figure 3-5 G-I, I inset). When z-stacks of epidermal cells were reconstructed to reveal the orthogonal view, the outside face displayed accumulation in the cell wall (Figure 3-5 A inset). These results indicated that the observable pool of YFP-LTPG was composed of a plasma membrane-localized population as well as a cell wall-associated or -localized population.

Some yeast GPI proteins are known to localize to both the plasma and the cell wall as observed for YFP-LTPG (Caro et al., 1997; Frieman and Cormack, 2003). To better understand the observed localization, examination of z-series or three-dimensional reconstruction of serial optical sections was performed (Figure 3-6 A,C,E). The serial optical sections showed that, in

addition to plasma membrane localization, YFP-LTPG was found in the cell wall subtending the cuticle but excluded from the primary cell wall. This finding was verified by comparison of YFP-LTPG localization pattern with an engineered secreted YFP (Figure 3-6). Moreover, YFP-LTPG accumulated over anticlinal cell walls, over the middle lamella (Figure 3-6 E). One explanation for these results was that the hydrophobic cuticle may impart changes to the path and trajectory of light emitted from plasma membrane-localized YFP-LTPG causing light scattering or reflective artifact. To examine this hypothesis, I examined the localization of secreted YFP (secYFP) to the cell wall (Figure 3-6 B, D, and F). This gene product directs entry to the protein secretory pathway through an amino terminal signal sequence and is driven by the LTP promoter (Appendix D), eliminating potential disparities between non-equivalent promoters. Exactly as observed for YFP-LTPG, secYFP accumulated in the apoplast over the middle lamella of anticlinal cell walls (Figure 3-6 F). Unlike YFP-LTPG, secYFP does not have a plasma membrane-localized population that may contribute to refraction and or reflection, making it highly unlikely that the cell wall localization observed in YFP-LTPG is due to optical distortions imparted by the waxy cuticle. Taken together these results indicate that YFP-LTPG localizes to both the plasma membrane and cell wall.

3.6.1 YFP-LTPG is found in expanding regions of the stem

The epidermal cells of rapidly expanding stems are under developmental pressure to deposit a waxy cuticle (Suh et al., 2005; Kunst and Samuels, 2009). Since the absence of LTPG resulted in reduced wax on the surface of stems, I examined whether YFP-LTPG was localized to regions of stems undergoing rapid expansion. To this end, I examined three regions of the stem, relative to the floral apex: 1. 0-1 cm; 2. 2-3 cm; 3. 4-7 cm (Figure 3-7). As suggested by the *ltpg-1* phenotype, YFP-LTPG was localized primarily to the areas of the stem undergoing rapid expansion (Figure 3-7A). The localization in the youngest region of the stem containing the least expanded epidermal cells showed that YFP-LTPG was associated with the endomembrane

system as well as the plasma membrane (Figure 3-7A'). This may reflect a phase of rapid YFP-LTPG biosynthesis or the endomembrane system is more pronounced in unexpanded cells. Once epidermal cells became more mature or became more expanded (2-3 cm from the floral apex), the YFP-LTPG fluorescence was mostly associated with the periphery or plasma membrane (Figure 3-7B). The region 4-7 cm from the floral apex containing fully expanded cells was a transition zone (Figure 3-7C). In this area of the stem, YFP-LTPG was still strongly expressed but expression ceased 5-7 cm from the floral apex. There was variability as to where the fluorescence of YFP-LTPG was terminated within this 5-7 cm zone. In all individuals examined, no fluorescence was observed farther than 7 cm from the floral apex. These results suggest YFP-LTPG expression is necessary when epidermal cells are rapidly expanding and not in fully expanded cells of mature stems.

3.7 A recombinant LTPG has a hydrophobic cavity

The functional characteristic of LTPs is thought to be the presence of a hydrophobic cavity that binds lipophilic cargo (Kader, 1996; Yeats and Rose, 2008). Such LTP cavities have been shown to bind cargo as large as prostaglandin B_2 (Tassin Moindrot et al., 2000) suggesting a great deal of torsional flexibility in the hydrophobic cavity and increasing the likelihood of binding large substrates like nonacosane. To test lipid binding, I expressed a recombinant LTPG (rLTPG), which lacked both the NTSS and hydrophobic transmembrane or GPI-domain. My first choice of recombinant protein expression systems was *Pichia pastoris*. *Pichia* is a methylotrophic yeast; subsisting on sugars and/ or methanol (Daly and Hearn, 2005; Cregg, 2007). The usage of methanol as a food substrate provides an experimental tool for Pichia protein expression because linearized constructs can be driven by the strong, methanol-inducible, AOX1 promoter after integration into this locus (Daly and Hearn, 2005). Unique to Pichia is the inability to ferment sugars to toxic ethanol, allowing growth at extremely high density, large biomass and theoretically greater amounts of desired recombinant protein (Cregg, 2007).

Proteins can be fused to the α-factor signal secretion sequence. By taking advantage of the mating α-factor secretion signal sequence, Pichia protein expression vectors allow the direction of fusion proteins into the culture medium, facilitating protein purification (Cregg et al., 1993; Cregg, 2007). These properties also make fermentation in bioreactors possible, and have been employed to generate functional, single-chain antibody fragments (Fischer et al., 1999). Moreover, Pichia has eukaryotic protein folding and glycosylation that has been used widely to express proteins that may have multiple cysteine bonds and resultant folding patterns (*e.g.* snake venom protein, hook-worm antigen and human α-amylase (Rydberg et al., 1999; You et al., 2004; Goud et al., 2005). As well as containing 8 conserved cysteine residues, my sequence analysis of LTPG shows two N-glycosylation sites at amino acid sequence LHNAS and TNNAT, determined by the *in silico* tool, NetNGlyc (Julenius et al., 2009). Some LTPs are *bona fide* glycoproteins (Motose et al., 2004). In light of the eight-cysteine motif/four disulfide bridges and potential glycosylation, I chose to use the *Pichia* expression system.

3.7.1 *Pichia* expressed rLTPG is hyperglycosylated

The rLTPG protein was expressed in Pichia using both pPICZalpha to direct secretion into the culture medium and pPICZ to express the protein with the native amino terminal secretion signal sequence. Pilot expression studies indicated that the protein was detected by Western blotting after 72 to 96 hrs of methanol induction. I used a c-myc antibody in order to detect the myc epitope fused to rLTPG. The pPIC vectors fuse c-myc in frame to recombinant proteins (reviewed in Pelengaris et al., 2002). Pichia is not known to express any proteins resembling the proto-oncogene, c-myc. The expected masses of the protein generated in pPICZalpha and pPICZ were 19 kD each. Western blots using anti-c-myc antibody (Pelengaris et al., 2002) revealed that rLTPG was detected as multiple proteins ranging in mass from 50 – 80 kD (Figure 3-8, lanes 2 and 3). Western blots of protein harvested from untransformed or empty vector control Pichia

displayed no anti-c-myc cross-reactivity (Figure 3-8, lane 1). These results suggested that the rLTPG was becoming post-translationally modified, acquiring a larger than predicted mass.

Since rLTPG was directed through the secretory system and yeasts may hyperglycosylate proteins, I hypothesized that rLTPG became hyperglycosylated. Therefore I treated these protein fractions with EndoH, which cleaves high mannose residues from asparagines (Alberts et al., 2002). Treating rLTPG fractions with PNGase resulted in a reduction of mass from 50- 80 kD to approximately 20 kD (Figure 3-8, lanes 5 and 6). At this point, the *Pichia* system was abandoned because of concerns with altered solubility of the protein and possible obstruction of the putative hydrophobic cavity by glycosylation. As a result of removing the GPI domain, N residues became proximal to the opening of the hydrophobic. Glycosylation may have obstructed the opening of the hydrophobic core. In collaboration with Drs. Trevor Yeats and Joceyln Rose, I next tried an *E. coli* protein expression system. I engineered rLTPG to be expressed without the domains from the NTSS and from the GPI-domain as above for Pichia. The resulting construct was introduced into *E. coli,* Rosetta-Gami (Novagen/EMD). This bacterium is genetically altered to yield codons optimized for eukaryotic protein expression.

3.7.2 Expression of rLTPG in E. coli and binding assays

In order to probe the lipid binding capacity of LTPG, the rLTPG was used as an analogue. I reasoned that the functional region of LTPG was the four alpha helices held in proximity by the 8 cysteine-motif. No evidence existed that the NTSS or GPI domain were responsible for lipid binding. When rLTPG was expressed and purified from *E. coli.,* SDS-PAGE showed an 18 kD band corresponding to rLTPG (Figure 3-9 A). A minor product was detected at approximately 9 kD. This may have been a decomposition product resulting from purification of the protein.

To determine if LTPG possesses a hydrophobic binding cavity we used the electrical potential probe, 2-(p-toluidinyl) naphthalene-6-sulfonic acid (TNS; Wang and Edelman, 1971). TNS is non-fluorescent in aqueous solution but becomes fluorescent once transferred to a hydrophobic

environment (*e.g.* a solution or region of protein). When rLTPG was mixed with TNS, fluorescence intensity increased steadily as TNS was titrated up to 25 µM (Figure 3-9 B, circles). This result indicates that rLTPG, and LTPG by structural analogy, possesses a hydrophobic cavity. Since a 10 kD protein contaminant was observed by SDS-PAGE, further testing was required. I reasoned that a protein with multiple disulfide bonds should lose activity once in a reducing, denaturing environment. The TNS assay was repeated after rLTPG was treated with Urea and dithiothreitol to denature the protein and reduced disulfide bonds (Figure 3-9 B, squares). Binding activity was abolished after this treatment suggesting that the TNS binding protein isolated possesses cysteine bonding, sensitive to a reducing environment.

3.8 Discussion

The results presented in this chapter indicated that LTPG is involved directly or indirectly in the movement of cuticular wax (DeBono et al., 2009). When *LTPG* expression is disrupted by T-DNA mutagenesis and RNAi, a reduction in stem cuticular wax is observed. This reduction is due to reduction in the major alkane, nonacosane. This result is unexpected for a single LTP given that at least 70 non-specific LTPs exist in the Arabidopsis genome (Beisson et al., 2003). The relative amount of alkane was altered, but not total cuticular wax, was reported by Lee and coworkers using a different T-DNA allele of *LTPG* (Lee et al., 2009). An explanation for their result is that Lee and colleagues used a Syngenta SAIL line, which was generated in the Col-3 background (http://arabidopsis.info/CollectionInfo?id=94). However, recent evidence shows that significant genetic differences are accrued between ecotypes and within an ecotype (Clark et al., 2007). Such differences may impact on transcriptional networks involved in cuticular wax deposition, which could alter the manner by which individuals interact and perceive their environments. Transcriptional networks are known to have an influence on the biosynthesis and deposition of cuticular lipids (Aharoni et al., 2004; Broun et al., 2004; Zhang et al., 2005; Raffaele et al., 2008). My own observations, and those of Kosma (Kosma et al., 2009), of

Arabidopsis grown with and without water deficit indicate differences in the amount of soluble wax. The interaction of altered genotype and environment may result in alterations in amounts of cuticular wax observed by Lee et al., (2009).

YFP-LTPG has a dual plasma membrane and cell wall localization pattern, indicating that this protein resides in the correct cellular domain to function as a component of the cuticular wax transport machinery. The presence of YFP-LTPG at the plasma membrane is not surprising given that it is a GPI protein. Dupree's group, in their pioneering global proteomics studies isolated Arabidopsis GPI proteins from callus tissue with phospholipase C (Borner et al., 2003) and it was also identified in detergent resistant fractions of plasma membranes (Borner et al., 2005).

The presence of LTPG at the plasma membrane may allow coordination with other proteins via lipid rafts. Since LTPG, through GPI-linkage, contains uncharacterized lipid tail, it may confer association with detergent resistant membranes or lipid rafts (Borner et al., 2005; reviewed in Lingwood and Simons, 2010). An examination of proteins isolated by Borner shows that *bona fide* wax-related ABC transporters were not found in detergent resistant membranes from callus tissue (Borner et al., 2005) but it is not known if they were expressed in those cells. The relationships between lipid rafts and protein function are being identified. ABCB19 was found to be associated with lipid rafts and to contribute to the function of the PIN1 polar auxin transport (Titapiwatanakun et al., 2009). The REMORIN protein, a lipid raft resident protein of *Solanacae* with several uncharacterized homologues in Arabidopsis, is known to alter the pathogenicity of *Potato virus X* (Raffaele et al., 2009), suggesting that lipid raft proteins can influence the path of movement of microorganisms and possibly macromolecules such as waxes. These studies suggest that stabilization or interaction of proteins and association with lipids may provide a vehicle to export or import biomolecules or microbes in plant cells. It is possible then that the GPI-domain, by associating with as yet unidentified proteins in lipid rafts, is responsible

for the observed wax export defect in *ltpg-1* individuals. Indeed human pathogenic bacterium *Aeromonas hydrophilia* co-opts host GPI proteins (Abrami et al., 2000). *Aeromonas* forms an interaction with host GPI mannose residues (NB: these are membrane proximal) to gain entry to host cells (Abrami et al., 2000). Coxsackie virus is a picoRNA virus, responsible for meningitis and myocarditis. It uses well characterized GPI protein decay accelerating factor (DAF) to gain entry into host epithelial cells (Shieh and Bergelson, 2002; Marsh and Helenius, 2006). The virus then crosslinks itself to DAF, gaining entry to lipid rafts and concomitantly activating raft associated kinases. The kinases rearrange the cytoskeleton allowing injection of viral RNA (Coyne and Bergelson, 2006; Marsh and Helenius, 2006). These data are exciting given that recent work on Arabidopsis Formin1, a cytoskeletal protein, indicates that there exists an intimate connection between cytoskeleton, plasma membrane, and cell wall (Martinière et al. 2011). These researchers show, using fluorescence recovery after photobleaching, that when the cell wall is removed from the cell environment, membranes proteins become more mobile. Given that viruses are known to co-opt GPI proteins and that there appears to be a direct link between the cytoskeleton and the cell wall, it is possible then, that plants may use, in contrast to viruses endocytosed into cells, an exocytosis based method for exporting complex biomolecules such as cuticular waxes.

This hypothetical model can integrate well into the popular, ABC transporter-requiring paradigm (discussed in Kunst and Samuels, 2009). ABC transporters extruding cuticular lipids are met by GPI LTPs representing the first biomolecule exchange, with the net effect of moving lipid cargo toward the cell wall. Next, the cargo may be passed on to LTPA type LTPs. Somerville and others hypothesize a model where LTPs, presumably of the LTPA type, consistently cycle between plasma membrane and cell wall (Somerville et al., 2000). The fundamental problem with their model is the lack of control, given that wax deposition is developmentally coordinated (Suh et al., 2005). Given that that LTPG participates in wax export

and is GPI-linked, I have refined this model. It is known that GPI linkage can confer the localization of proteins to nanospaces named lipid rafts or detergent resistant membranes (Bhat and Panstruga, 2005). In my refined model, I hypothesize that GPI-linked LTPs interact with arabinogalactan proteins (AGPs; Figure 3-10). AGPs are small, GPI-linked peptides that are heavily glycosylated and, as a result of the large arabinogalactan oligosaccharides that they contain, are primarily carbohydrate by mass (Seifert and Roberts, 2007; Ellis et al., 2010). AGPs may structure the extracellular environment for the LTP in the region between the plasma membrane and cell wall. They may interact with portions of the cell wall, creating a functional continuum between the cell wall and plasma membrane. In so doing, organizing AGPs could cordon an area of the plasma membrane, to associate tightly with the cell wall. Within this area, the GPI-linked LTP could exchanges its cargo with a soluble LTP (LTPA). This model, however, does not account for the data showing LTPG in the cell wall environment. Removal of LTPG from the plasma membrane may be coordinated by phospholipases (Borner et al., 2003).

GPI proteins, especially in yeasts, are known to localize to the plasma membrane and/ or, the cell wall (Orlean and Menon, 2007; Kinoshita et al., 2008). Most GPI proteins in *Saccharomyces* (yeast) are known to be cell wall proteins (Frieman and Cormack, 2004). The default path of the yeast GPI protein is the cell wall where it is thought to cross-link with the cell wall environment (Frieman and Cormack, 2004). Of the few Arabidopsis GPI proteins studied, only COBRA appears in hypocotyl epidermal cell wall (Roudier et al., 2005). Somerville's group showed, using plasmolysis, that root epidermal cell GPI protein SKU5 is associated with the plasma membrane and cell wall (Sedbrook et al., 2002). By comparison with secreted YFP, my results show that LTPG is present in both the plasma membrane and the cell wall. An interesting observation from studying secYFP, and similarly YFP-LTPG, is the apparent movement of protein through the region corresponding to the middle lamella of cell walls. These data closely match the results presented for LTP1 and WAX9 (Thoma et al., 1993; Pyee et al.,

1994; Thoma et al., 1994). The YFP-LTPG that is not associated with the plasma membrane appears abundant in middle lamella region as well. The localization of a synthetic protein, with no defined biological role, such as secYFP and of YFP-LTPG, suggests that middle lamella region of the cell wall is an exit point from cells. Electron microscopical examination of epidermal cells from different plant species indicates that the middle lamella is highly osmiophilic or rich with lipids (Pyee et al 1994; Jeffree, 2006). Perhaps the involvement of LTPG in wax movement, and its localization to the cell wall as well as its osmiophilic nature of the middle lamella region of the cell wall may be a path through which lipids are moved out of the cell. This idea is supported by the fact that LTPG is not polarly localized as is the case for mammalian GPI proteins (Orlean and Menon, 2007; Kinoshita et al., 2008).

Whether LTPG moves lipids directly or indirectly is not clear according to my data. Its localization to the cell wall and its capacity for binding the lipid probe TNS is intriguing. My data suggest that the LTPG structure possesses a hydrophobic cavity. This hydrophobic cavity may bind lipidic cargo like nonacosane molecules extruded from epidermal cell membranes by ABC transporters. The *ltpg* phenotype predicts the lipid carried by LTPG would be nonacosane. With the TNS assay, it is possible to test lipid specificity using a loss of fluorescence displacement assay. However, I was unable to test the binding of nonacosane to LTPG, due to the technical difficulty associated with solubilizing such long hydrocarbons. If a solvent exists that can maintain the native folding of LTPG, and solubilize nonacosane, I would predict that the hydrophobic cavity could accommodate this molecule. Testing the ability of LTPG to bind short chain lipids such as stearate (Zachowski et al., 1998) would provide little more information than identifying the presence of a hydrophobic pocket with TNS. My data show that the LTPG cavity is required for TNS binding activity, as reduction of disulfide bonds conferred by cysteines abolishes activity. Similarly, a tobacco LTP involved in cell expansion was identified and required native disulfide bonding to maintain its function based on the protein's ability to induce

expansion of cucumber hypocotyls *in vitro* (Nieuwland et al., 2005). This study suggests the possibility for an LTP to possess cell wall modifying properties (Nieuwland et al., 2005). With respect to the observation of LTPG in the cell wall, perhaps this represents a cell wall population of LTPG and/or others, among the annotated GPI LTPs that become integrated into the cell wall via glycosylation, creating a proteinaceous, lipid trafficking tunnel, without going through the primary cell wall. Perhaps the observed cell wall localization is indicative of an LTPG population that modifies the cell wall while a plasma membrane population may deal with lipid traffic. This idea is not supported by the *ltpg-1*, phenotype which bears no obvious changes from normal growth and development that would indicate cell wall defects. However, approximately 70 LTPs exist and functional redundancy may mask or make subtle interesting single gene phenotypes.

The experiments performed in this chapter implicate LTPG in wax export. The reduction in cuticular wax in *ltpg-1* mutants in addition to the presence of LTPG at the plasma membrane and cell wall places the protein in the right domain of the cell to perform wax export. The GPI domain of LTPG is energetically expensive and requires multiple coordinated steps (Orlean and Menon, 2007). This post-translational modification is likely to have an impact on function *in vivo*

Table 3-1: Listing of LTPs studied for this thesis work with transcript enrichment data from an epidermis microarray.

	EXPRESSION[a]	
ACCESSION NUMBER	AVERAGE TOP EPIDERMIS[a]	TOP EPIDERMIS: TOP STEM[a]
At1g27950/LTPG	11826.85	3.79
At2g15050/LTPA1	18269.60	4.29
At3g43720/LTPE23	13127.35	3.22
At3g51600/LTPA8	28334.75	2.75
At5g59320/LTPA13	38084.70	1.61

[a]Raw data from Affymetrix Arabidopsis microarray produced and reported by Suh et al. (2005) Plant Physiol. 139: 1649-1665.

© DEBONO ET AL., 2009 THE PLANT CELL

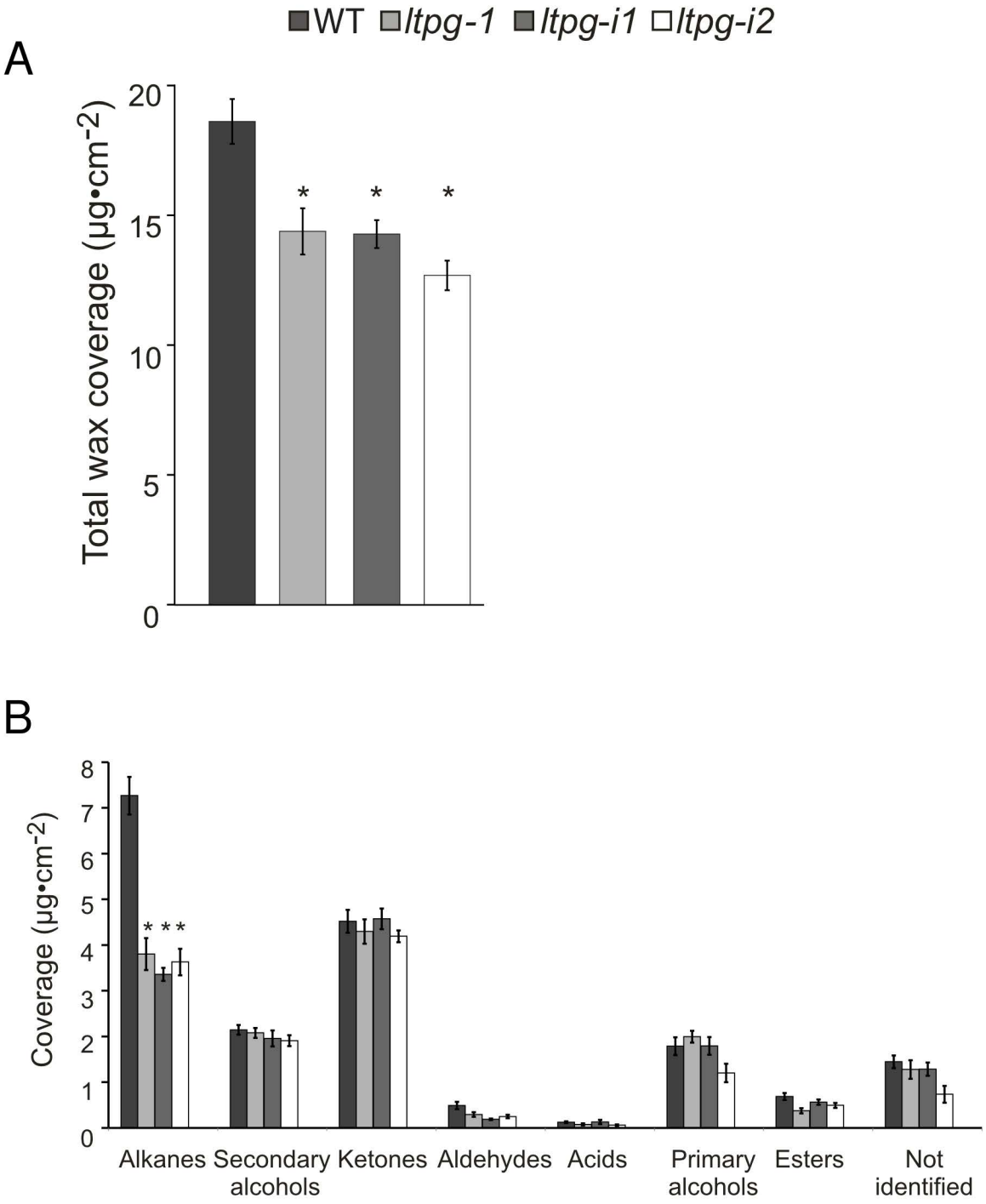

Figure 3-1: Gas-chromatography analyses of soluble cuticular waxes. (A) Stems of *ltpg-1* mutants and RNAi transgenics (*ltpgi1* and *ltpgi2*) display reduced cuticular wax. (B) The observed reduction in wax is a result of reduced alkanes. n = 10. * indicates difference from WT by ANOVA. $P < 0.01$. Three biological replicates are shown.

© DEBONO ET AL., 2009 THE PLANT CELL

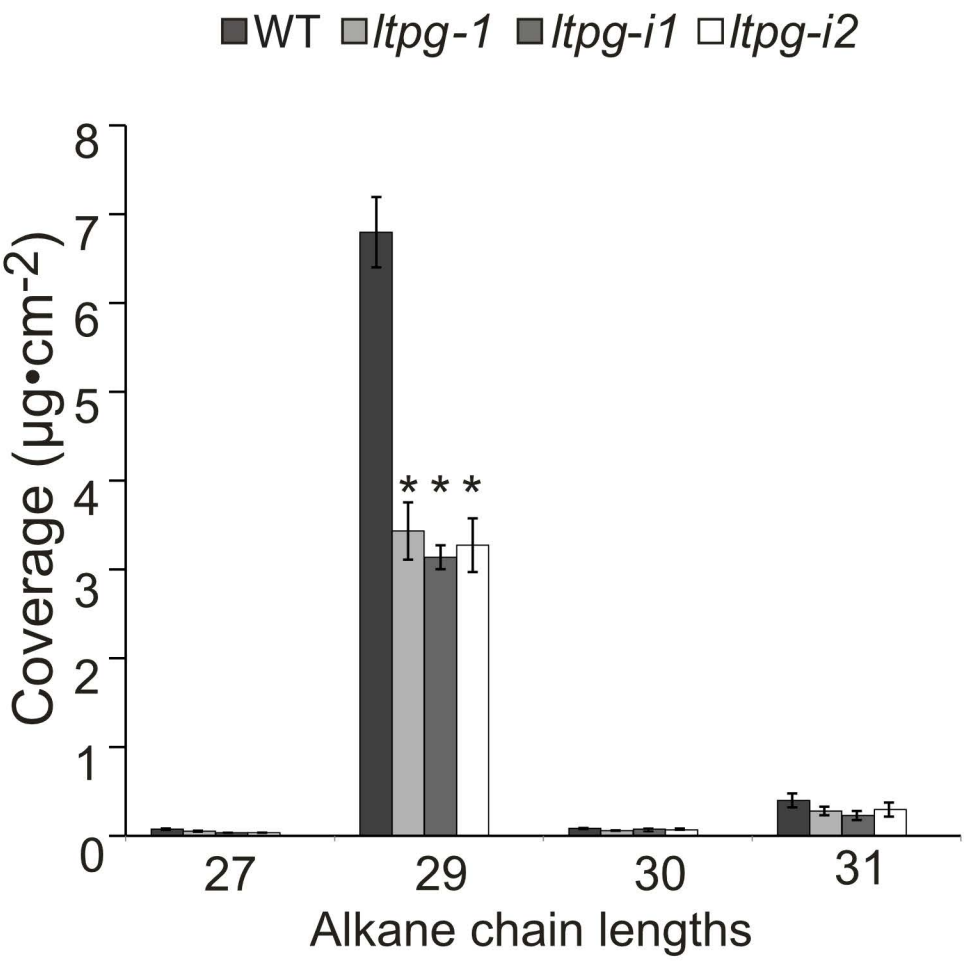

Figure 3-2: Gas chromatography analysis of alkane chain lengths. Nonacosane or the 29-carbon long alkane is reduced compared with WT. No significant differences in the other alkanes are observed. ANOVA $P < 0.01$. $n = 10$. Three biological replicates are shown.

© DEBONO ET AL., 2009 THE PLANT CELL

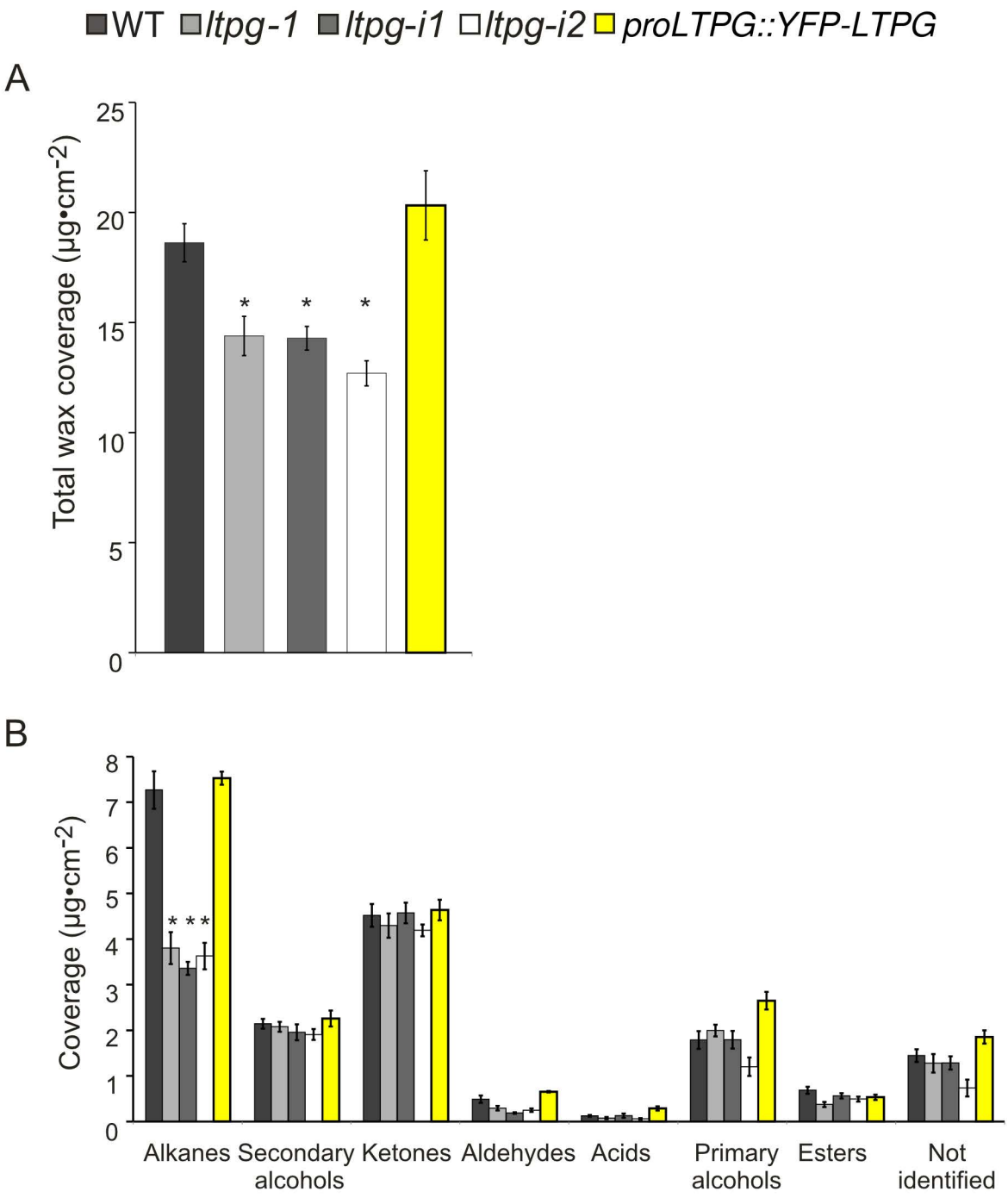

Figure 3-3: Complementation by *proLTPG::YFP-LTPG* of the *ltpg-1* stem wax deficiency. (A) When a genomic copy of LTPG is internally tagged with YFP and expressed under the control of the LTPG promoter, wax is restored to *ltpg-1* stems. ANOVA $P < 0.01$ (B) The *proLTPG::YFP-LTPG* transgenic individuals have alkane amounts that are indistinguishable from WT. ANOVA $P < 0.01$. n=10. Three biological replicates are shown.

© DEBONO ET AL., 2009 THE PLANT CELL

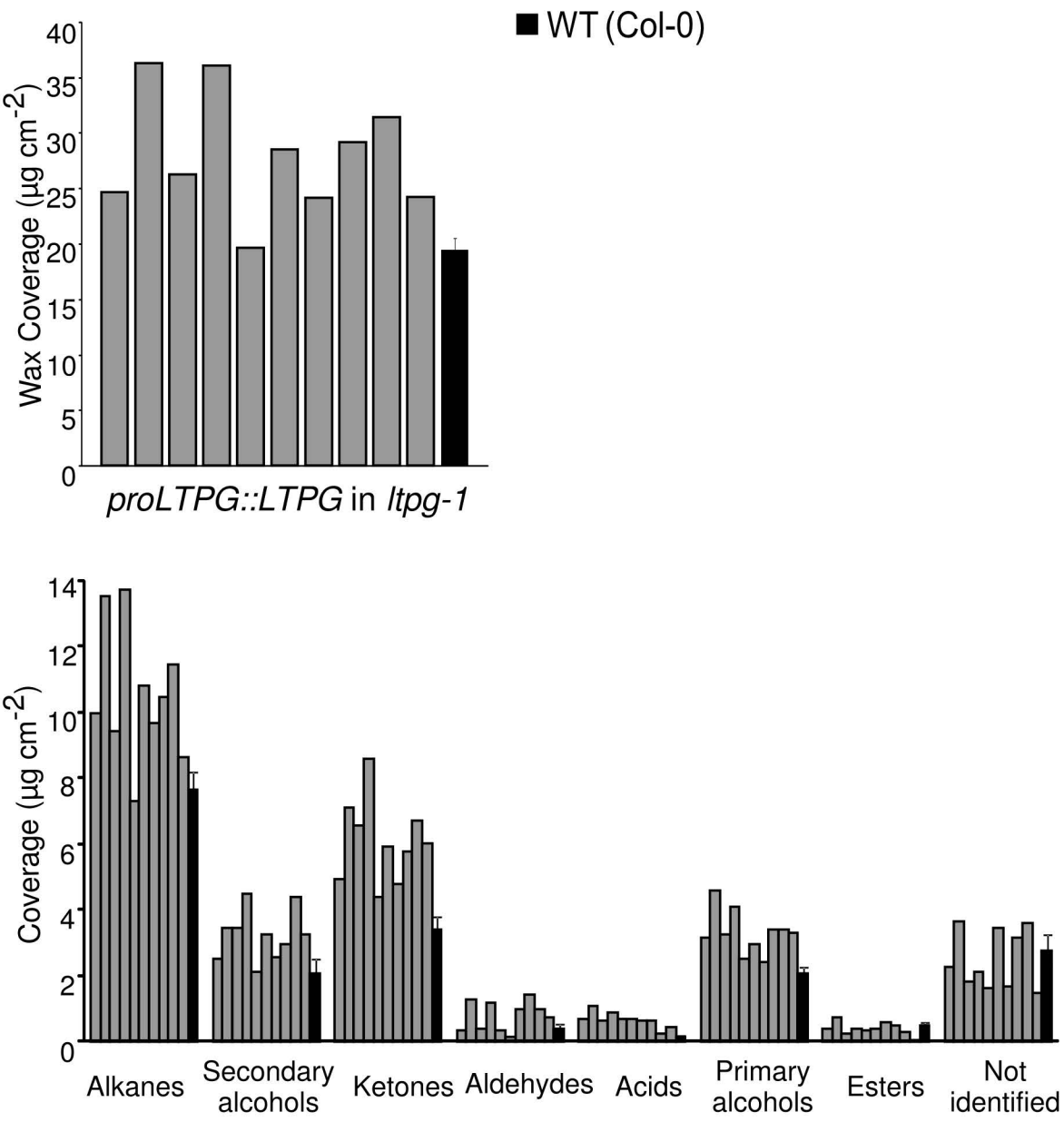

Figure 3-4: Native promoter driven, non-epitope tagged LTPG rescues the *ltpg-1* wax phenotype. The total cuticular wax extracted from primary inflorescence stems of ten individual plants expressing the native promoter driven *LTPG* in *ltpg-1* mutants (grey bars) and WT (Col-0; black bar). Complemented plants have restored wax (A) and alkane levels (B) compared to WT. For WT mean with SE is shown. n=6.

© DEBONO ET AL., 2009 THE PLANT CELL

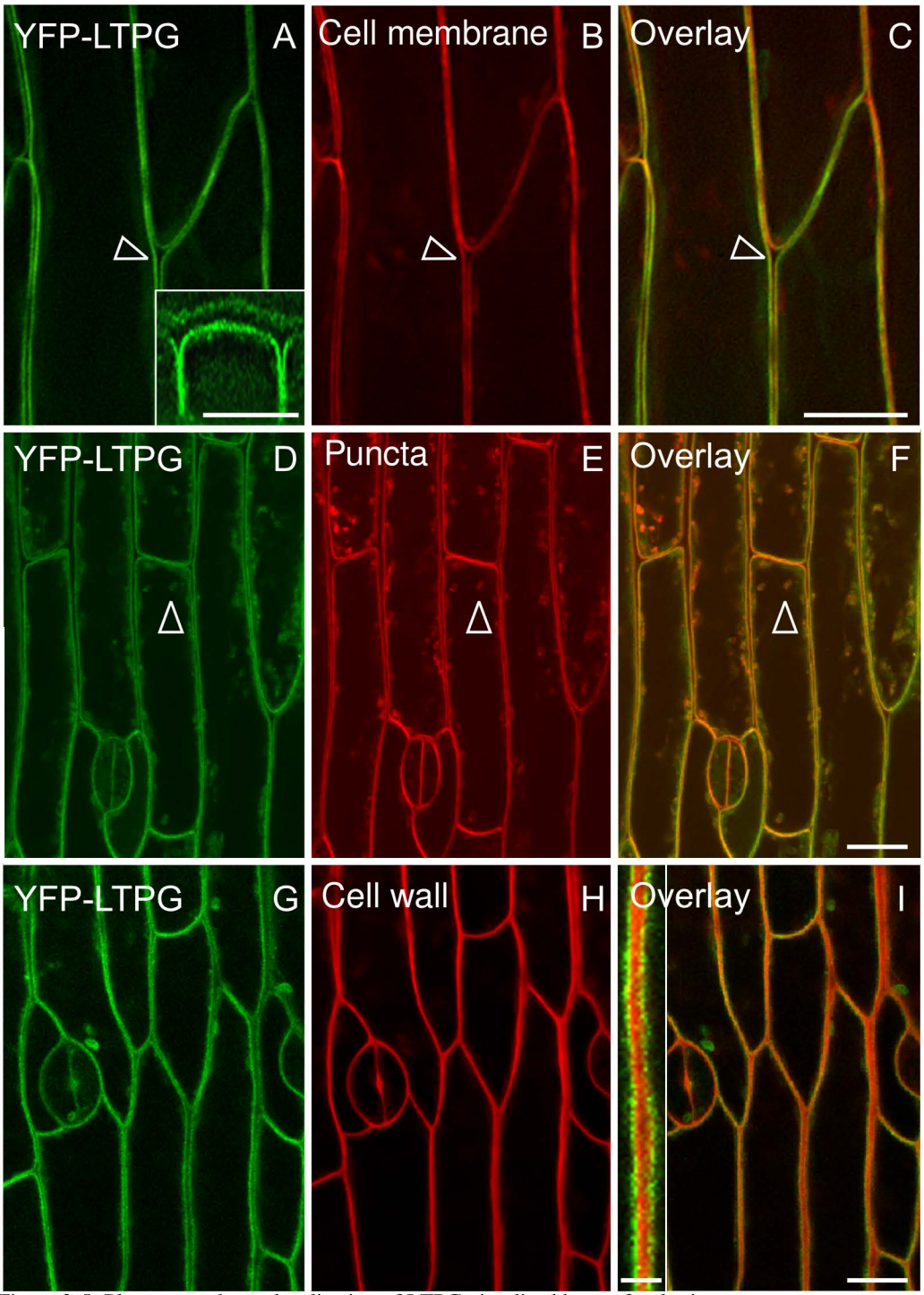

Figure 3-5: Plasma membrane localization of LTPG visualized by confocal microscopy.
(A) YFP-LTPG is observed at the plasma membrane (arrow heads). (A, inset) XZ plane indicates YFP-LTPG is present in the cell wall near the cuticle. (B) Cell membranes of epidermal cells stained with FM4-64. (C) YFP-LTPG colocalizes with cell membranes stained with FM4-64. (D) During late cell expansion, YFP-LTPG is found in puncta throughout the cytoplasm (arrow heads). (E) Epidermal cells stained with FM4-64 showed puncta, indicating endocytosis of FM4-64. (G) YFP-LTPG. (H) Cell walls stained with propidium iodide. (I) Overlay of G and H. (I, inset) YFP-LTPG is not coincident with the cell wall. Scale bars 10 μm. Inset A,8 μm. Inset I 2.5 μm.

© DEBONO ET AL., 2009 THE PLANT CELL

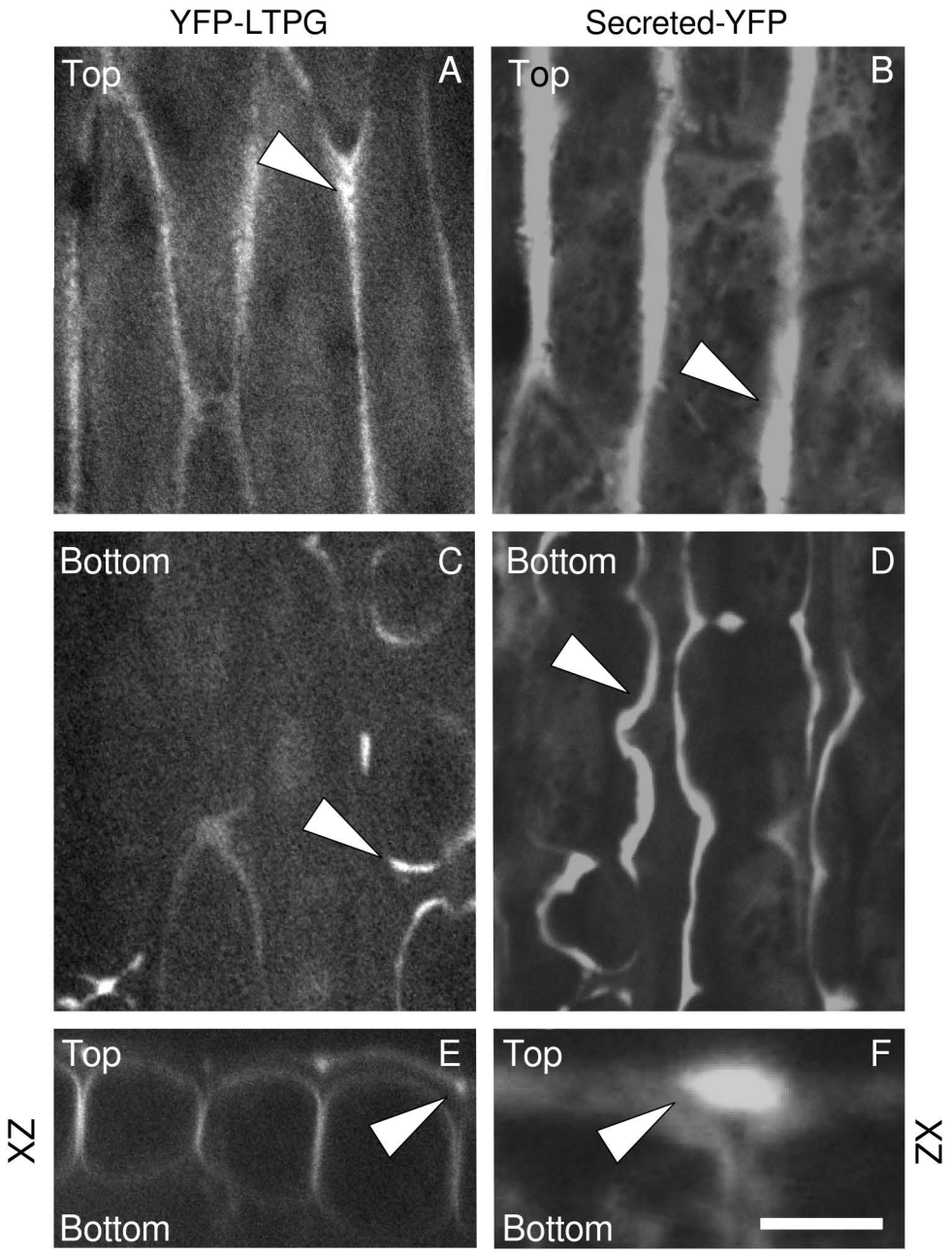

Figure 3-6: Comparison of YFP-LTPG cell wall localization with secreted-YFP. Each pair of images compares equivalent optical slices (A-D). YFP-LTPG (A,C,E) and sec-YFP (B,D,F) are shown. Top indicates the outside face of stem epidermal cells, facing the cuticle. Bottom indicates the inside face of epidermal cells, facing the cortex. Panels E and F compare the XZ planes or collection of optical sections. Open arrows in each image displays accumulation of YFP-LTPG or secreted-YFP. The accumulation of each fluorescent chimera appears most intense over the junctions between two epidermal cells (E, F). Bar = 10 μm

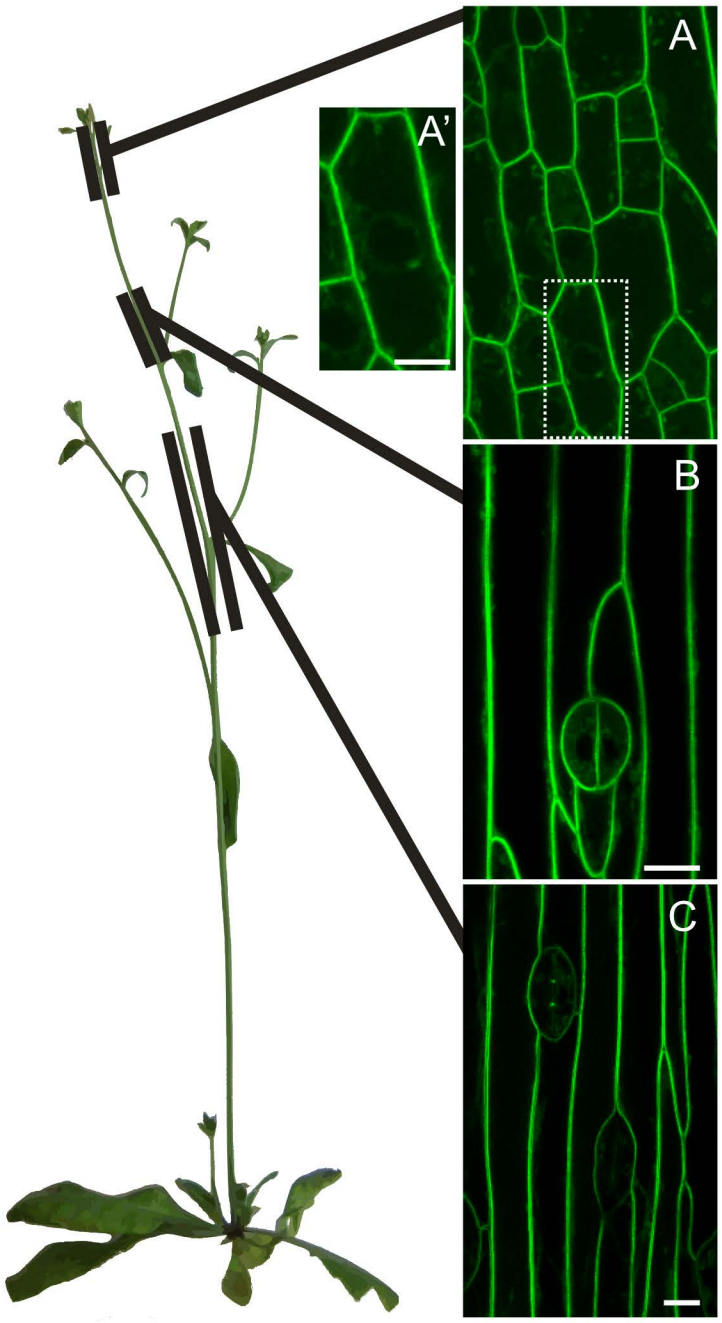

Figure 3-7: Localization of YFP-LTPG over the length of the Arabidopsis stem shows high expression in regions of rapid expansion. (A) 0-1 cm from the shoot apical meristem: Fluorescence was found at the plasma membrane with some internal localization (A') Inset shows YFP-LTPG in the interior of immature cells, in perinuclear distribution and puncta resembling endomembranes. (B) 2-3 cm from the shoot apex: YFP-LTPG signal was localized to the plasma membrane. (C) 4-7 cm: In mature cells localization was also primarily at the plasma membrane. Scale bars 10 μm. Inset 14 μm.

© DEBONO ET AL., 2009 THE PLANT CELL

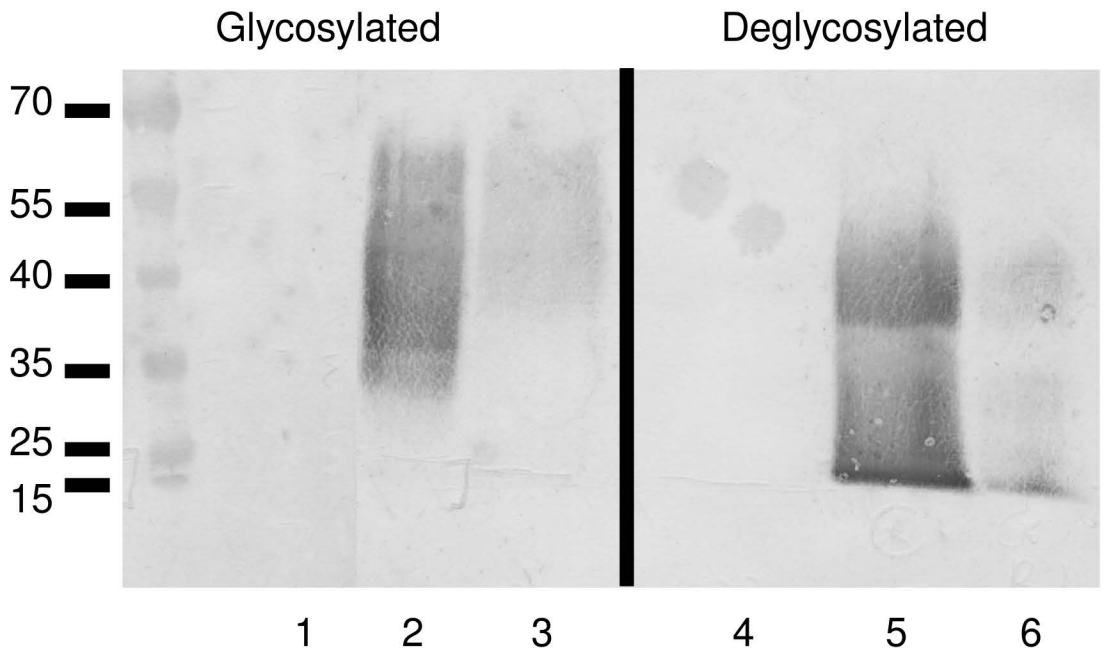

Figure 3-8: Western blot detecting *Pichia* X-33 expressed recombinant LTPG with α-c-myc. Equal amounts of filtered media loaded. Lane 1: Wild type. Lane 2: α-factor-rLTPG. Lane 3: rLTPG using native amino terminal signal secretion sequence. Lanes 4-6 exactly as lanes 1-3 except each fraction is treated in parallel with mannosidase (500 U PNGase). Molecular mass markings in kD are shown.

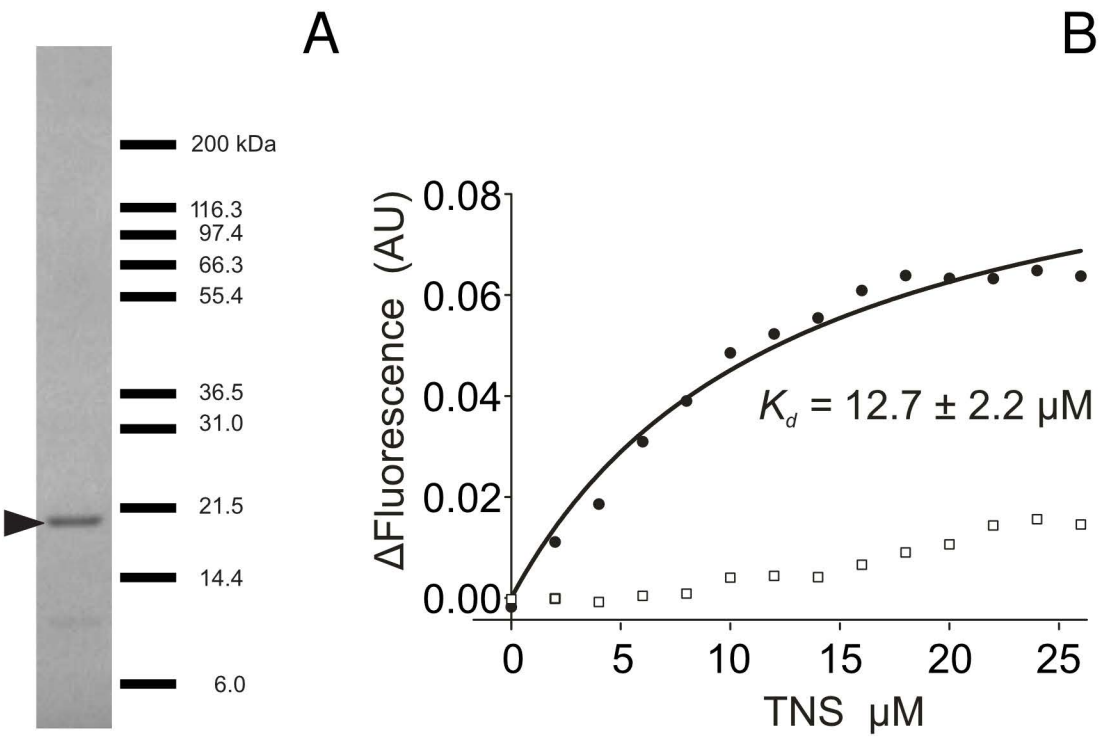

Figure 3-9: Recombinant purified LTPG binds lipophilic probe TNS. (A) SDS-PAGE of recombinant LTPG fraction used for binding studies. An 18 kD band corresponding to recombinant LTPG was observed (arrow head). (B) Recombinant LTPG was engineered to resemble the mature processed protein by omitting the amino terminal signal secretion sequence and GPI domain, then purified following overexpression in *E. coli*. Recombinant LTPG was incubated with increasing concentrations of 2-p toluidinonapthalene-6-sulfonate (TNS), and exhibited saturation binding defined by Kd = 12.7 ± 2.2 μM (circles). No saturation binding was observed (squares) if the protein was denatured by boiling in a solution of 6 M urea and 200 mM DTT.

© DEBONO ET AL., 2009 THE PLANT CELL

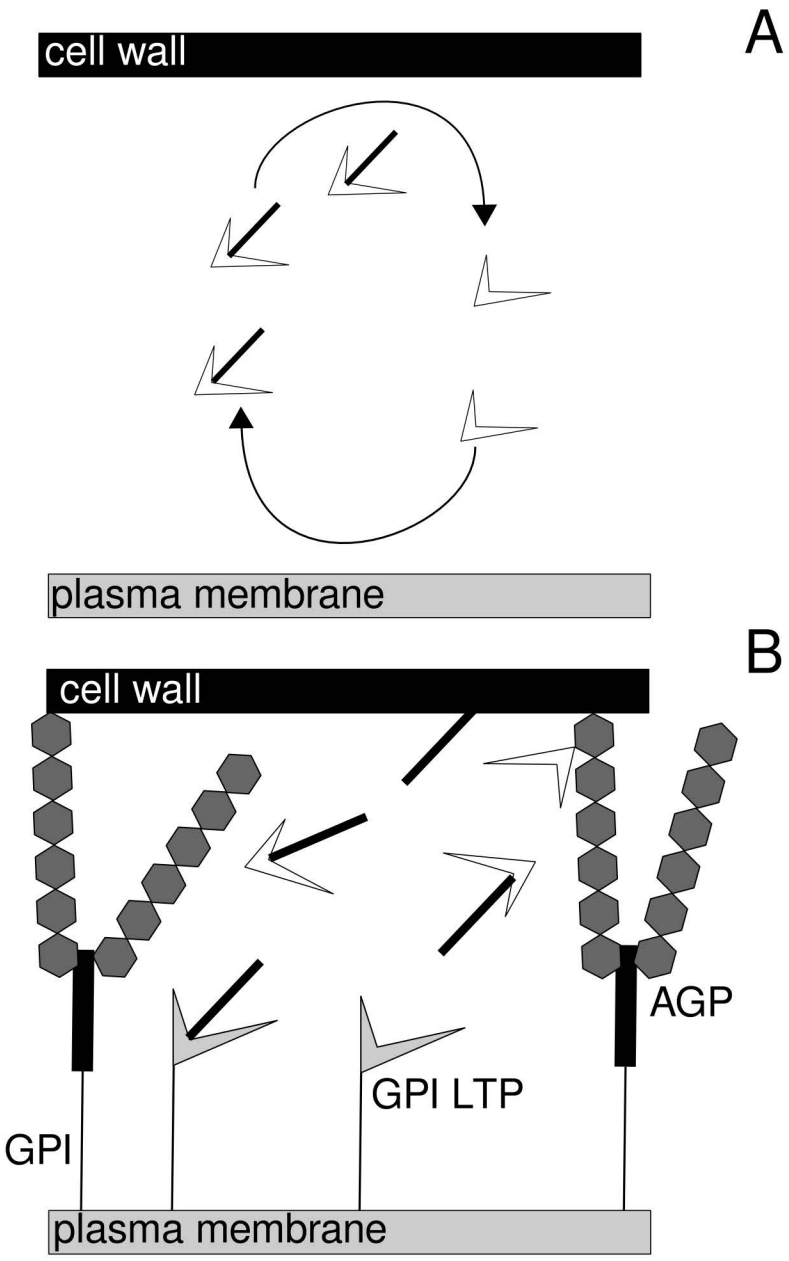

Figure 3-10: Proposed model describing functional interactions of AGPs, LTPG and LTPAs. (A) Somerville's model (modified from Buchanan et al., 2000) displays LTPs (white triangles) as shuttles cycling between the plasma membrane and the cell wall, carrying lipidic cargo (thick black line). LTPs are free to float in all directions. The shuttle model uses a GPI LTP as the first portion of the lipid relay from the plasma membrane into the apoplast (grey triangle & thin black line). AGPs organize the extracellular space by glycosylation (grey hexagons). LTPs are restricted in their degree of mobility about the apoplast increasing the chance that they will encounter a wax donating GPI LTP or a recipient area in the cell wall/cuticle interface. (B)

4. *LTPA* double and triple mutants do not have altered stem cuticular wax

4.1 Synopsis

The aim of the experiments presented in this chapter was to test if soluble cell-wall LTPs (non-GPI-linked), which are strongly expressed in the epidermis, are required for wax export to the cuticle. These LTPs included At2g15050, At3g51600, and At5g59320. Chemical analysis of stem cuticular wax harvested from LTP mutants revealed that the wax phenotypes of single mutants in the top three LTP candidates were indistinguishable from wildtype (DeBono et al., 2009). This observation led to the second objective of this thesis chapter. What is the role of LTP functional redundancy in wax export? Since 70 LTPs are annotated in the Arabidopsis genome, I expected some functional redundancy. Of the LTPs expressed in the epidermis, I define a subtype of Arabidopsis LTPs as 'A-type LTPs.' To test the role of functional redundancy, I generated higher order mutants: double and triple mutants, and performed chemical analyses on their soluble cuticular waxes. The wax loads of the double and triple mutants were statistically indistinguishable from the wax loads of wild-type stems.

4.2 Bioinformatics and definition of A-type LTPs

The microarray upon which this study is based (Suh et al., 2005) identifies strongly upregulated LTPs in the epidermis of Arabidopsis stems, correlated with cell expansion and associated cuticle deposition. My phylogenetic analysis of LTPs shows the existence of a subtype of LTPs that cluster together or are different from the remainder of annotated LTP genes (Figure 4-1). I define these as the A-type LTPs because their kind were the first LTPs reported and characterized structurally (Shin et al., 1995; Gomar et al., 1996; Lee et al., 1998; Charvolin et al., 1999; Tassin Moindrot et al., 2000). Historically, LTPs reported in the literature (Thoma et al., 1993; Pyee et al., 1994; Chae et al., 2009) fall into the LTPA subtype. Using the *in silico* tool Bigπ, the soluble or A-type LTPs investigated in this chapter are not expected to be tethered to the PM by GPI-linkage (Eisenhaber 2003; Table 4-1, *bold face*). LTPAs are reported in

Arabidopsis, broccoli, barley, gingko, maize, rice, sunflower, and wheat. The functions of LTPAs are enigmatic because they display wide substrate binding promiscuity and appear associate with many biotic phenomena (*e.g.* defense response, fertility, drought ; Molina and Garcia-Olmedo, 1997; Regente and De La Canal, 2000; Cameron et al., 2006a; Isaac Kirubakaran et al., 2008; Sawano et al., 2008; Yeats and Rose, 2008; Chae et al., 2009; Edstam et al., 2011).

Similar to LTPG, the LTPAs bear an eight cysteine motif common to all LTPs and LTP-like proteins (Jose-Estanyol et al., 2004). LTPAs are smaller than LTPG, the only LTP implicated in wax export. LTPAs are 100-120 amino acids in length with masses of 9-10 kD versus 193 amino acids or approximately 20 kD for LTPG. This discrepancy is partially owed to the different carboxy-terminus, the carboxy-terminus of each LTPA bears no detectable GPI-linkage motif (Eisenhaber et al., 2003). They represent excellent candidates for participation, with LTPG, in the wax export machinery. They are found in the cell wall (Thoma et al., 1994) and were found in broccoli leaf wax (Pyee et al., 1994) and secreted from carrot cell suspension cultures (Sterk et al., 1991). Based on a nucleotide-derived phylogeny of LTPAs, I determined that *LTPA1*, *LTPA8* and *LTPA13* were closely related to one another and the remainder of the LTPAs (Figure 4-1, indicated in yellow) and could perform similar, overlapping, functions.

Grouping of genes into such clades with overlapping functions is observed for the duplication of *CYCLOIDIA* genes of *Helianthus annuus* (Chapman et al., 2008). According to the epidermis microarray (Suh et al., 2005), these *LTPs* were strongly expressed in the epidermis harvested from the tops of developing stems. For these reasons, I decided to test whether LTPA1, LTPA8 and LTPA13 are required for wax export in the inflorescence stems of Arabidopsis. I hypothesized a working model for cuticular wax export involving LTPAs to either complete the transfer/export of wax or assist in its export by interacting with LTPG, another protein and / or a cell wall domain (recall Figure 3-10).

As with LTPG, T-DNA insertional mutants for each LTPA candidate were verified as homozygous, then GC was used to assess their wax phenotypes. For each *ltpa* mutant two alleles were tested where available. None of the single *ltpa* mutants mentioned displayed altered cuticular wax load (DeBono et al., 2009). Given that these LTP candidates displayed strong expression and a high degree of amino acid and nucleotide similarity, functional redundancy may have played a role in masking putative wax phenotypes. For this reason, all combinations of LTPA double and triple mutants were generated: *ltpa1 ltpa8, ltpa1 ltpa13, ltpa8 ltpa13,* and *ltpa1 ltpa8 ltpa13.*

4.3 The stem wax of double *ltpa* mutants is indistinguishable from wildtype

To test for LTPA functional redundancy, I generated all double mutants from 'best' candidates by crossing homozygous T-DNA lines and determining genotypes by PCR. Crosses from *ltpa1, ltpa8,* and *ltpa13* resulting in the following double mutant: 1. *ltpa1 ltpa8* 2. *ltpa1 ltpa13,*and 3. *ltpa8 ltpa13.*

Double mutant plants were phenotypically equivalent to wild-type plants, displaying no obvious changes in development or appearance. Phenotypes associated with altered cuticles such as post-genital organ fusions were not observed, indicating that the cuticle was not severely compromised. To test for subtle changes in cuticle integrity, stem samples were stained with toluidine blue (Tanaka et al., 2004). Briefly, excised tissue is immersed in the toluidine blue stain for two minutes. Plants with cuticle defects become colored blue (Tanaka et al., 2004). No differences in staining with toluidine blue were observed for the *ltpa* double mutants suggesting no defects in cuticle integrity (Figure 4-2 A-D). In contrast, the ABC transporter mutant *wbc11-3/abcg11-3,* which is known to have cuticle defects (Bird et al., 2007; Panikashvili et al., 2007) was found to stain intensely with toluidine blue (Figure 4-2F). Similarly, wax harvested from the bolting stems of double mutants displayed no difference in cuticular wax load compared with wild type plants (Table 4-2, ANOVA, $P > 0.05$). Examination of the five most abundant

compounds in the cuticular wax showed no statistically significant differences from WT (Table 4-3).

4.4 Triple *ltpa* mutants have wild-type wax load

Since single (DeBono et al., 2009) and double *ltpa* mutants did not display cuticle disorganization and/or reduced cuticular wax, triple mutants were generated from the available double mutants. Double mutants *ltpa1 ltpa13* and *ltpa1 ltpa8* were crossed in order to generate a triple mutant *ltpa1 ltpa8 ltpa13.* As observed for double mutants, triple *ltpa* mutants appeared indistinguishable from wild-type plants. Stem cuticular wax from triple mutant plants was examined by GC. Triple mutant plants displayed statistically similar wax compositions to wild-type plants (Table 4-4). As observed with double *ltpa* mutants, the five most abundant compounds did not differ from WT plants (Table 4-4). The integrity of *ltpa* triple mutant plant cuticles was tested with toluidine blue staining as described for double mutants. The cuticle of stems from *ltpa* triple mutants did not appear compromised compared with wild type plants (Figure 4-2).

4.5 Discussion

In this chapter, mutants for *ltpa1, ltpa8, and ltpa13* were tested for changes in wax and cuticle integrity. These LTPAs were categorized by amino acid and nucleic acid sequences as a subtype of LTPs that are similar to, but distinct from LTPG. Despite the sequence similarity between the LTPAs, and their strong expression as determined by an epidermal peel microarray (Suh et al., 2005), mutants lacking these LTPs did not display differences in stem cuticular wax from wild-type plants and, moreover, displayed intact cuticles according to toluidine blue impermeability. That no cuticular wax related phenotypes were observed in all *ltpa* mutants examined may indicate that *LTPA1, LTPA8,* and *LTPA13* play no role in cuticular wax transport. There may, however, be a role for other LTPAs. LTPAs and LTPA-like proteins from other plants display affinity for all lipidic molecules tested (Lerche et al., 1997; Zachowski et al., 1998; Tassin

Moindrot et al., 2000). This suggests that these LTPs have some role in lipid binding. Although some LTPAs can bind lipids, protein crystal structures collected over the past 20 years indicate a lack of catalytic domains, excluding a biosynthetic function. Sequence analysis and localization data of LTPs suggest that LTPAs have secretion signals (Sterk et al., 1991; Fleming et al., 1992; Thoma et al., 1994; this work) in Arabidopsis, carrot and tobacco, indicating a function outside of cytoplasm. Moreover, these LTPs have been detected outside of the cell, expelled from carrot suspension cells and in the cuticular wax of broccoli (Sterk et al., 1991; Pyee et al., 1994). Although the combinations of *ltpa* mutants that I studied do not have cuticular wax deficiencies, binding data described in chapter 1 and localization data described above support a role for LTPAs in cuticular wax transport. The absence of cuticular wax differences between wild-type plants in single, double and triple mutants of LTPAs may imply that 1. other LTPAs must be impaired to elicit a phenotypic change in wax quantity, and 2. LTPAs may have functions in the cell wall, unrelated to wax transport. An experiment that fulfills scenario one is described in chapter 5.

These results are not entirely unexpected since thirteen LTPAs exist in total. Targeting three LTPAs may not have been sufficient to inhibit LTP function or overcome functional redundancy. Unfortunately my attempts at *in silico* design of microRNA (miRNA) directed against multiple LTPA transcripts were unsuccessful (Schwab et al., 2006). I was unable, using Weigel's web-based microRNA designer (WMD), to generate suitable miRNAs primarily due to the lack of consensus regions required by the *in silico* algorithm (discussed at length in Schwab et al., 2006). Despite strong overall *LTPA* sequence similarity, very little sequence similarity existed over the short sequences required for suitable miRNA generation. In chapter 1, LTPs are described as having a signature eight-cysteine motif and four alpha helices. Two codons are required to produce a cysteine (TGT, TGC). However, these cysteine residues are found in the four alpha helices. Alpha helices can sustain a considerable level of sequence diversity; an alpha helix can

be generated with many combinations of amino acids. This problem was exacerbated by the lack of obligate catalytic domains (*e.g.* ABC transporter Walker domain).

It is a still a possibility that more than three LTPAs must become impaired before a wax related change can be observed. Instead of a miRNA approach, a co-suppression or post-transcriptional gene silencing approach could be used in combination with gene stacking (Wu et al., 2005; Li et al., 2010; Lu et al., 2011) to introduce multiple cDNA copies of LTPAs to induce *LTP* gene silencing. Independent groups have used gene stacking to alter the composition of oil seeds (Wu 2005; Li et al., 2010) by inserting multiple enzymes into the plant genome as a cassette. This is considered as a significant advance in plant biotechnology (Lu et al., 2011). Therefore, production of multigene co-suppression cassettes may be a method to knock down more LTPAs and decipher their function.

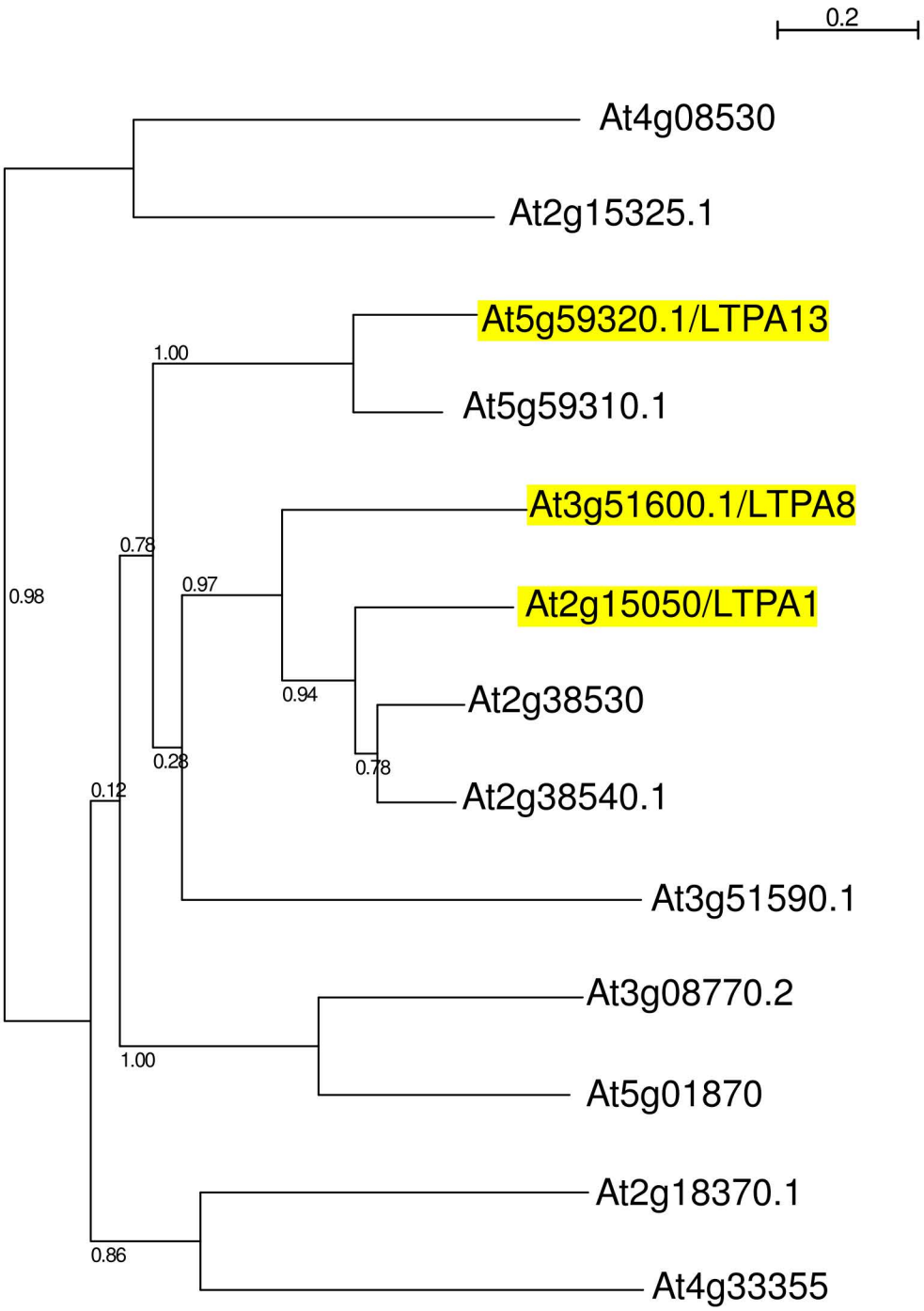

Figure 4-1: PhyML phylogenetic tree displaying relationships among the LTPA family of LTPs. Nucleotide sequences are used to assemble tree. Numbers indicate confidence values after 1000 bootstrap replicates. Arabidopsis genome identifiers are shown at branch ends. LTPAs used to generate double and triple mutants are displayed on yellow backgrounds.

Table 4-1: Bigπ analysis of LTPAs

AGI identifier/LTP	Predicted best GPI site (amino acid)	Big πScore	Amino acid sequence length
LTPG / At1g27950	S residue #160	+12	193
At2g15325	S	-29	121
At4g08530	N	-60	103
At5g01870	A	-61	116
At3g08770	N	-111	116
At2g38530	S	-50	118
At2g38540	S	-59	118
At2g15050/LTPA1	R	-64	118
At3g51600/LTPA8	N	-47	118
At3g59320/LTPA13	I	-87	115
At3g59310	S	-115	112
At3g51590	L	-58	117
At4g33355.1	D	-52	119
At4g33355.2	D	-52	117
At2g18370	N	-33	116

LTPAs are not GPI linked. LTPAs are compared with LTPG using *in silico* GPI linkage prediction tool, Bigπ. Table displays AGI number or unique identifier; Bigπ predicted site; and the length of each LTP. The Bigπ score assigns a positive score when structural criteria are met. These criteria are as follows: A short unstructured region and a hydrophobic domain at a given protein's carboxy-terminus surrounding compact amino acids to which a GPI is added. LTPAs have no appropriate GPI linkage sites shown as negative scores.

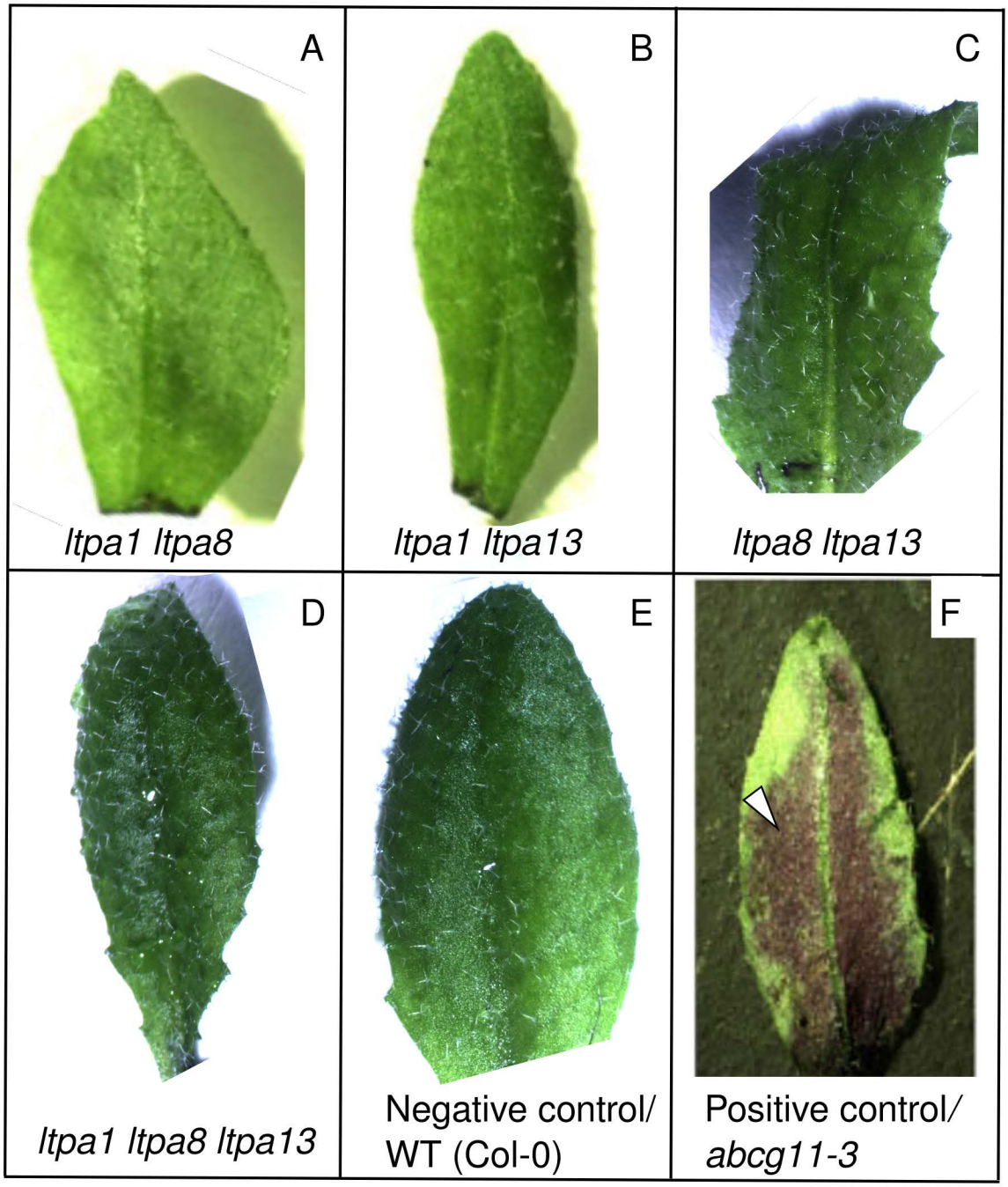

Figure 4-2: Toluidine blue staining analysis of double and triple *ltpa* mutants. (A-D) The leaves from double and triple mutants do not display toluidine blue staining. (E) A WT leaf does not display toluidine blue staining. (F) The mutant *wbc11-3/abcg11-3,* which has a defective cuticle, shows intense staining (open arrow head). Results are indicative two biological replicates.

Table 4-2: Total stem wax loads of *ltpa* double mutants

Genotype	Total Wax	P-value
ltpa1 ltpa8	19.5 ± 4.20 μg/cm^2	0.12
WT (Col-0)	14.2 ± 7.76 μg/cm^2	
ltpa1 ltpa13	16.1 ± 4.97 μg/cm^2	0.13
WT (Col-0)	12.5 ± 3.96 μg/cm^2	
ltpa8 ltpa13	12.7 ± 4.3 μg/cm^2	0.10
WT (Col-0)	08.5 ± 2.3 μg/cm^2	

Total wax loads ± SD of stems harvested from double *ltpa* mutants are compared with corresponding WT stems. P-values from ANOVA indicate no differences from corresponding WT plants. n = 5-10. Data for three biological replicates is shown.

Table 4-3: A comparison of the five most abundant compounds by abundance, extracted from the stems of *ltpa* double mutants with WT.

	ltpa1 ltpa8	*ltpa1 ltpa13*	*ltpa8 ltpa13*	WT (Col-0)
Nonacosane	7.8 ± 1.36 μg/cm^2	6.1 ± 1.12 μg/cm^2	4.7 ± 1.30 μg/cm^2	4.6 ± 1.14 μg/cm^2
Hexacosanol	0.3 ± 0.08 μg/cm^2	0.3 ± 0.14 μg/cm^2	0.3 ± 0.08 μg/cm^2	0.1 ± 0.06 μg/cm^2
Nonacosanone	4.3 ± 0.82 μg/cm^2	3.1 ± 0.52 μg/cm^2	2.9 ± 0.64 μg/cm^2	1.8 ± 0.48 μg/cm^2
Nonacosan-15-ol	2.0 ± 0.23 μg/cm^2	1.3 ± 0.20 μg/cm^2	1.3 ± 0.29 μg/cm^2	0.8 ± 0.21 μg/cm^2
Octacosanol	0.4 ± 0.12 μg/cm^2	0.5 ± 0.15 μg/cm^2	0.4 ± 0.09 μg/cm^2	0.2 ± 0.07 μg/cm^2

Average ± SD is shown, for at least 10 indivduals in three biological replicates. P-values for ANOVA indicate no differences ($P > 0.05$) from wild-type plants.

Table 4-4: A comparison of the total wax loads and most abundant compounds extracted from stems of *ltpa1 ltpa8 ltpa13* triple mutants with WT (Col-0).

	ltpa1 ltpa8 ltpa13	WT (Col-0)
Total Wax	17.8 ± 3.72 μg/cm^2	19.0 ± 2.16 μg/cm^2
Nonacosane	7.3 ± 0.9 μg/cm^2	6.4 ± 0.9 μg/cm^2
Hexacosanol	0.4 ± 0.0 μg/cm^2	0.3 ± 0.1 μg/cm^2
Nonacosanone	4.9 ± 0.6 μg/cm^2	3.9 ± 0.6 μg/cm^2
Nonacosan-15-ol	2.5 ± 0.4 μg/cm^2	2.5 ± 0.4 μg/cm^2
Octacosanosol	0.7 ± 0.1 μg/cm^2	0.5 ± 0.2 μg/cm^2

Average ± SE is shown. P-values for ANOVA indicate no differences ($P > 0.05$) from WT plants. At least 10 individuals are shown for two biological replicates.

5. LTPG membrane dynamics and non-homogeneous distribution at the cell surface during cuticle secretion

5.1 Synopsis

Lipid transfer protein glycosylphosphatidylinositol anchored (LTPG) is a GPI protein detected in detergent resistant membranes (DRM), suggesting that it is a component of lipid rafts (Borner et al., 2003; Elortza et al., 2003). The GPI domain confers the addition of a post-translational modification to proteins that may allow LTPG to interact with other proteins through lipid microdomains and/or, through release from the plasma membrane, into the cell wall. Little information exists indicating how plant GPI proteins behave in the plasma membrane. Two factors influence the behavior of GPI proteins such as LTPG: 1. The effect of the plasma membrane lipid composition and 2. The interaction of LTPG with its non-lipidic environment. Less information is available regarding the nature of proteins that are capable of traversing the plasma membrane-cell wall-cuticle interface. Thus, the objective of the work presented in this chapter was to understand how LTPG behaves at the cell surface (defined below); this was accomplished using fluorescence recovery after photobleaching (FRAP). My secondary objective was to examine what properties of LTPG were responsible for its observed behavior at the cell surface. To achieve this objective, I used molecular biology to generate fluorescent LTP chimeras and confocal microscopy to image them.

5.1.1 Is LTPG a highly diffusible membrane protein?

In light of the results described in chapter 3, YFP-LTPG was considered primarily a plasma membrane protein. My first objective was to characterize the behavior of YFP-LTPG at the plasma membrane. To complete this objective, I performed FRAP on outside, periclinal membranes (*e.g.* immediately underneath the plant cell wall, facing the cuticle and the external environment), in order to measure the two-dimensional recovery of YFP-LTPG in the plasma membrane. Surprisingly, LTPG was relatively immobile. This behavior was compared with plasma membrane proteins: wax related ABC transporter, ABCG12/CER5 (Pighin et al., 2004)

and non-wax related GFP-LTI6b (Capel et al., 1997; Cutler et al., 2000). These proteins displayed relatively low mobilities as well. To refine my study and to confirm that large mobilities could be observed using the imaging paradigm that I developed, I designed and tested highly diffusible proteins: 1. Cytoplasmic YFP (cyto-YFP) and 2. YFP-GPI, a chimera consisting of the LTPG amino-terminal signal sequence and the GPI domain on either side of citrine YFP. The engineered controls were highly mobile.

LTPG is involved in cuticular wax transport and is found in detergent resistant membranes (Borner et al., 2005; DeBono et al., 2009). The cuticular wax that appears on the cell surface likely moves through the plasma membranes of epidermal cells. In a computer simulation performed by Tielman et al., a membrane composed of 1,2-dioleoyl-sn-glycero-3-phosphocholine (DOPC) showed that nonacosane can adopt conformations that are stabilized by DOPC acyl tails (Coll et al., 2007). It is possible that nonacosane that is oriented parallel to acyl tails of membranes results in regions of local fluidity reduction. I considered that the observed immobility of LTPG may have been a function of the lipid environment it experienced. Therefore, I examined LTPG dynamics in three mutant backgrounds that result in altered fluxes of cuticular lipids from epidermal cells. I used *cer5-2*, *mah1-1* and the co-suppressed *cer6* (Millar et al., 1999; Pighin et al., 2004; Greer et al., 2007). The *cer5-2/abcg12* mutant exhibits a decrease in total wax load and specifically, nonacosane (Pighin et al., 2004), which would be similar to desaturating the plasma membrane, increasing fluidity. In this genetic background, nonacosane would not be available in the same quantities to associate with the acyl tails of membrane lipids. *Mah1-1* mutant does not have reduced cuticular wax, but its wax composition is altered: it is deficient in mid-chain oxygenated wax molecules (*e.g.* nonacosan-15-one and nonacosan-15-ol). The chemical profile of *mah1-1* is hypothesized to result in an increased alkane content of the plasma membrane owing to the absence of loosely packing oxygenated chemical species, resulting in lower fluidity. The co-suppressed *cer6* (hence forth '*cer6*') has

severely reduced wax of all species owing to a defect in VLCFA elongation (Millar et al., 1999; Fiebig et al., 2000). It is hypothesized that the severe reduction of wax in *cer6* epidermal cells results in a nearly wax-free plasma membrane; absence of wax is predicted to increase plasma membrane fluidity.

5.1.2 How does LTPG accumulate at the plant surface and what factor(s) is/are responsible?

While developing the FRAP protocol used for this work, many observations of the cell surface of Arabidopsis stem epidermal cells were made. In chapter three, I described the accumulation of YFP-LTPG over the long periclinal walls, the cell walls parallel to the axis of growth. This led me to ask what factor(s) influence(s) the accumulation of YFP-LTPG at the cell wall-cuticle interface. I used four-dimensional imaging to show that YFP-LTPG at the cell surface is non-uniformly distributed and has dynamic and static properties. Furthermore, I showed that YFP-LTPG accumulates on the surface of epidermal cells in a way that dark spots or pock marks are interspersed in the YFP fluorescence. I will refer to these pockmarks as areas of fluorescence occlusion. I demonstrated that these pockmarks and the accumulation of YFP-LTPG were altered by the flux of wax moving out of cells (using the wax deficient mutants described in section 5.1.1). Next, I addressed whether the accumulation of YFP-LTPG above the long walls was a functional localization that contributes to wax accumulation. I engineered a synthetic LTP using LTPA1; an LTP, which when mutated did not result in detectable changes in wax, fused to the GPI domain of LTPG. Using analytical chemistry, I showed that this synthetic chimera functionally complements the *ltpg-1* mutant. The results discussed in this chapter indicate that LTPG is an immobile GPI protein when resident in the plasma membrane that accumulates in the cell wall non-homogenously. Moreover, the cell wall fraction of LTPG is involved in wax transport.

5.2 Protein mobility can be gauged by fluorescence recovery after photobleaching

Fluorescence recovery after photobleaching (FRAP) is a technique pioneered by Webb in the 1970s. Although other groups were performing FRAP experiments at the time, Webb generated the algorithms used to generate recovery curves that are still used today, and used in this study (Axelrod et al., 1976; Zagyansky and Edidin, 1976). FRAP is based on the observation of fluorescent molecules and, as of the GFP era, fluorescent proteins (FP), in a planar area of a known size. A cell is illuminated by low intensity photo-irradiation and the fluorescent molecules in the region of interest are irreversibly bleached by high intensity laser pulse. The bleached or blackened area, devoid of fluorescence, is monitored over time in order to observe and measure the re-population by fluorescent proteins or fluorescent probes (Sprague and McNally, 2005). This imaging paradigm gives important pieces of information: first, the mobility of a given protein, *i.e.* the relative amount of fluorescing molecules that replace photo-bleached molecules (Figure 5-1 A) and second, the speed with which mobile molecules diffuse into the bleached zone. This speed is expressed as the half-time of recovery or time at which the bleached region returns to 50% of the initial fluorescence intensity (Figure 5-1 B).

5.3 FRAP does not damage the cells of the stem epidermis

Quantitative studies of protein mobility in Arabidopsis have, to-date, focused on expanding leaf epidermal cells, cell wall-free plant cells (Martinière et al. 2011), and root epidermal cells (Feraru et al., 2011). My study is the first that attempts to quantify protein dynamics in Arabidopsis stem epidermal cells actively secreting wax. Therefore, it was not established what levels of laser irradiation would bleach FPs expressed in epidermal cells. Moreover, the constructs that I designed for this study are based on citrine YFP, a third generation FP with strong acid stability (Griesbeck et al., 2001); citrine YFP yields twice the fluorescence of enhanced GFP (eGFP; Shaner et al., 2005). Therefore, imaging parameters capable of bleaching

epidermal cells without damaging cells was needed. I developed a test to determine whether the FRAP event damaged cells. This required manipulation of several key FRAP event parameters.

The FRAP event is manipulated by varying the following parameters: area, intensity, and dwell-time. Area is the size of the photo-bleached region of interest. The intensity of the laser, or the power in mW, is expressed as a percentage of maximum output of a given laser line. Finally, dwell time represents the amount of time the laser irradiates the area at the desired photobleaching laser intensity. While these parameters must be balanced, so too must a balance be made between irreversible photo-destruction of FPs while maintaining cell health and integrity and cell death. It is a concern if an imaging paradigm is developed where cells are damaged and/or destroyed in the process of photo-bleaching. Using the viability marker propidium iodide, I empirically determined the conditions that reliably photo-bleached constructs based on citrine YFP. Stem segments were stained in propidium iodide as described for cell wall staining in Chapter 3. Next, stained tissue was exposed to high and low bleaching laser paradigms (Figure 5-2). If cell integrity was compromised by the bleaching laser, propidium iodide would enter the cytoplasm of epidermal cells and cause nuclei to fluoresce intensely. Laser power output of the laser diodes was measured in June 2010; the most powerful laser line, 488 nm, measured approximately 2.5 mW. The measurements of laser power can be found in section 2.7.1. The diameter of the bleached area in all experiments was held to approximately 3μm. With 'Low intensity' bleaching parameters consisting of 100% 488 nm laser power output, 250 iterations for four sec of total dwell-time, no damage occurred to epidermal cells as determined by the absence of fluorescing nuclei (Figure 5-2 A, C, E, G). Using ‘high intensity’ bleaching settings consisting of 100% 488 nm laser power output, 1000 iterations for four sec total dwell-time, cells became ruptured as indicated by the glowing nuclei (Figure 5-2 F, H, asterisks). The parameters used for the acquisition of all FRAP data presented in this chapter were 70% laser intensity, 50 iterations, and 500 ms dwell time. The FRAP parameters used for

data acquisition are well below the intensity of the 'low intensity settings, the settings that did not cause cell rupture. This result indicates that the FRAP results shown are indicative of *bona fide* FP bleaching and not cell damage or death.

5.4 Relating LTPG dynamics and wax secretion

LTPG is associated with detergent resistant membranes (DRMs; Borner et al., 2005), and it is well established that GPI proteins are covalently linked to lipids (Orlean and Menon, 2007). Computer simulations show that nonacosane, nonacosan-15-one and nonacosan-15-ol are stabilized by acyl tails of membrane composed entirely of DOPC (Coll et al., 2007); by analogy plasma membrane lipids may stabilize wax molecules *in vivo*. Therefore if wax is moving through the plasma membrane, wax may interact with LTPG through the GPI lipid tails. The objective of the following experiments was to determine whether the flux of cuticular lipids moving through the plasma membrane could affect the mobility of LTPG, due to the presence of specialized regions in the plasma membrane that provide the lowest free energy environment for wax molecules (Coll et al., 2007). I considered two possible scenarios that would affect the dynamics of YFP-LTPG. 1. YFP-LTPG resides in the microdomain of the membrane known to form DRMs; the tails of sphingolipids associated with the DRMs may stabilize wax molecules in a similar fashion to the DOPC membrane examined *in silico*. In this scenario, YFP-LTPG is predicted to be immobilized in wax molecule-filled, crowded, subspace. Once an area is bleached, YFP-LTPG would recover slowly due to association with DRMs. When wax is absent, recovery is predicted to be faster. 2. Wax may not have an appreciable resident time in the plasma membrane, resulting in no observable changes in YFP-LTPG dynamics when alterations in the flux of cuticular wax are made.

To evaluate the effects of different fluxes of wax moving from epidermal cells to the surface of Arabidopsis stems, three genotypes were used. CER5/ABCG12 is an ABC transporter responsible for moving wax components out of epidermal cells (Pighin et al., 2004). The *cer5-1*

point mutant displays a strong reduction of alkanes (Pighin et al., 2004). *Cer5-2* is allelic to *cer5-1*, the former is a transcriptional knockout and phenocopies *cer5-1* closely (Pighin et al., 2004). The *CER6* gene encodes a keto-acyl Co-A synthase; disruption of *CER6* results in an absence of wax crystals on the surface of stems and a chemical profile showing a reduction in all wax components of chain lengths greater than 24 carbons (aldehydes, primary alcohols, alkanes, ketone and secondary alcohols) as well as an increase in carboxylic acids of chain lengths shorter than 26 carbons. These alterations in the chemical profile of *cer6* result in a reduction in stem wax load (Millar et al., 1999). *MAH1* encodes a mid-chain alkane hydroxylase (Greer et al., 2007) responsible for the production of secondary-oxygenated cuticular wax compounds; *mah1-1* mutants display trace amounts of the second and third most abundant chemical species in cuticular wax, nonacosan-15-one and noncosan-15-ol while having increased amounts of nonacosane (Greer et al., 2007). I hypothesized that the altered flux of cuticular lipids moving through the epidermal plasma membrane would render it either less fluid, which would result in reduced LTPG mobility (*mah1-1*), or more fluid, resulting in increased LTPG mobility (*cer5-2*, *cer6*; Figure 5-3).

5.4.1 YFP-LTPG is relatively immobile and does not appear to be influenced by the absence of nonacosane, nonacosane-15-ol, and nonacosan-15-one

In order to study the dynamics of YFP-LTPG in the plasma membrane, cell and molecular biology resources were required that did not exist. Before discussing YFP-LTPG dynamics in various backgrounds, it is of particular importance to briefly mention the cell biology tools that I developed in order to acquire data with meaningful controls. Since both the plasma membrane lipid environment and interaction with the cell wall could affect the mobility of YFP-LTPG, a GPI-anchored YFP that lacked the LTPG domain was generated. While metazoan systems have long had synthetic GPI proteins, chimeras that are directed to be GPI linked when they are not normally so, (Moran and Caras, 1991a; Moran and Caras, 1991b), only one such protein has

been reported in the plant biology literature. Arabinogalactan protein (AGP) 14 is a confirmed GPI protein (AGP14; Sherrier et al., 1999); Borner developed PAT (phosphinothricin acyl transferase)-GPI, a double-myc tagged synthetic GPI as a biochemical marker of plant lipid rafts (Borner et al., 2005). This was the only available synthetic GPI protein available in plants. PAT-GPI was not suitable for my study since it lacked a FP, and since it used the last 56 C-terminal amino acids of AGP14. AGPs are known to be heavily glycosylated proteins which may confer unwanted post-translational modifications such as glycosylations in addition to GPI linkage (Borner et al., 2005; Ellis et al., 2010). Therefore, I developed a YFP-GPI by fusing the LTPG amino-terminal signal secretion sequence (ending in amino acids GALADE) to the amino-terminus of citrine YFP. The detection of the amino-terminal signal secretion sequence is discussed in Chapter 3. Next, I fused the region encoding the final 46 amino acids of LTPG (starting PATPAT) to the carboxy-terminus of citrine YFP. The chimeric gene was expressed using the LTPG promoter. This gene allowed me to test how the GPI domain influences protein mobility. YFP-GPI localizes to the plasma membrane exactly as YFP-LTPG (Figure 5-4 A). When secant planes are examined, the junctions between cells clearly indicate fluorescence on either side of the non fluorescing cell wall (compare Figure 5-4 A and B, open arrow heads). The YFP-GPI targets correctly to the plasma membrane and was used for FRAP experiments as a control.

In order to demonstrate that a full recovery after photobleaching could be captured with my acquisition parameters and system, a protein that is freely mobile was required. I designed an LTPG promoter-driven cytoplasmic YFP (cyto-YFP) in order to establish a base line for full recovery after photobleaching (Figure 5-4 C). Studies of fluorescein diacetate (FDA) and micro-injected GFP in mammalian cells as well as the lumen of the mitochondrion had indicated that full recovery is reached at ambient temperature (Partikian et al., 1998; Verkman, 2002; Vink et al., 2006; Takao and Kamimura, 2008). Therefore, I reasoned that a full recovery should be

achieved with cyto-YFP. Cyto-YFP displayed a nearly complete recovery (approximately 90%; Figure 5-4 D). This demonstrates that a nearly complete recovery is possible with the image acquisition parameters developed for my study.

To test membrane protein mobility in stem epidermal cells, two proteins were examined: ABC transporter GFP-CER5/GFP-ABCG12 and GFP-LTI6b (Figure 5-4 D). These membrane protein control constructs displayed surprisingly low mobilities regardless of their differences in kD in the bilayer. GFP-LTI6b displayed the lowest mobility, at approximately 20%. Examination of the cDNA sequence of *LTI6b* (Capel et al., 1997) showed at least two transmembrane domain regions are predicted. GFP-CER5 displayed approximately 40% mobility and it has six predicted transmembrane domains.

Representative recovery curves for the outside periclinal membranes from stem epidermal cells with genotypes *YFP-LTPG ltpg-1*, *YFP-LTPG cer5-2*, *YFP-LTPG cer6*, *YFP-LTPG mah1-1* are shown (Figure 5-4 E-G). In contrast to cyto-YFP, YFP-LTPG *ltpg-1* appeared highly immobile with approximately 60% immobile fraction, a shallow recovery curve and large $T^1/_2$ (Figure 5-4 E). YFP-LTPG *ltpg-1* mobile fraction was similar to that of GFP-CER5 and larger than that of GFP-LTI6b. Surprisingly, YFP-GPI, bearing an identical GPI linkage to YFP-LTPG, was highly mobile (approximately 80% mobile) and displayed a steep recovery curve, compared with YFP-LTPG *ltpg-1* (Figure 5-4 F). These results suggest that the GPI domain of LTPG, independent from the remainder of the LTP, is able to recover to pre-bleach fluorescence. When *YFP-LTPG* is expressed in each of the *cer5-2* and *mah1-1* backgrounds, the mobile fraction did not differ from *YFP-LTP ltpg-1*. However, the $T^1/_2$ of YFP-LTPG *ltpg-1* is slower, displaying a shallower recovery than that of YFP-LTPG *mah1-1* and YFP-LTPG *cer5-2* (Figure 5-4 G).

Next, I performed statistical analyses to quantify observed difference in $T^1/_2$ recovery values and to determine if other subtle changes in mobilities exist among the genotypes (Figure 5-5;

grey bars indicate $T^1/_2$; yellow bars indicate mobile fractions). Cyto-YFP, YFP-GPI, and GFP-LTI6b displayed $T^1/_2$ values that were statistically indistinguishable; values ranged from 1.1 to 2.4 sec (Figure 5-5) The $T^1/_2$ value of GFP-CER5 *cer5-2* was longer than that observed for LTI6b (6.6 sec vs. 1.4 sec; Figure 5-5). The YFP-LTPG *ltpg-1* $T^1/_2$ value was significantly larger than that of YFP-LTPG measured in the *cer5-2* and *mah1-1* genetic backgrounds (13.2 sec vs. 7.0 sec and 5.4 sec; Figure 5-5). This result suggests that altering the membrane composition by changing the flux of the cuticular lipids moving through the plasma membrane results in significantly reduced YFP-LTPG $T^1/_2$ values (Figure 5-5). That YFP-LTPG *ltpg-1* has a slow $T^1/_2$ suggests some hindrance either through association with the plasma membrane, through lipids or a plasma membrane protein highly sensitive to lipid traffic through the membrane. These results suggest that YFP-LTPG is relatively immobile; immobility is independent of the content of the plasma membrane that is changed by manipulating wax flux. The $T^1/_2$ of YFP-LTPG in each of *cer5-2* and *mah1-1* appear to be influenced by wax flux through the membrane as these values are smaller in these genetic backgrounds when compared with *YFP-LTPG ltpg-1*. This difference appears subtle as indicated by the representative curves (Figure 5-4 G).

Conspicuously absent from the FRAP analyses is *YFP-LTPG* expressed in the *cer6* genetic background. Unexpectedly, upon expression of *YFP-LTPG* in this genetic background, the localization of YFP-LTPG was altered in comparison with the *ltpg-1* background. In the *cer6* background, YFP-LTPG did not accumulate on the outer periclinal face of the plasma membrane. These results are discussed below.

5.5 YFP-LTPG localization is altered in the *cer5-2*, *cer6*, and *mah1-1* mutants compared with the *ltpg-1* genetic background

During FRAP acquisitions, many observations of the surfaces of the outer periclinal membranes of stem epidermal cells were made. By examining three-dimensional data from z-series, I compared the cell wall and plasma membrane populations of YFP-LTPG expressed in various

genetic backgrounds. A schematic diagram of the xz orientation of two adjoining plant epidermal cells, indicating the 'top' and 'secant' focal planes used in these experiments is shown in Figure 5-6 A. YFP-LTPG accumulates over the long cell walls (Figure 5-6 B, closed arrow heads) and its surface fluoresces non-uniformly (Figure 5-6 B, open arrow heads). In comparison, secant planes of YFP-LTPG epidermal cells display no detectable wall localized fluorescence (Figure 5-6 F, arrowhead). The surface distribution of fluorescence gives the appearance of dark pock marks, areas where fluorescence is occluded (Figure 5-6 B). The distribution of fluorescence at the surface of YFP-LTPG expressed in epidermal cells of *cer5-2*, *cer6*, and, to a lesser extent, *mah1-1*, is altered when compared to the *ltpg-1* genetic background (Figure 5-6 C-E). The differences in distribution are explained below.

In the *cer5-2* background, YFP-LTPG accumulates strongly over the long walls as observed for YFP-LTPG *ltpg-1* (Figure 5-6 C, closed arrow head). However, the surface is different in two ways: instead of displaying 'pock marks, ' the areas of fluorescence occlusion are ovoid (Figure 5-6 C, open arrow heads).

In the *cer6* genetic background, YFP-LTPG did not accumulate appreciably over the outside periclinal surface, with the exception of long wall regions (Figure 5-6 D, closed arrow heads). YFP-LTPG in *cer6* appears visible only over long walls. Some cells appear to display ovoid occlusion of YFP-LTPG, albeit at irregular intervals (Figure 5-6 D, open arrowhead). In the *cer6* mutant, a large oval area that did not display fluorescence filled the central areas on epidermal cell surfaces. For this reason, it was impossible to perform FRAP on *YFP-LTPG* expressed in the *cer6.*

YFP-LTPG in the *mah1-1* genetic background appeared to display a more uniform localization of extracellular fluorescence than YFP-LTPG *ltpg-1* (compare Figure 5-6 E with B). Despite differences observed at the outer face of epidermal cells, proximal to the surface of the plant, no differences were observed among these genotypes when secant planes were examined (Figure 5-6 F-I). The established membrane protein GFP-CER5 (Pighin et al., 2004) does not display long cell wall localization (Figure 5-6 J, closed arrow heads). YFP-GPI, like YFP-LTPG displays accumulations of fluorescence signal over long cell walls (Figure 5-6 K). Secreted YFP accumulates over the same areas (Figure 5-6 L). As a negative control, cyto-YFP was examined and compared with the other constructs (Figure 5-6 M); no fluorescence is observed over the long cell walls (closed arrow heads). At secant planes, GFP-CER5, YFP-GPI and secreted-YFP only display membrane localization (Figure 5-6 N-P). These results suggest that the differences in the flux of cuticular lipids result in differences in how YFP-LTPG accumulates in the cell wall. YFP-LTPG, like GFP-CER5, is a membrane protein, but a subset of YFP-LTPG in the *ltpg-1*

genetic background appears to display non-uniform accumulation at areas of the outer periclinal face of the epidermal cell.

5.6 When linked to a GPI domain, LTPA1 accumulates over long cell walls.

GPI linkage tethers YFP-LTPG to the plasma membrane and, by analogy to other systems (*e.g.* yeasts: Kapteyn et al., 1999; Frieman and Cormack, 2003), may assist in distributing the protein in the cell wall. I hypothesized that the GPI linkage to the LTP domain confers function in the export of cuticular lipid export. In the bioinformatic analyses made in Chapter 4, the amino acid sequence GGSASA was predicted to include the ω-site using the *in silico* predictive algorithm Bigπ (Eisenhaber et al., 2003). The simplest way to test this hypothesis was to delete the GPI domain of LTPG, however, the resultant deletion mutants incorrectly accumulated inside the cell (Figure 5-7).

Since all LTPs have an eight-cysteine motif that allows the formation of a four α-helix bundle, I hypothesized that the primary structure can vary considerably so long as the sequence is amenable to producing a hydrophobic cavity. With this sequence data, I tested whether linking the LTPG GPI domain to LTPA1 would create a functional pseudo LTPG capable of complementing *ltpg-1*. I used LTPA1 to create a synthetic LTP with a GPI domain known as YFP-LTPA1ω (Figure 5-8). LTPA1 was well suited for this study because its mutant displays no detectable change in wax accumulation or composition, nor does its mutation affect wax as a member of a double or triple mutant (Chapter 4). To control for differences in expression levels between LTPA1 and LTPG (Suh et al., 2005), YFP-LTPA1ω was expressed from the LTPG promoter. The localization of YFP-LTPA1ω was examined by acquiring z-series, allowing a comparison of xy, xz, and yz planes (Figure 5-9). The YFP-LTPA1ω protein displays two localization fates: 1. at the cell wall, over long walls and 2. inside the cell centre, in a pattern consistent with vacuolar localization. When the surface of YFP-LTPA1ω plants was compared

with that of secreted YFP, fluorescence in both was detected over the long cell wall of epidermal cells (compare Figure 5-9 A with B).

When viewed in the xz or yz plane, the fluorescence was observed as either a concentrated area of fluorescence above cell walls or a diffuse fluorescence in the cell. The xz plane of YFP-LTPA1ω shows clearly that, in addition to the cell wall localization, there is an accumulation of fluorescence in the cell centre, presumably in the vacuole (Figure 5-9 A, closed arrow head). These observations indicate that removal of the native LTPA1 stop codon and fusion with the LTPG GPI domain, in frame, creates a synthetic LTP that is mislocalized inside the cell and accumulates above the long cell wall in a pattern similar to secreted YFP and YFP-LTPG (Section 5.5).

5.7 The synthetic YFP-LTPA1ω restores wax to the surface of *ltpg-1* stems.

I hypothesized that the accumulation of YFP-LTPG in the cell wall is the functional localization of this protein. Since YFP-LTPA1ω displayed a similar cell wall accumulation, I reasoned that because the protein accumulates in the cell wall, it could be functionally carrying lipids there. I transformed YFP-LTPA1ω into the *ltpg-1* genetic background to test for changes of nonacosane and total wax (recall the phenotype displayed by *ltpg-1, ltpgi1,* and *ltpgi2* is a reduction of nonacosane and total wax). The *ltpg-1* mutant displays its reported (DeBono et al., 2009) nonacosane and wax reduction of approximately 40-50% and 30%, respectively (Figure 5-10). When YFP-LTPA1ω is introduced into the *ltpg-1* genetic background, the nonacosane and total wax loads are wild-type levels. These results suggest that the LTP domains of LTPG and LTPA1 are largely functionally exchangeable.

5.8 In addition to non-uniform distribution, YFP-LTPG displays regions of non-homogeneous dynamics.

In section 5.7, I detailed the appearance of YFP-LTPA1ω in the cell wall and its ability to rescue the *ltpg-1* mutant. This suggested that localization to the cell wall allowed the fusion protein to be biologically functional. These results prompted a reexamination of the YFP-LTPG at the cell wall/cuticle interface. I hypothesized that the accumulation of YFP-LTPG over long walls should be dynamic since wax profiles correlate with age (Suh et al., 2005); if LTPG moves wax, it may accumulate according to the level of wax secretion. I performed four-dimensional microscopy in order to determine whether the cell wall accumulation of YFP-LTPG coincided with periods of known wax deposition. Figure 5-11 displays a single optical slice taken from a z-series at 20 time points, each separated by 1 minute in time. In each panel, four square areas of different colors are shown; each square of a given color indicates the same area in each micrograph. The trend emerging from observations of epidermal cell surface is that two populations of cell wall-localized YFP-LTPG exist; one population is relatively static, the other is dynamic. An area of fluorescence at the junction of three cells (Figure 5-11, orange square outline) shows solid fluorescence, and then at time 5 min (4 images later in the sequence) the fluorescence appears to recede leaving a dark line visible at time 6 min. After this time, the observed recession of fluorescence stops and remains static for the remainder of the time-lapse. The area marked with a cyan square outline shows a region that is relatively dark (time 1 min), then after 13 min the area becomes filled with YFP-LTPG and, by time 16 min, the area is completely illuminated (compare time 1 min with 16 min). At time 1 min, the magenta square outline shows an area with two dark spots on either side of a fluorescing line. The fluorescence in this region changes, giving the appearance that the dark spot is moving (compare time 1 min with time 15 min). These changes occur over a twenty-minute interval and result in shifting of fluorescence associated with YFP-LTPG. The slow movement of fluorescence is apparently due to shifting patterns of pock marks described in section 5.5. Taken together with results presented

in section 5.5, YFP-LTPG fluorescence associated with the cell wall is dynamic, albeit over long periods of time.

Since YFP-LTPG outside of the cell is dynamic, I reasoned that it was possible to observe the protein in the cell wall upon plasmolysis. Plasmolysis with mannitol resulted in poor separation of the plasma membrane, leading to the conclusion that YFP-LTPG is entirely plasma membrane localized; any possibility of cell wall localization was extremely tentative and was explained as a probable optical artifact (DeBono et al., 2009). Reports using sodium chloride, to isolate cell wall-linked arabinogalactan proteins suggested that this osmoticum could disrupt a putative association between YFP-LTPG and cell wall, enough to clearly separate the externally localized fluorescence signal from the plasma membrane population (Sardar et al., 2006). I plasmolyzed stem epidermal cells expressing YFP-LTPG with 4% sodium chloride (1 M). Immediately upon plasmolysis (within 30 sec), the protoplast retracted from the cell wall, and revealed bright foci in the regions where tricellular junctions occur (Figure 5-12 A, open arrow heads). A characteristic of plant cell plasmolysis is the formation of Hechtian strands, thread-like areas of plasma membrane in zones of adhesion to the cell wall. As plasmolysis increased, the protoplast retraction revealed Hechtian strands.(Figure 5-12 B, closed arrow heads) and foci that remained in the corners or tricellular junctions of epidermal cells (open arrow heads). Fluorescence found in the cell wall was difficult to detect after plasmolysis, indicating a weak association with the cell wall. When post-plasmolysis fluorescence was detected in the cell wall, it appeared as a fine outline around a membrane (Figure 5-12 A, magenta arrow head); in the case of fluorescence over long walls, a bright spot of fluorescence was observed, which occurred between two cells (Figure 5-12 B, magenta arrow head). At focal planes above the top-most region of the epidermal cells, bright spots corresponding to what were likely areas of the plasma membrane adhered to the cell wall above (Figure 5-12 C, arrow heads).

These results indicate that LTPG is associated with the plasma membrane and may associate with the cell wall at cell corners; this region subtends the region where the YFP-LTPG appears over the long cell wall. Plasmolysis of YFP-LTPG closely approximates results obtained from cells (tobacco BY-2) expressing AGPs (Zhao et al., 2002; Sun et al., 2005; Sardar et al., 2006; Yang and Showalter, 2007). Using 4% sodium chloride, the plasma membrane of Arabidopsis epidermal cells plasmolyzes in 30 sec; with the identical concentration of sodium chloride, the plasma membrane of tobacco BY-2 cells required up to 15 min to achieve comparable levels of retraction from the cell wall (Sardar et al., 2006; Yang and Showalter, 2007).

5.9 Discussion

In this chapter, I detailed the behavior of YFP-LTPG at the plasma membrane-cell wall interface. My previous understanding of wax transport involving LTPG was guided by the concept that membrane behavior would be determined by the lipid tail of the GPI linkage. I believed LTPG would associate with lipid rafts allowing for interactions with other proteins. An attractive idea was that GPI linkage provided mobility to LTPG allowing for association between ABCG12/CER5 (referred to hereafter as CER5) and LTP, analogous to ABCAs and ABCBs that interact with sterol carrier proteins (Maxfield and Menon, 2006). I used different genetic backgrounds to examine the impact of cuticular lipid flux through the plasma membrane during plant cuticle development and wax deposition. I studied YFP-LTPG in its native membrane environment (rescued *ltpg-1* mutant) and in genetic backgrounds that had different wax amounts or compositions. LTPs have been considered downstream from ABC transporters on a 'wax transport pathway' (Kunst and Samuels, 2009). Because LTPG may be a terminal point of wax transport or near terminal, this dissuaded me from genetic approaches where double mutants are generated and changes in wax are assessed by gas-chromatography.

5.9.1 Lipid flux does not appear to be a critical factor in LTPG mobility.

By making comparisons with equivalent engineered proteins, I showed that YFP-LTPG is not a highly mobile protein when compared to cyto-YFP and to YFP-GPI, the latter bearing the same LTPG GPI domain. Furthermore, I demonstrated that the flux of cuticular lipids moving through the plasma membrane does not have an effect on the LTPG mobile fraction; where measurable, neither the reduced amounts of nonacosane nor the absence of nonacosan-15-ol and nonacosan-15-one alter the amount of the mobile fraction of YFP-LTPG.

The original hypothesis was that reductions in the total wax load and nonacosane attributed to the *cer5-2* mutation would impart increased fluidity; absent nonacosan-15-ol and nonacosan-15-one cuticular species attributed to *mah1-1* were expected to decrease fluidity. Therefore *cer5-2* and *mah1-1* were expected to increase and decrease recovery times of YFP-LTPG, respectively. My hypotheses were only partially supported; YFP-LTPG recovers more quickly in both genetic backgrounds. This could reflect that cuticular lipid packing in the bilayer is not well predicted by computer simulations of DOPC (Coll et al., 2007), or that the flux of lipids through the plasma membrane contributes indirectly to interactions between YFP-LTPG with other proteins. A secondary result from these experiments is that mobility of plant membrane proteins in the bilayer is not well predicted by mass. GFP-CER5 recovers in half the time required by YFP-LTPG and shares a statistically similar mobile fraction. These proteins differ considerably in terms of mass and interaction with the membrane; the monomeric forms of these proteins, once processed, and including their respective FPs, have masses of 96 kD and 41 kD, respectively, yet no difference was observed in their $T^{1/}_{2}$. The difference in masses between these proteins, indicates that plant plasma membrane proteins may not necessarily be restricted in mobility by mass, but, instead, interactions with the cell wall or other proteins residing in the plasma membrane or inside the cortical cytoplasm. This was further supported by the low mobility

demonstrated by GFP-LTI6b compared with GFP-CER5; GFP-LTI6b is a protein that is small and compact relative to the six transmembrane domain bearing GFP-CER5.

Mobility of proteins is a function of membrane composition and interactions among proteins and their environments (Sprague and McNally, 2005). Plasma membrane lipid tail saturation and the modulation by sterols will alter the behavior of the proteins residing within. Increasing saturation results in a less fluid membrane and increasing sterols allows for equilibration of fluidity at temperature extremes (Alberts et al. 2002). Proteins are not passive in the plasma membrane. Transmembrane domain proteins may have domains that associate with the cytoplasm resulting in protein mobility changes (Edidin et al., 1991; Edidin et al., 1994). In metazoan systems, the cytoskeleton serves as a transient, restrictive force, "corralling" proteins with a "cytoskeleton-fence" in the plasma membrane (Tsuji et al., 1988; Kusumi et al., 2005; Lajoie et al., 2009). The behavior of plant plasma membrane proteins was largely unknown. Progress has been made by Martinère et al. (2011), demonstrating a linkage formed between the actin cytoskeleton, plasma membrane and cell wall mediated by FORMIN1.

YFP-LTPG is a GPI-linked protein. Proteins with such post-translational modifications reside in the membrane through covalent linkage to a lipid. The lipid linkage in plants is largely unknown, but a pear arabinogalactan protein (AGP) contains a ceramide lipid (Oxley and Bacic, 1999). Presumably, YFP-LTPG contains a similar GPI linkage; the GPI tail may interact with the plasma membrane in different ways if the lipid composition in the membrane is altered. YFP-LTPG displayed low mobility; mobility was unaffected by expression in genetic backgrounds that alter lipid flux through the plasma membrane (*cer5-2* and *mah1-1*). Two conditions were established by expression of YFP-LTPG in two distinct genetic backgrounds: 1. *cer5-2* results in a cytoplasmic accumulation of untransported wax (Pighin et al., 2004); membranes no longer are a transient stop point for exported wax. 2. *mah1-1* represents the condition where the less-fluid plasma membrane may contain increased nonacosane and a near

absence of mid chain hydroxylated compounds, nonacosan-15-ol and nonacosan-15-one (Greer et al., 2007). Surprisingly, these conditions did not alter the mobile fraction of YFP-LTPG but they significantly reduced the recovery (T ½) of YFP-LTPG.

T ½ indicates whether there is complicated recovery entailing binding or association of proteins with their immediate environment (Sprague and McNally, 2005). Complicated recoveries, which contain elements of both diffusion and binding, result in a curve that appears shallow and result in slow T ½ (large value). Recoveries comprised of simple diffusion alone have fast T ½. The control constructs examined in my FRAP experiments are indicative of simple diffusion; cyto-YFP and YFP-GPI displayed rapid T ½, less than two sec. YFP-LTPG displayed a slow, complicated recovery; the recovery was twice as fast when YFP-LTPG was expressed in the *cer5-2* and *mah1-1* mutant backgrounds. No change in T ½ was observed between *YFP-LTPG cer5-2* and *YFP-LTPG mah1-1*. Neither an abundance of nonacosane nor an absence of secondary oxygenated cuticular lipids alone, play a role in the slow recovery observed in *ltpg-1*. Any change in these cuticular lipids results in a faster T ½ value of YFP-LTPG. It is known that plant plasma membranes can remodel membrane lipids to maintain cellular homeostasis, specifically, to maintain plasma membrane fluidity (Tjellström et al., 2010). My observations may reflect the fact that plant plasma membranes change to adjust membrane fluidity. Alternatively, it may reveal that LTPG associates with itself (*e.g.* forms multimers) or associates with membrane proteins such as an ABC transporter. Since *cer5-2* is a knock-out mutant therefore *YFPLTG cer5-2* contains no CER5 protein; the absence of CER5 protein in these mutants could result in an alteration of the T ½ through absence of one member involved in the putative interaction. A protein-protein interaction between YFP-LTPG and MAH1 is negated because these proteins do not share subcellular compartments. It is clear that impairment of *MAH1* indirectly influences YFP-LTPG, increasing its observed recovery time as compared to plants with a wild-type genetic background.

5.9.2 The LTPG mobile fraction and recovery may be influenced by the cell wall

YFP fused to the LTPG GPI domain, but lacking the LTP domain, displayed nearly complete recovery after FRAP. This result suggests that a feature of the LTP domain causes the observed, reduced mobility of YFP-LTPG. Thus, YFP-LTPG is not restricted for mobility by the GPI linkage, and unlike FORMIN1, is not known to be tethered by a cytoskeletal fence. Instead, it may be bound to the cell wall through oligosaccharides or stable association with the cell wall proteins. An LTP-like xylogen protein was isolated and found to contain over 80 kD of endoH-susceptible glycosylation (Motose et al., 2004). Observations made in Chapter 3 indicate that glycosylation on the LTPG domain is likely; a subset of YFP-LTPG is indeed in the cell wall domain. Therefore, it is reasonable to imagine that LTPG may become associated with the cell wall via interaction between protein-attached oligosaccharides and the cell wall, thereby reducing mobility. *S. cerevisiae* is known to take GPI proteins and integrate them into the cell wall through covalent cross-linking (Frieman and Cormack, 2004). If YFP-LTPG is associated with the cell wall, then static, photo-bleached YFP-LTPG would impede the repopulation of a photobleached area of the plasma membrane with fluorescing proteins. Experiments with FORMIN1 indicate that withdrawal of the protoplast from the cell wall by plasmolysis and /or cell wall removal results in a large increase in mobility owing to loss of the physical constraint by the cell wall (Martinière et al. 2011). Similarly, the auxin transporter PIN2-GFP gains lateral mobility upon cell wall degradation (Feraru et al., 2011).

Plasmolysis of YFP-LTPG results in Hechtian strands derived from the labelled protoplast and bright foci, corresponding to the protein remaining in the cell wall. The fluorescence is in the cell corners roughly subtending the bright foci observed during three-dimensional imaging (*e.g.* Section 5.5). Although all FRAP experiments were performed on the outside periclinal membrane, it is unknown if fluorescence in the cell corners caused reduced mobility. It is plausible that the reduced mobility of YFP-LTPG is due to the constraint by and/ or weak

association with the cell wall. It was difficult to observe YFP-LTPG found over long cell walls after plasmolysis. In previous experiments, the osmoticum mannitol did not plasmolyze epidermal cells of Arabidopsis stemsYFP-LTPG appreciably at concentrations up to 0.75 M (using the protocol of Oparka et al., 1994). Sodium chloride worked well to plasmolyze epidermal cells where mannitol failed. At the concentrations used, sodium chloride (1 M) is known to disrupt the association of cell wall proteins with the cell wall (Rose et al., 2000), and is used in modern protocols to isolate cell wall proteins (Jamet et al., 2008). The difficulty to recover YFP-LTPG along long walls during plasmolysis may, in part, be due to extraction of LTPG or cell wall protein(s) to which LTPG may associate. Furthermore, it suggests that cell wall-associated YFP-LTPG is not covalently linked to the cell wall matrix like yeast cell wall proteins.

5.9.3 Extracellular accumulation of LTPG appears non-uniform and is biologically functional.

Multiple attempts to establish FRAP allowed for close examination of the cell wall-cuticle interface. Three findings emerged: 1. YFP-LTPG is non-uniform at the cell wall-cuticle interface; 2. the non-uniform localization is altered by changes in flux of wax through the system and/ or wax accumulated in the cuticle; and 3. the non-uniform accumulation changes over time. In chapter 3, I showed that YFP-LTPG accumulates on top of and in the long walls of epidermal cells. The cell wall-cuticle interface of epidermal cells expressing YFP-LTPG appears pock marked and has areas lacking YFP-LTPG fluorescence. What I have defined as areas of occlusion may be sites of wax deposition. Since these areas occur on the outside face of the epidermal cell wall, where wax is trafficked, it is reasonable to hypothesize that these may be sites of wax deposition. Although not impossible, it is difficult to imagine how LTPG can make a return trip from the cuticle to the epidermal cell plasma membrane. However, it is a seemingly wasteful means to traffic lipids, using LTPG only once for a single purpose. The occurrence of

YFP-LTPA1ω in the cell wall and rescue of *ltpg-1* suggests that the GPI domain may be sufficient for placing an LTPG where it can contribute to wax transport, but that the LTP eventually makes its way to the cell wall-cuticle interface.

5.9.4 The middle lamella region of the cell wall as an exit point for biomolecules.

The genotypes *YFP-LTPG ltpg-1; YFP-LTPG cer6; YFP-LTPG cer5-2*, *YFP-GPI* in WT and *secreted YFP* in WT consistently displayed fluorescence accumulation over long cell walls in a region consistent with the middle lamella. This localization is consistent with the localization reported for YFP-LTPG (DeBono et al., 2009). This may suggest that proteins and biomolecules can use the middle lamella as an exit point from the epidermal tissue. Kolattukudy described, with immunocytochemistry, a path taken by the broccoli LTP, WAX9, through the anticlinal cell wall subtending the area where fluorescence accumulates for the constructs listed above (Pyee et al., 1994). In addition, the fungal pathogens *Phytophthora nicotinae*, *Phytophthora cinammoni* and alfalfa fungus penetrate their host tissues through the anticlinal epidermal cell wall; the area over which YFP-LTPG and the others accumulated (Hardham, 2001; Cosgrove, 2005; Hardham, 2007). Is a special property associated with the region where the anticlinal wall meets the plant surface? This region is continuous with the middle lamella and is pectic (Caffall and Mohnen, 2009). The pectic cell wall regions control cell wall porosity and gel properties (Cosgrove, 2005). Taken together: 1.YFP-LTPG and derivatives including secreted YFP are found in a region of the cell wall that contributes to porosity; 2. the pectic region is used for ingress by fungal pathogens. Two testable hypotheses are immediately evident: 1. Small proteins use the middle lamella region of cell wall to escape the plant cell wall; and/or 2. LTPG integrates into the cell wall in order to serve as a hydrophobic acceptor in the cell wall and allow the movement of the osmiophilic, lipophilic regions to the surface (Pyee et al., 1994; Jeffree, 2006). These hypotheses will be discussed in the following chapter.

5.9.5 Comparison of LTPG with known plant GPI proteins

The accumulation of YFP-LTPG in the cell wall implies that the localization at the plasma membrane may be a means to gather and accumulate protein, whereas the functional localization is in the cell wall. This compares with two of the best characterized plant GPI proteins: COBRA and SKU5. COBRA is a root protein involved in anisotropic cell expansion localized to both the plasma membrane and the cell wall (Roudier et al., 2005). Cell fractionation indicated that COBRA is N-glycosylated and GPI-anchored at the plasma membrane; immunocytochemistry with a COBRA antibody revealed that it was primarily found in the plasma membrane where its distribution is microtubule dependent as well as being predominantly associated with longitudinal cell walls (Roudier et al., 2005). No biochemical or live-cell imaging localization exists for COBRA at this time. Research on GPI-linked SKU5 is most pertinent to LTPG. When *SKU5* is mutated, Arabidopsis seedling roots become twisted (Sedbrook et al., 2002). SKU5 was isolated from purified plasma membrane fractions and probed with a SKU5 antibody; the protein was in the plasma membrane (Sedbrook et al., 2002). Re-probing of proteins harvested from GFP-SKU5 seedlings after a salt wash detected SKU5 in the cell wall. Free GFP was detected in the cell wall fluid harvested from these seedlings; the researchers concluded that free GFP could not be excluded as a factor contributing to cell wall fluorescence. A body of evidence suggests that observation of free GFP is quite common. Somerville's group created a series of GFP-tagged AGP and hydroxyproline-rich glycoprotein deletion mutants known collectively as synthetic glycomodules (SynGMs; (Estevez et al., 2006). Upon Western blotting, they observed 27 kD bands corresponding to free GFP in their SynGMs plant protein preparations (Estevez et al., 2006). Their conclusion was that proteolysis occurred during heat denaturation prior to sample loading, showing that heating protein above 60^{o}C resulted in release of GFP. Furthermore, temperatures above 70^{o}C nearly removed all GFP from their chimeric proteins (Estevez et al., 2006). Although GFP is, itself, highly resistant to proteolysis (Heim and Tsien, 1996), associated linkers may not be, and may introduce structure that is especially labile

if the structure permits nucleophilic attack of residues susceptible to acyl shifts (Xu et al., 1999). The data I have acquired suggest that I am not observing free FP. When I generated a YFP-LTPA1ω, I found that fluorescence accumulated in the cell wall. Performing wax analysis, I showed that the construct was able to functionally complement the *ltpg-1* mutant. Therefore, while it is possible that I have observed some free FP in the cell wall, my data do not support a scenario where the cell wall is entirely populated by free YFP.

5.9.6 Protein localization and mis-localization may be influenced by post-translational modifications

The functional synthetic GPI-linked LTP, YFP-LTPA1ω was localized to both the vacuole and over the long wall region of the cell wall. LTPA1 is not natively a vacuolar protein. The accumulation of the protein in the vacuole is likely a result of extending the native carboxy-terminus. It is known that modification of plant protein carboxy-termini can result in aberrant targeting (Brandizzi et al., 2002). Vacuolar protein localization requires a stretch of hydrophobic amino acids at the carboxy-terminus (Dombrowski et al., 1993; Saalbach et al., 1996). A considerable modification of LTPA1 was made when the GPI domain of LTPG was fused in frame. The carboxy-terminus of LTPA1 ends with residues YIC; adding the GPI domain extended this carboxy-terminus by 28 amino acids, starting with LTPG residues PATPAT. Included in the amino acids that confer the GPI domain, is a stretch of amino acids AVVALAVAL, which may have been confused by the protein sorting machinery as a potential vacuolar targeting sequence. The combination of the primary structures from the GPI domain and LTPA1 domain may have resulted in vacuolar targeting. Dombowski et al. (1993) showed that altering where glycosylation occurs at the carboxy-terminus can influence whether a protein is targeted to the vacuole.

An intriguing aspect of YFP-LTPA1ω localization was that it was targeted to the region over long cell walls similar to YFP-LTPG, without any visible association with the plasma membrane

based on comparison and identical cell wall localization with sec-YFP. Several lines of evidence suggest this lack of residence at the plasma membrane may be a function of altered susceptibility to phospholipase cleavage due to changes that GPI proteins undergo when native post-translational modifications are altered. GPI protein structure may change with alterations in glycosylation status. Some membrane proteins are recalcitrant to immunocytochemistry and evade antibodies and advanced high-pressure tissue preservation techniques (Wiese et al., 1996; Weise et al., 2000). Similarly, the GPI protein β2-glycoprotein I of red blood cells is not recognized by antibodies until the protein is deglycosylated by PNGaseF (de Laat et al., 2006). Therefore, YFP-LTPA1ω, a non-natively GPI-linked protein presenting different glycosylation, may be processed differently from YFP-LTPG. This may explain why YFP-LTPA1ω does not accumulate appreciably at the plasma membrane.

Surprisingly, YFP-LTPA1 complemented the reduction of wax phenotype of *ltpg-1*. This result supports the assertion made in chapter 4; two LTPs may have little amino acid sequence consensus and yet share similar tertiary structure. The amino acid sequences of LTPG and LTPA1 differ considerably; the former is 50% larger, yet both possess the eight cysteine motif common to all LTPs. The *ltpa1* mutants showed no detectable changes in wax; addition of the LTPG GPI domain placed the LTPA lipid binding domain in the correct location where it could complete a wax transport function. Over-expression of soluble YFP-LTPA in *ltpg-1* mutants may also result in complementation but this has not been tested. More testing is required to determine whether the GPI domain is required for LTPA to functionally complement the *ltpg-1* mutant.

5.9.7 Cuticular lipid flux influences YFP-LTPG distribution at the epidermal cell wall-cuticle interface.

When YFP-LTPG was expressed in the *cer5-2, cer6,* and *mah1-1* genetic backgrounds, pockmarks on the cell surface were not observed. The amount of wax in the genetic

backgrounds tested is lowest in *cer6* followed by *cer5-2*. *mah1-1* has wax with an altered composition. The surface localization of YFP-LTPG was altered from wild type in the same order of wax reduction. The absence of fluorescence in the *YFP-LTPG; cer6* genetic background due to a shift in fluorescence accumulation strongly implies that the altered localization at the surface is partially dependent on the wax moving through the plasma membrane and / or the arrangement of cuticular wax in the cuticle. Therefore, the final distribution of LTPG in the apoplast appears to be controlled, at least indirectly, by cuticular lipids, moving from and accumulating on epidermal cells.

By performing the first quantitative FRAP study of LTPs, I showed that cuticular lipid flux does not determine the mobile fraction of YFP-LTPG but influences rate of recovery. Surprisingly dynamic accumulation in the cell wall-cuticle interface and radical reorganization in the absence of wild-type wax indicates that LTPG is complex and is modulated in subtle and unexpected ways by the very substrate it is thought to move.

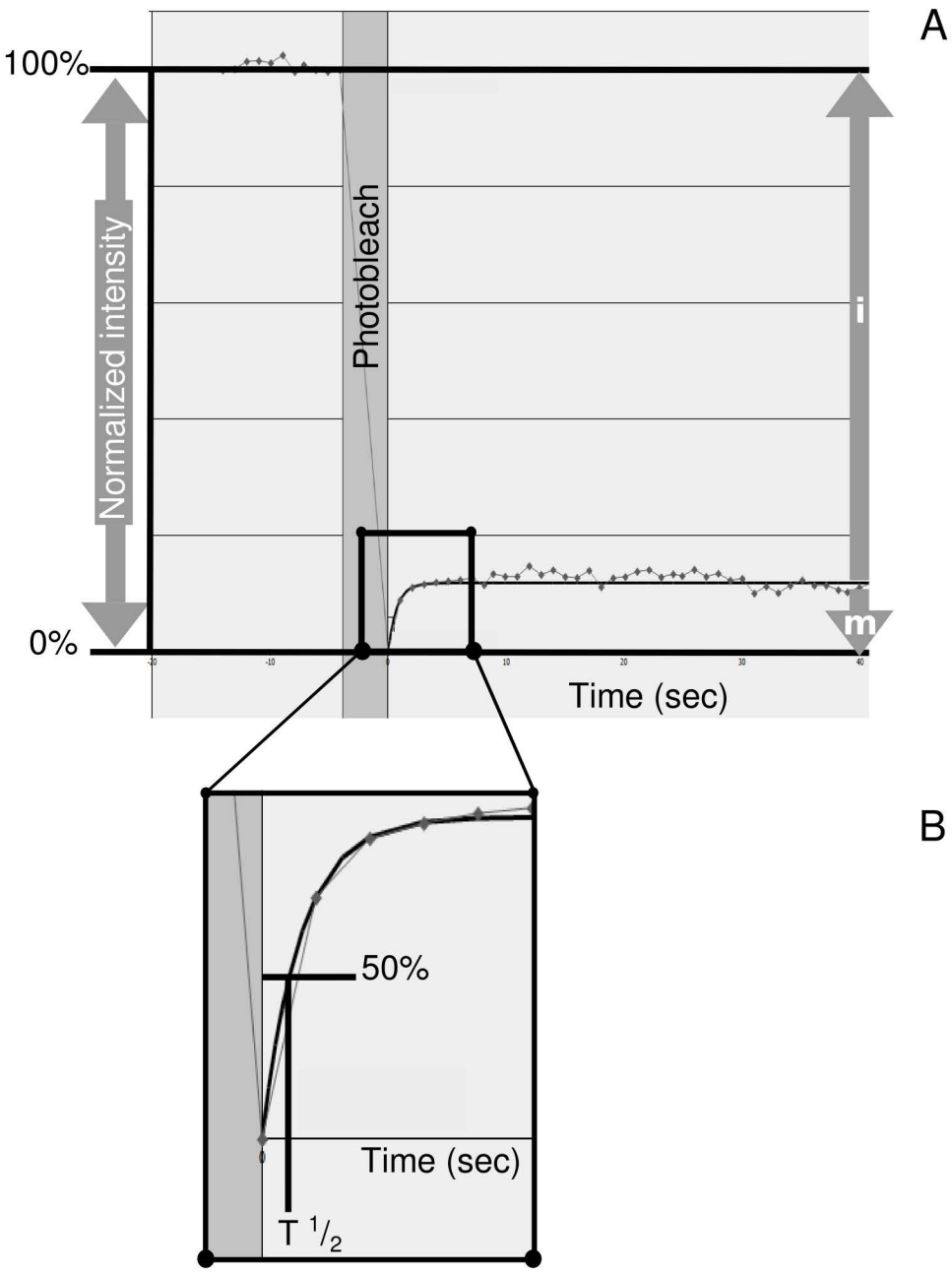

Figure 5-1: The information presented in a fluorescence recovery after photobleaching (FRAP) curve. (A) FRAP is a time series acquired before and after a photobleaching event. The y-axis indicates pixel intensity, normalized to 100%. The x-axis indicates time. The prebleach fluorescence is compared with postbleach fluorescence after a fluorescence plateau is reached to guage the mobility of a population of fluorophores. Fluorescence at photobleaching is zero or nearly zero. The recovered fluorescence (increase from zero fluorescence) is known as the mobile (m) fraction. Conversely the fluorescence that fails to return to the bleached region is known as the immobile (i) fraction. (B) $T\ ^{1}/_{2}$ is a time at which 50% of the maximum fluorescence is reached.

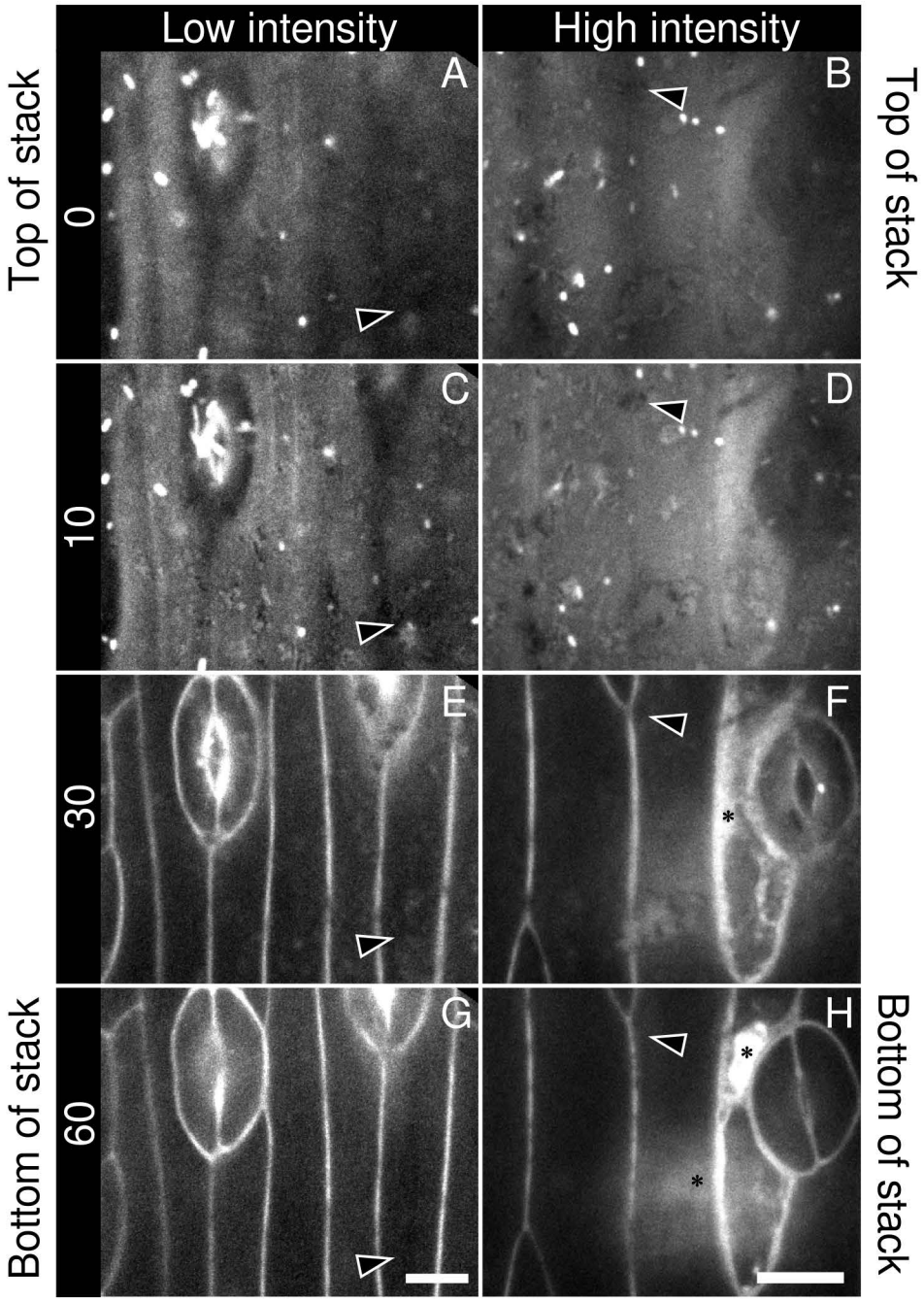

Figure 5-2: Establishing FRAP parameters that do not damage stem epidermal cells. The columns of micrographs represent two z-series acquired after irradiation with the photobleaching laser. Fluorescence is from propidium iodide. The numbers represent the depth of the image shown in the z-series. Zero is the the top of the z-series and 60 approaches the middle of the cell. (A,C,E,G) An arrowhead indicates the approximate area where photobleaching occurred. (F,H) Asterisks indicate nuclei. The low intensity settings used were 250 ms dwell time, the time that the laser spent bleaching the sample, at 100% laser intensity. (B,D,F,H) High intensity settings included 1000 ms laser dwell time at 100% laser intensity. In both experiments the bleaching laser was the 488 nm laser. Bar = 8.5 μm.

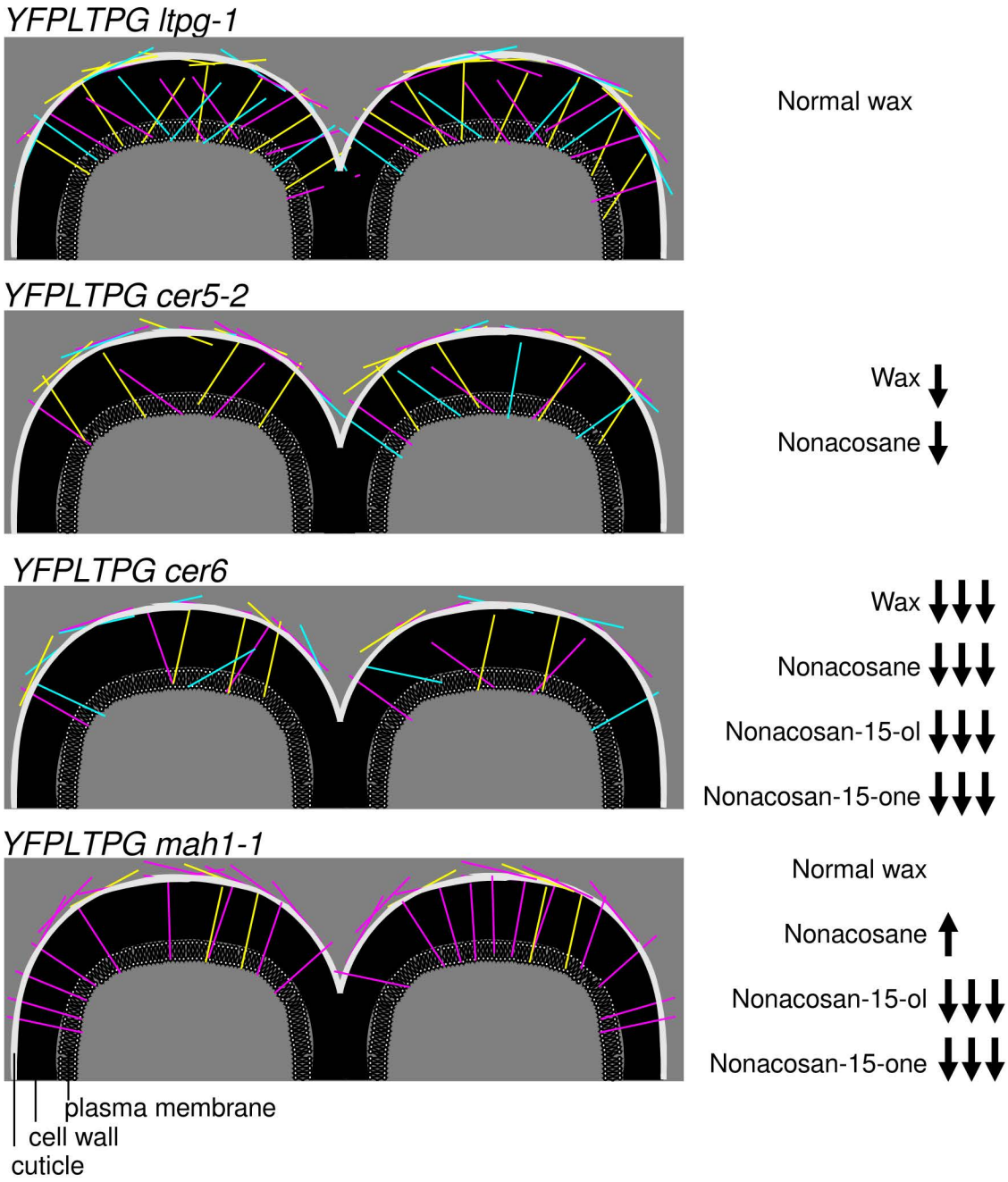

Figure 5-3: Models depicting hypothesized flux of cuticular lipids moving through the epidermal cells of *YFP-LTPG* in *ltpg-1* background compared with those of genotypes *YFP-LTPG* in *cer5-2, YFP-LTPG* in *cer6*, and *YFP-LTPG* in *mah1-1*. *YFP-LTPG ltpg-1* is a complemented line with the wild type wax load. Magenta, yellow, and cyan lines indicate nonacosane, nonacosan-15-ol, and noncosan-15-one, respectively. The cytoplasm is omitted from the diagram. Cells are not drawn to scale.

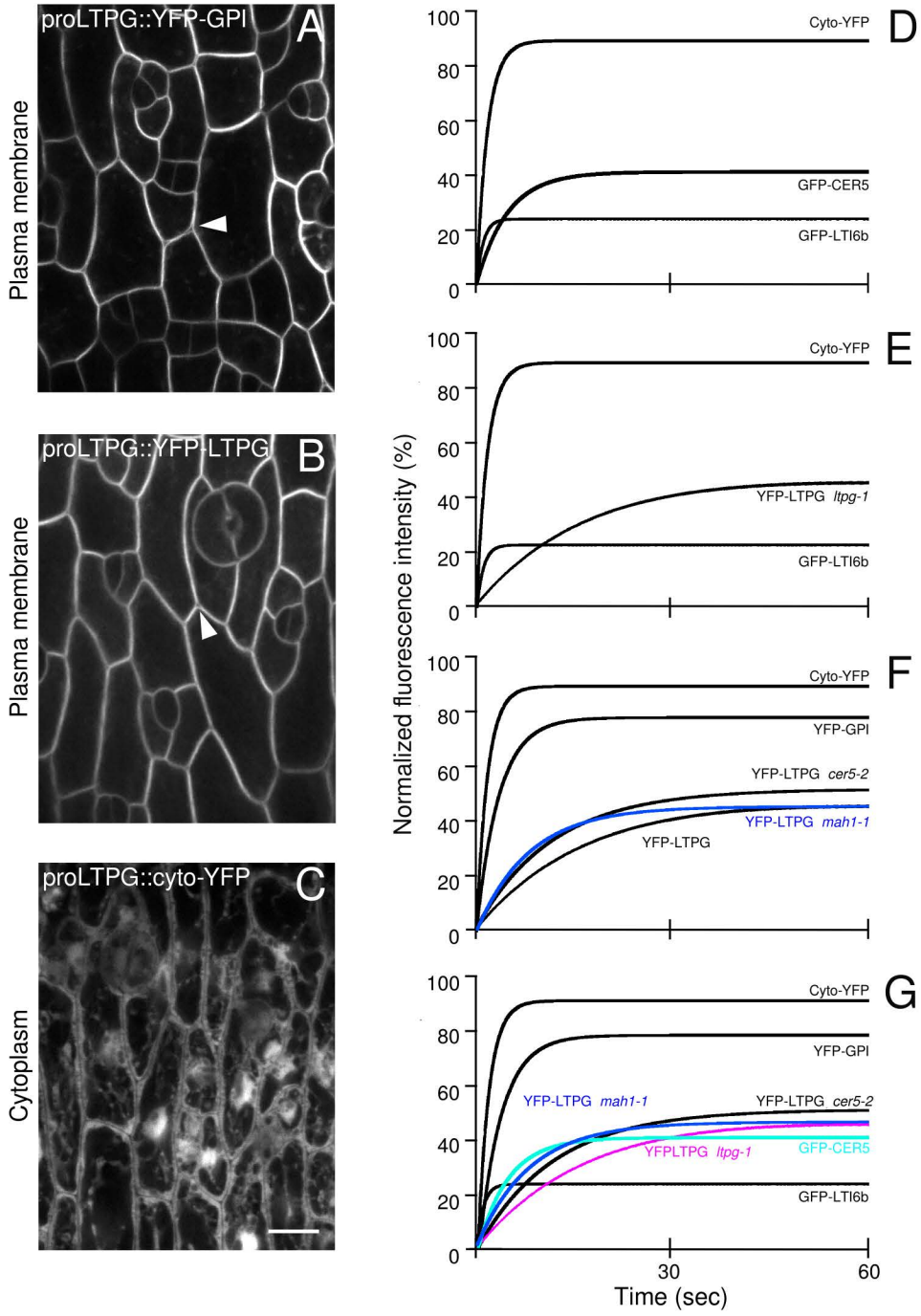

Figure 5-4: Localization of YFP-GPI and cyto-YFP compared with YFP-LTPG and representative fluorescence recovery curves for indicated constructs expressed in various genetic backgrounds. Synthetic YFP-GPI targets to the plasma membrane (A) exactly as YFP-LTPG (B). Arrowheads indicate areas where plasma membranes are distinct from one another. (C) Cyto-YFP accumulates in the cytoplasm (D-G) Normalized fluorescence is on the y-axis and time is shown on the x-axis. (D-G) The fluorescence recoveries of cyto-YFP and YFP-LTPG are compared with each genotype indicated. (G) The recovery curves shown in panels D through F are superimposed. Colored lines are used to distinguish overlapping recovery curves. Bar = 10 μm.

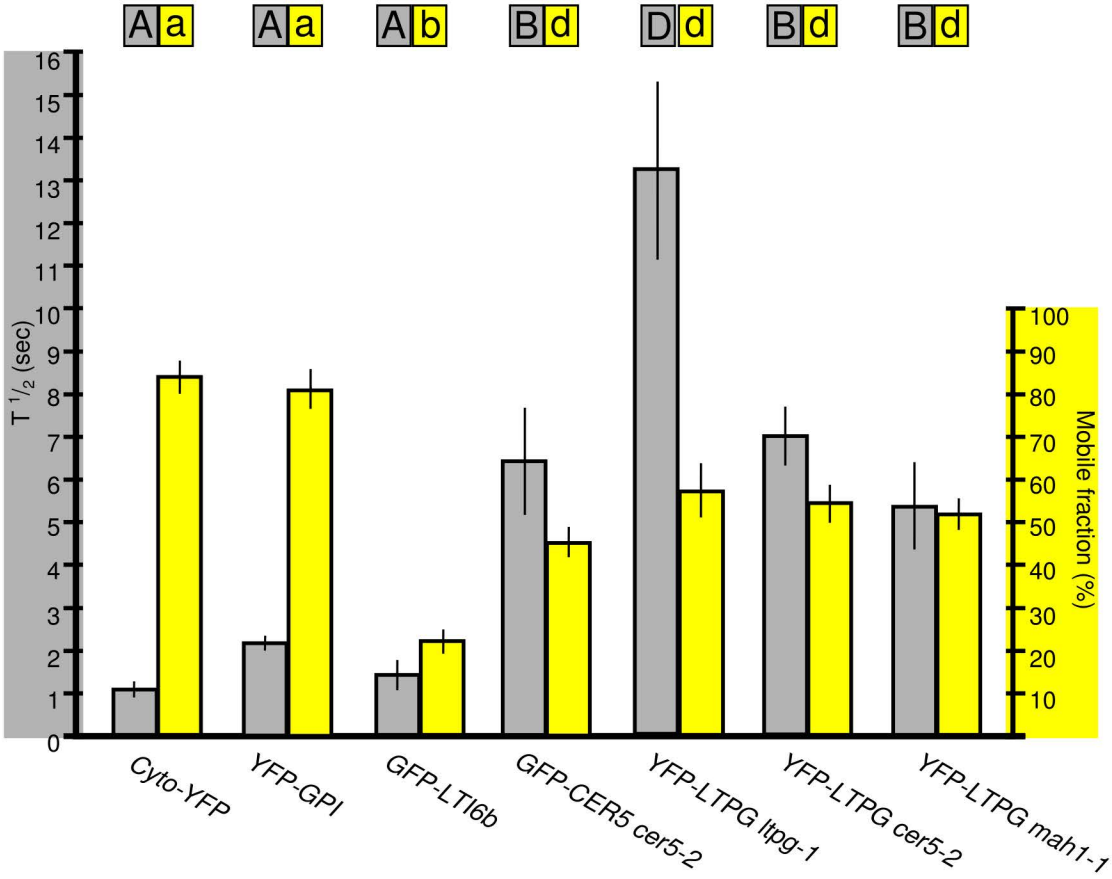

Figure 5-5: A comparison of the mobile fractions and half-times of recovery ($T_{1/2}$) for plant lines expressing the constructs shown (x-axis). Bars shown in gray and yellow indicate averages with standard error for $T_{1/2}$ and mobile fractions. *Cyto-YFP, YFP-GPI,* and *GFP-LTI6b* are expressed in the WT (Col-0) genetic background. *YFP-LTPG* and *GFP-CER5* are expressed in the genetic backgrounds indicated. Data points not linked by the same letter are significantly different, $P < 0.05$, as determined by Kruskal-Wallis analysis. Data is for a maximum of 3 FRAP events per cell for 6-12 plants per genotype. At least 2 biological replicates are shown.

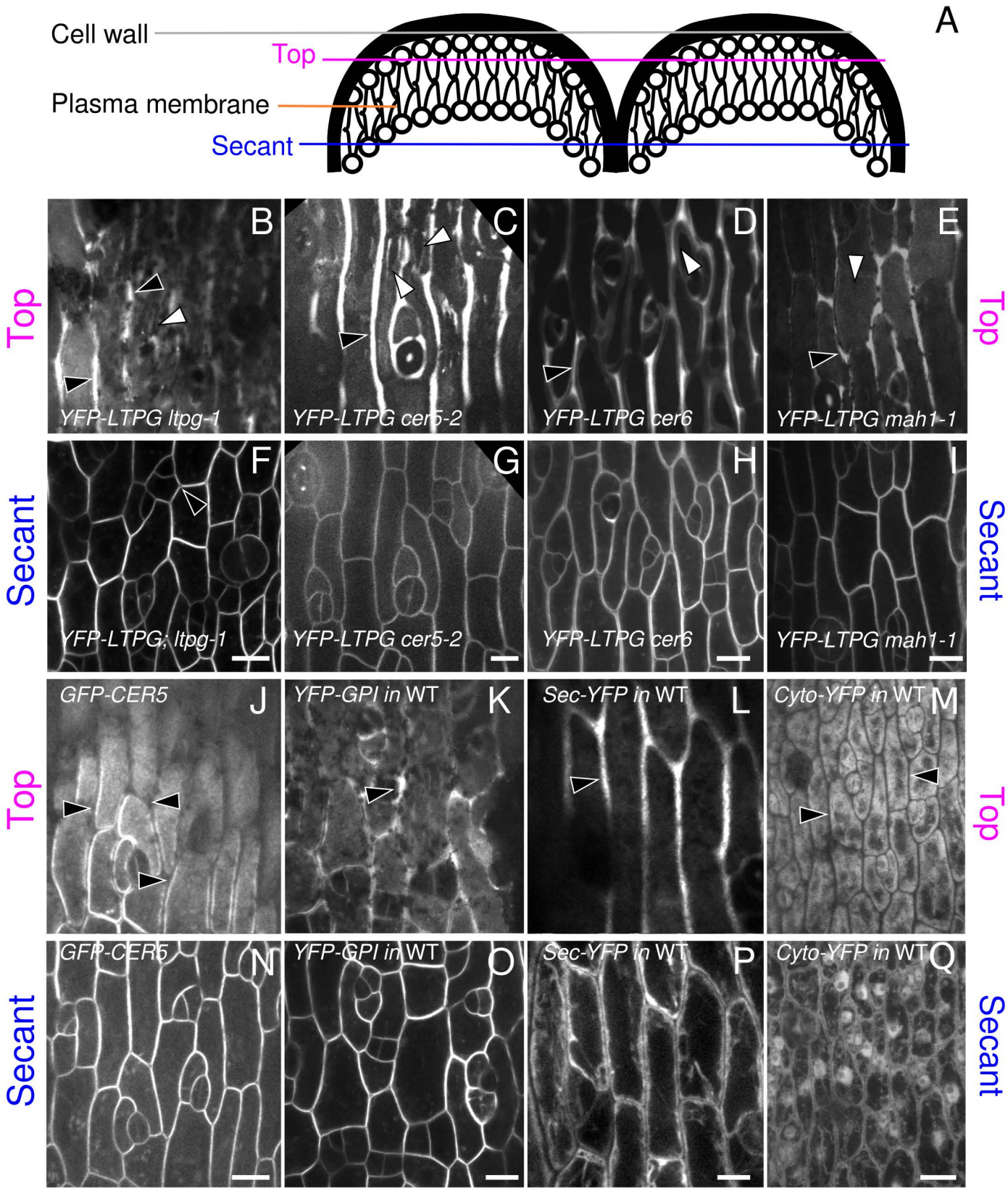

Figure 5-6: Comparison of the top and secant planes of stem epidermal cells expressing the indicated constructs.

Figure 5-6: *Continued from previous page*. Comparison of the top and secant planes of stem epidermal cells expressing the indicated constructs. (A) Top refers to the plane of an epidermal cell that is proximal to the external environment. Secant refers to a plane approximately at the midline of the epidermal cell. (B-E) Cells expressing YFP-LTPG display an accumulation of fluorescence along cell walls (closed arrow heads). (F-I) The observed cell wall accumulation does not occur in the secant planes of the same cells. (B) YFP-LTPG displays accumulation of fluorescence along long walls (closed arrow heads) and its surface displays spots from where fluorescence is absent (open arrow). (C-D) In the *cer5-2* and *cer6* genetic backgrounds, YFP-LTPG accumulates at the cell wall region such that ovoid areas appear to occlude fluoresence (open arrow heads). (J) The tops of cells expressing *GFP-CER5* do not display fluorescence in the cell wall. (K-L) Like YFP-LTPG, YFP-GPI accumulates over long cell walls of epidermal cells (closed arrow heads). (M) Negative control, cytoplasmic YFP (cyto-YFP), does not display cell wall fluorescence. (N-P) Exactly as *YFP-LTPG* expressing cells, GFP-CER5, GPI-linked YFP (YFP-GPI), and secreted YFP (sec-YFP) do not display cell wall localizations at secant planes. (Q) Cyto-YFP is is expressed in the cytoplasm only and is used as a negative control. Bars = 8.5 µm.

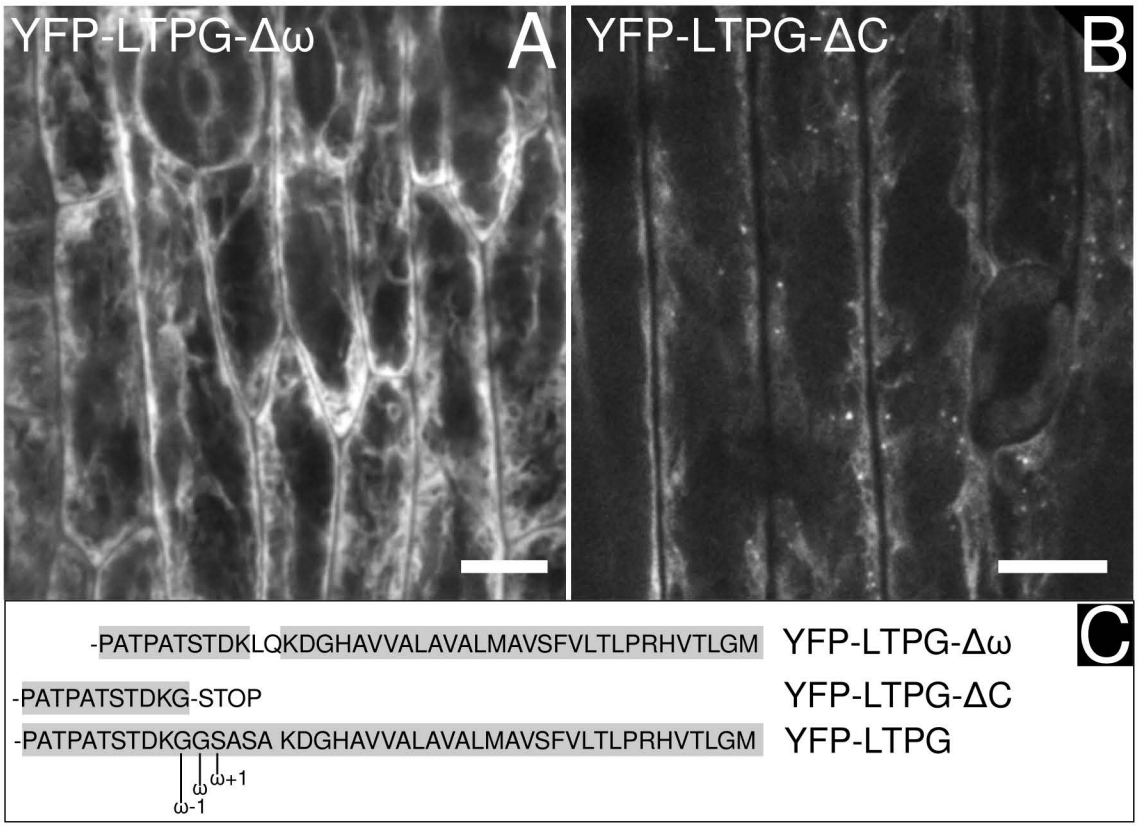

Figure 5-7: When the ω-site or carboxy terminus of YFP-LTPG is altered, mislocalization occurs. (A) YFP-LTPG-Δω contains a deletion of the predicted ω-site residue and the amino acids on either side. (B) The carboxy terminus of YFP-LTPG-Δc is deleted in the predicted ω-site residue and is replaced with a stop codon. In both transgenic plants, this construct is mislocalized, accumulating intracellularly. The fluorescence is consistent with ER, and bright foci which are consistent with the endomembrane system. (C) The final 43 amino acids of YFP-LTPG are compared (grey background) with the carboxy terminii of YFP-LTPG-Δω and YFP-LTPG-Δc. The ω-region of YFP-LTPG is indicated. Amino acid sequences not on grey background represent introduced changes to the primary sequence.

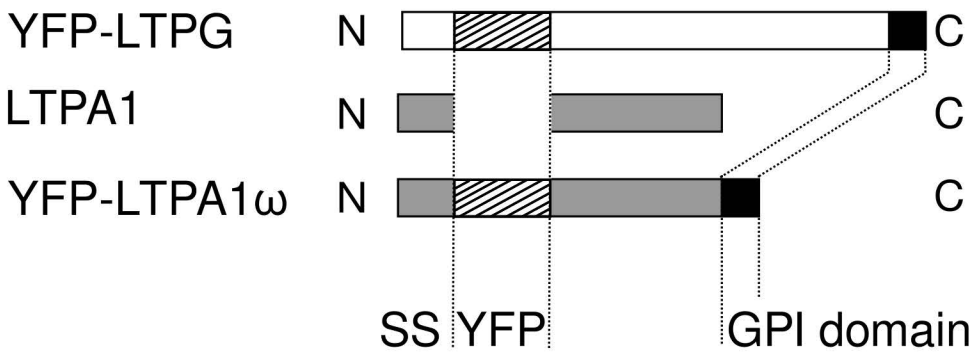

Figure 5-8: YFP-LTPA1ω is a fusion of the LTPA1 amino-terminal signal secretion sequence (SS), YFP and the GPI domain from LTPG. LTPG (white), LTPA (grey) and YFP (hatched) are shown The GPI domain is depicted as a closed box.

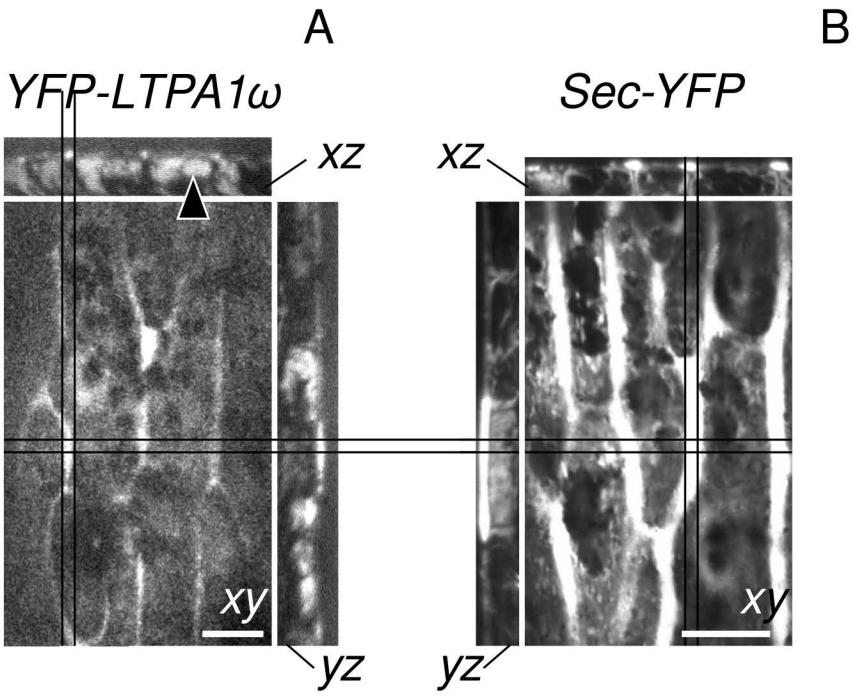

Figure 5-9: The surfaces of epidermal cells expressing YFP-LTPAω, and sec-YFP are compared using orthogonal series. Cross hairs relate the postition of fluoresence displayed in the XY plane with the XZ and YZ planes. (A) YFP-LTPAω accumulates in the cell wall, appearing as bright foci above the perimeter of epidermal cells. Closed arrow indicates fluorescence pattern consistent with vacuole. (B) Similarly, Sec-YFP is enginereed to accumulate in the cell wall. Sec-YFP accumulates heavily over the length of cell walls resulting in extremely bright foci. Bars 8.5 μm.

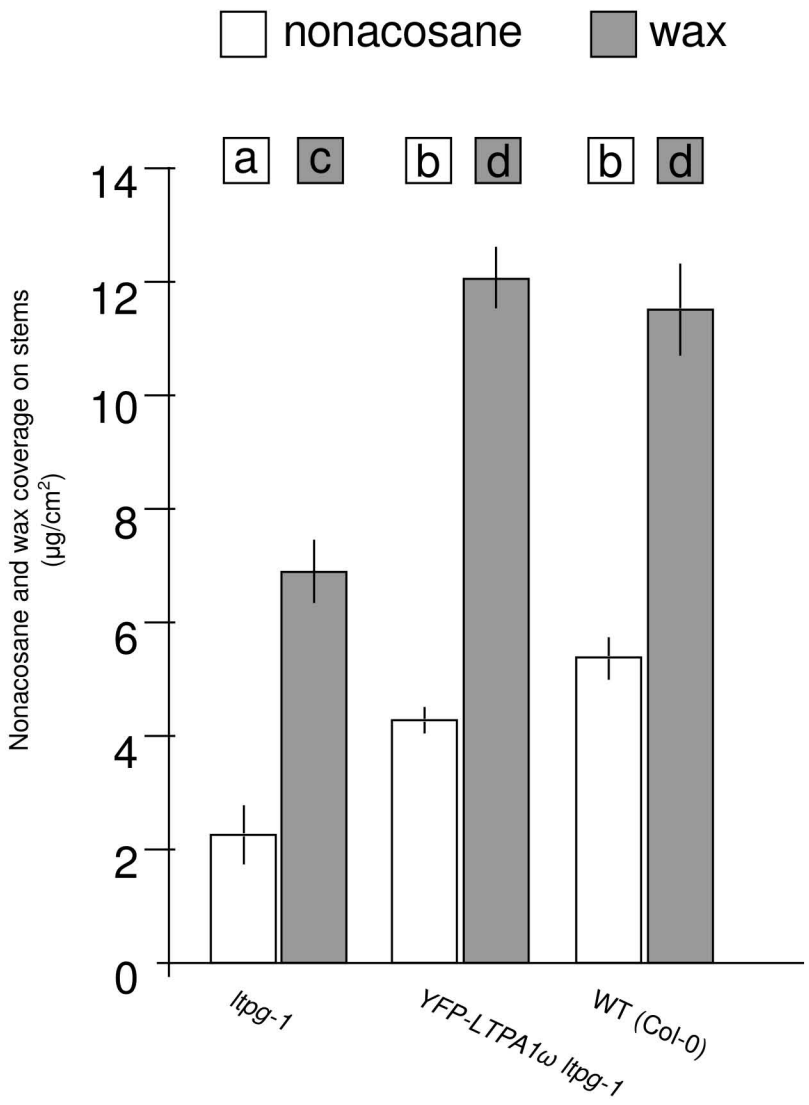

Figure 5-10: *YFP-LTPA1ω* restores the nonacosane and wax to the stems of *ltpg-1* mutants. Bars represent the average with standard error for a given compound. Bars not linked with the same letter are statistically significant, $P < 0.05$, after Kruskal-Wallis analysis. Data is representive of at least 5 stems from two independent biological replicates. WT (Col-0) and *ltpg*-1 n=10 each. YFP-LTPA1ω ltpg-1, n = 17.

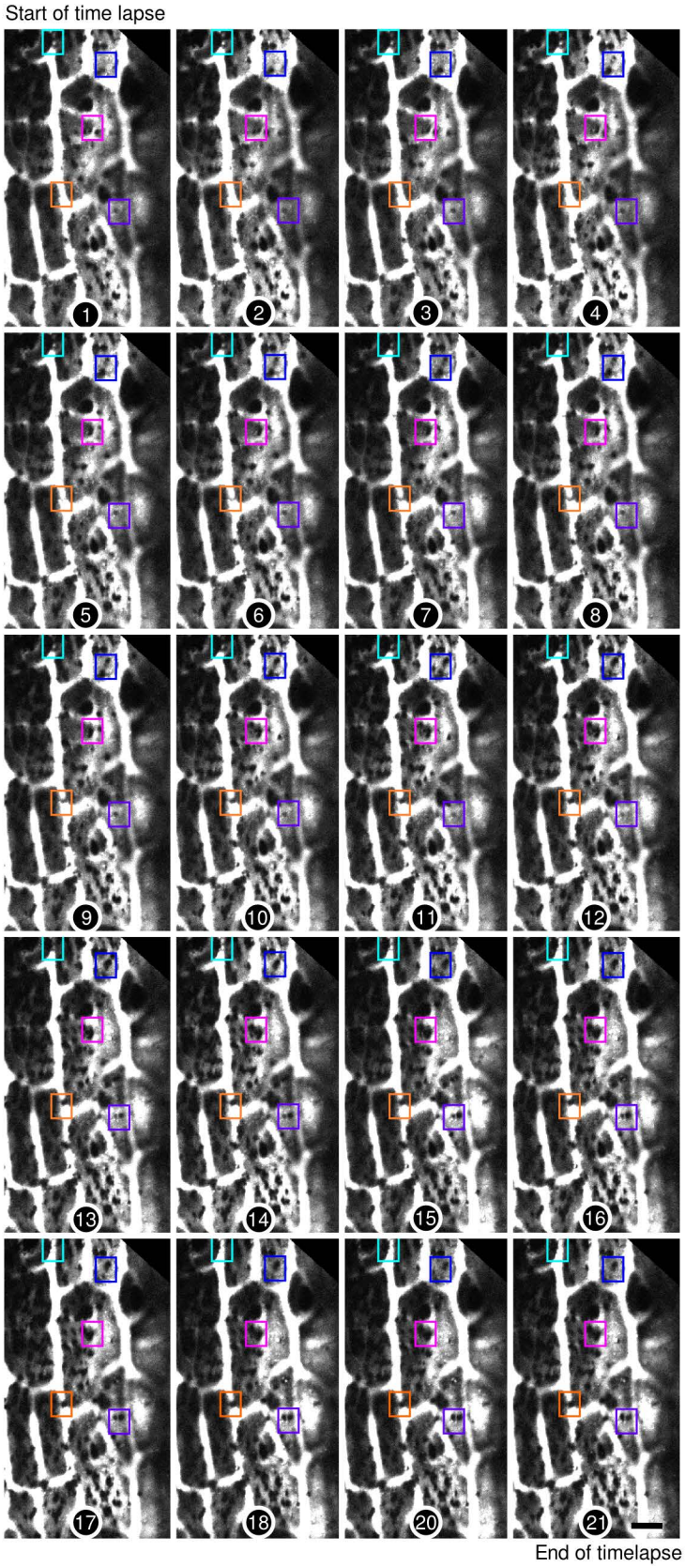

Figure 5-11: The dynamic nature of YFP-LTPG at the cuticle-cell wall interface. *Caption is continued on next page.*

Figure 5-11: *Continued from previous page.* The cuticle-cell wall interface of YFP-LTPG displays irregular areas that lack fluorescence. These spots are dynamic, and over time, become fluorescent (*i.e.* in-fill of spots with fluorescence). Conversely, fluorescing areas form where fluorescence becomes occluded (*i.e.* fluorescing region form spots without fluoresence). Each panel displays one optical section from a z-series acquired once per minute, over 20 min (time is shown in closed circles). Matched, colored, square outlines indicate a region of changing fluoresence. Bar is 10 μm.

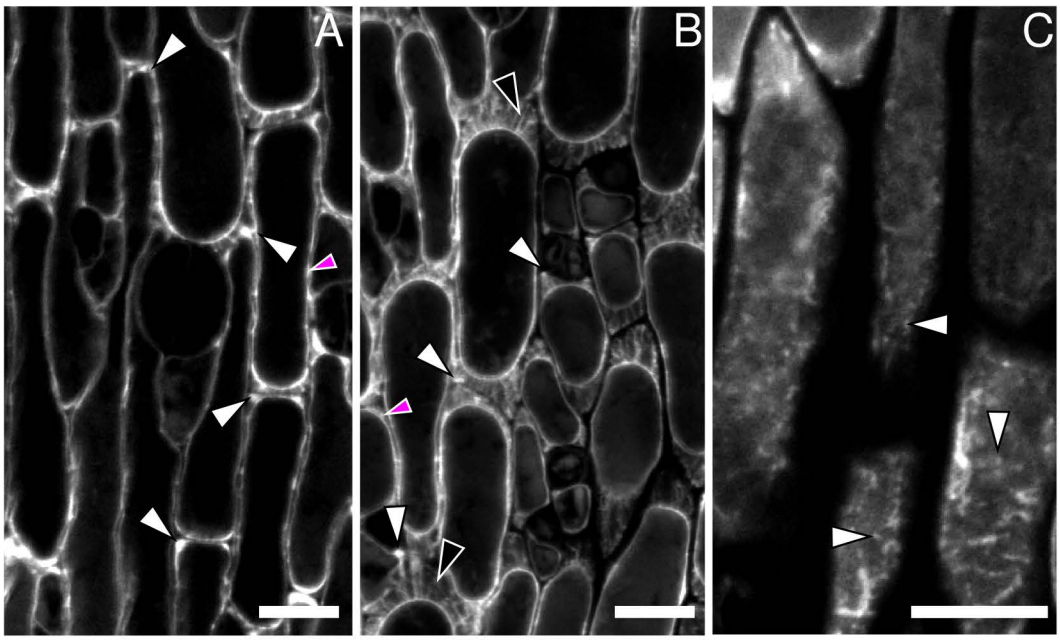

Figure 5-12: Plasmolysis of stem epidermal cells expressing YFP-LTPG reveals most fluorescence is associated with the plasma membrane and the junctions of epidermal cells. When cells were plasmolyzed with 4% NaCl for 30 s cells displayed Hechtian strands and intense fluoresence at the junctions or cell corners. (A) Mild plasmolysis shows YFP-LTPG displays fluorescence accumulation in cell corners (open arrow heads) prior to Hechtian strand formation. (B) When plasmolysis persists Hechtian strands are observed (closed arrow heads); bright foci at cell corners are still visible (open arrow heads). Magenta arrow heads indicate areas during plasmolysis where YFP-LTPG is found in the cell wall spaces. (C) At the surface of cells plasma membrane localized YFP-LTPG appears as small bright spots (arrow heads), presumed to be areas of adhesion where the membrane pulls away from the cell wall located directly above. Bars = 10 μm.

6. Future research directions

6.1 Research summary

LTPs were identified as intracellular lipid shuttles, moving phosphatidylglycerol between microsomal (ER derived) to chloroplast membranes (Kader et al., 1984). This line of thinking was abandoned when sequence analysis from an Arabidopsis LTP showed the presence of signal secretion sequences (Bernhard et al., 1991) and carrot cell cultures were shown to secrete an LTP into their growth medium (Sterk et al., 1991).

My thesis work addressed the objectives set out in chapter 1 (Section 1.9). By isolating homozygous mutants disrupted by T-DNA insertion and RNAi, I showed that LTPG is required in wax transport (Objective 1 and 2, Chapter 3). I found no evidence that three other strongly expressed LTPs in the cuticle are involved in wax transport (Objective 1, Chapter 3 and 4). Complementation of the *ltpg-1* mutant with the YFP-tagged and non-tagged versions of LTPG confirmed that mutation at this locus was responsible for the observed wax reduction phenotype (Objective 2, Chapter 3). By expressing LTPG in bacteria and testing binding to a lipophilic probe, TNS, I showed that this protein possessed a hydrophobic binding cavity (Objective 3, Chapter 3). By performing a sequence analysis, I showed that LTPs have little primary sequence consensus but they exhibit similar, alpha-helix secondary structures (Objective 1, Chapter 4). Alteration of the GPI domain resulted in aberrant trafficking of the modified LTPG indicating the importance of this post-translational modification for proper targeting. FRAP studies of YFP-LTPG showed the protein is relatively immobile and has a slow rate of recovery. While the cuticular lipid traffic through the plasma membrane had no effect on the mobile fraction, it appeared to increase the rate of lateral diffusion (Chapter 5, Objective 5). Finally, by creating a synthetic GPI-linked LTP, I showed that YFP-LTPA1ω accumulates in the cell wall and the vacuole, with this pattern of localization, complements *ltpg-1* mutants (Chapter 5, Objectives 6 and 7). The sum of these data places LTPG in the plasma membrane-cell wall- interface, as a

protein that is associated with the cell wall and involved in lipid transport. The cell wall may exert a restrictive force on LTPG resulting in its slow lateral diffusion in the plasma membrane. My bioinformatic analyses closely match the only other bioinformatics study that includes GPI-linked LTPs (Edstam et al., 2011); LTP secondary structure is largely similar. The similarity of secondary structure among LTPs, likely contributed strongly to the exchangeability of the LTPG domain for the LTPA1 hydrophobic cavity domain. A number of questions, however, are unanswered: 1. How does YFP-LTPG become wall associated? 2. Does wall association result in slow dynamics? 3. Is there a cytoplasmic component to the slow dynamics observed? 4. Are membrane proteins retarding LTPG dynamics? The following sections detail some experiments to address these questions and possible outcomes.

6.2 Studying cell wall associated LTPG

The experiments presented in chapter 5 show that LTPG accumulates in the cell wall. It is known that phospholipases can release GPI proteins from membranes although their action has not been documented *in planta* (Svetek et al., 1999). In this section, the following experiments will address tracking released YFP-LTPG and the development of an inducible system for GPI protein release *in planta*. Photoactivatable fluorescent proteins (FPs) can be used to study YFP-LTPG after release from the plasma membrane. Modern photoactivatable FPs are monomeric, photostable, and can be photoactivated to track a subset of proteins within the population without introducing unwanted dimerization (McKinney et al., 2009; Mathur et al., 2010). An example of such a protein is EOS (Mathur et al., 2010). Photoactivatable FPs change color over time upon photoactivation (*e.g.* green to red emission change). Moreover, my work with FRAP has determined a safe laser intensity threshold that will not damage stem epidermal cells. EOS is a fluorescent protein that has been used successfully *in planta* (Mathur et al., 2010). With this technology it may be possible to track the population of YFP-LTPG that putatively moves from the plasma membrane into the cell wall; real-time assessments of how long it takes for YFP-

LTPG to gain cell wall localization could be made and possibly related to rates of wax secretion *in planta*.

LTPG accumulates in the middle lamella region of the cell wall. Is the localization in the middle lamella region permanent or transient? EOS-tagged LTPG can be used to address this question. One scenario is that an EOS-tagged LTPG associates stably or transiently with the cell wall and does not leave the middle lamella region; EOS-LTPG would then undergo the green to red color change, and the two populations would not be separated in space. If EOS-LTPG were to become stably associated with the cell wall (starting as a green fluor), given enough time, the entire fluorescence signal corresponding to the middle lamella region would fluoresce green. New EOS-LTPG, upon photoactivation, would fluoresce red. Using spectral imaging-equipped instruments, such as the Zeiss Meta 510 and Olympus Fluoview Multiphoton microscopes, it is possible to perform ratiometric fluorescence quantification: an area is scanned for the fluorescence contribution of a red fluorophore or lingering green fluorophores.

Missing in the studies of plant GPI-linked proteins is a system to study the release of these proteins from the plasma membrane. The bacterial phospholipase of *Bacillus cereus* has been used to release GPI proteins from callus plant tissue (Sherrier et al., 1999; Borner et al., 2005). My attempts to use phospholipase C on intact plant tissue gave unreliable and highly variable results (data not shown). Briefly, some of the YFP-LTPG fluorescence corresponding to the outside periclinal face became dimmer. I propose future experiments to probe LTPG GPI-linkage cleavage involving an inducible promoter system to express human GPI-phospholipase D (GPI-PLD). If developed, this system would be comprised of the dexamethasone (DEX)-inducible promoter from pTA7001 (Aoyama and Chua, 1997), and *Homo sapiens* glycosylphosphatidylinositol-specific phospholipase D1 (GPLD1'; Genbank accession L11701). This promoter provides constitutive expression upon application of DEX at concentrations as low as 0.1 μM and is typically used at 1 μM (Wang et al., 2001). GPI-PLD is known to cleave

GPI protein linkage between phosphate and inositol in COS [CV-1 (simian) in Origin, and carrying the SV40 genetic material] cells, GPI-linked heparin sulfate proteoglycan from human bone marrow cells, and decay accelerating factor-expressing HeLa cells (Scallon et al., 1991; Brunner et al., 1994; Metz et al., 1994). When the sequence for hsGPI-PLD is compared with known Arabidopsis proteins, no homologues are found despite the presence of PLDs in multiple plant genomes. I propose that future studies of LTPG release consider the engineering of the DEX promoter fused to hsGPI-PLD and mRFP. In this way, GPI-PLD, can be induced with DEX and monitored for the red fluorescence emission from mRFP. The expected outcome for this construct would be the creation of a system that can release LTPG from the plasma membrane. This is predicted to increase cell wall-associated, while decreasing plasma membrane YFP-LTPG. Despite the rapid ontogeny of the model plant Arabidopsis, generating stable transformants is a long process. These constructs need not be stably introduced into the Arabidopsis genome. The FAST technique can be used to transiently transform Arabidopsis seedlings (Li et al., 2009); members of the Wasteneys lab have transformed at least five constructs into Arabidopsis seedlings, among which is YFP-LTPG (personal communication, Drs. Chris Ambrose and Sylwia Jancowski).

6.3 Protein-protein interactions as restrictive force?

In chapter 5, I demonstrated that YFP-LTPG has a relatively slow lateral diffusion in the plasma membrane, touching upon explanations such as interaction with membrane bound proteins or multimerization of LTPG among others. YFP-LTPG recovery was faster when expressed in the *cer5-2* genetic background. It is unknown whether there are *bona fide* interactions/associations of YFP-LTPG with other membrane proteins. I propose that future experiments addressing this take advantage of the microscopy technology by performing fluorescence resonance energy transfer (FRET) (Pietraszewska-Bogiel and Gadella, 2011).

Fluorescent constructs exist for all of the proteins studied and they are easily modified to have appropriate FRET fluorescent protein pairs (*e.g.* cyan-yellow; yellow-red). If LTPG recovers slowly as a result of multimerization or interaction with GFP-CER5, FRET can be used, with modified LTPG constructs to determine if LTPG interacts with itself or with GFP-CER5. This experiment would require alteration of GFP-CER5 from its present form to move the FP such that it faces the cell wall instead of the cytoplasm.

Alternatively, biochemical procedures can be used to investigate whether simple interactions occur. A traditional protein biochemistry approach will not distinguish recovery of a monomeric YFP-LTPG from putative multimeric YFP-LTPG. Fluorescence resonance energy transfer (FRET) is capable of determining LTPG-LTPG and LTPG-CER5 interaction whereas traditional biochemical experiments may discover unexpected associated proteins (*e.g.* an unexpected membrane protein). Both experimental approaches contribute information and may be used in a complementary fashion. Using α-GFP chromatography beads, it is possible to harvest YFP-LTPG protein from stems and determine if other proteins co-purify. This method requires that protein sequencing is performed to identify if other proteins co-purify with YFP-LTPG. Proteins associated/interacting with LTPG may help explain the observed membrane dynamics. If, however, these experiments fail to identify LTPG-associated proteins, then LTP glycosylation should be considered for further study.

6.4 Glycosylation as a restrictive force?

The slow recovery of YFP-LTPG could be, in part, due to the restrictive force exerted by the cell wall. How might the cell wall restrict YFP-LTPG recovery? Examination of the LTPG lipid-binding domain with *in silico* tool NetNGlyc (Gupta et al., 2004) suggests glycosylation may occur at amino acids NASI and NATT. This is further supported by my *Pichia* recombinant LTPG protein studies (Chapter 3). I propose that a version, or versions, of YFP-LTPG be created to delete glycosylation sites. Using these modified proteins in FRAP experiments; it may

be determined if the absence of glycosylation results in shorter recovery times, and whether LTPG, like FORMIN1, has its mobility restricted by the cell wall (Martinière et al. 2011).

6.5 Maximum protein size that can be secreted into the middle lamella of the cell wall.

YFP-LTPG was found in the middle lamella region of the cell wall. To investigate whether the protein moves through anticlinal cell walls to the cuticle, I propose that the secreted YFP construct be re-engineered as a multimer. Modifying secreted YFP by creating a number of constructs with varying numbers of YFP (*e.g.* from two to five), one would be able to use a common cell biology tool to determine the maximum protein size that can be exported from the epidermal cell wall; this information can be compared with, biochemical measurements (Tepfer and Taylor, 1981; Baron-Epel et al., 1988).

6.5.1 Linking pectin characteristics to wax export: creating a larger exit point.

Finding YFP-LTPG in the middle lamella region of the cell wall is highly intriguing. This result suggests there may be a link between cell wall biosynthesis and LTPG traffic. I propose using the *galacturonosyltransferase1* (*GAUT*) genes to study accumulation of YFP-LTPG in the middle lamella. GAUTs belong to a multigene family that catalyzes the synthesis of pectin (Sterling et al., 2006). The expression patterns of many GAUT genes have been characterized. Two members of the GAUT family, *guat8/At3g25140* and *guat12*/At5g54690 have publicly available SALK T-DNA insertion mutant lines that display reduced and abolished gene expression, respectively (Caffall et al., 2009). The middle lamella of *gaut* mutants is compromised owing to impaired pectin assembly (via homogalacturonic acid biosynthesis). Because such mutants have compromised middle lamellae they may display cell wall structural integrity problems in the region where YFP-LTPG is shown to accumulate, I hypothesize that YFP-LTPG will accumulate to a greater abundance than observed for YFP-LTPG *ltpg-1* plants. Expression of YFP-LTPG in *gaut* mutants may result in more stem cuticular wax than observed in wild type plants. On the other hand, the wax transport machinery may be limited by substrates

generated from the cuticular lipid biosynthetic machinery in the ER. Therefore, combining *gaut* mutants with multi-gene expression cassettes (discussed in Chapter 4; Wu et al., 2005; Li et al., 2010; Lu et al., 2011) containing crucial biosynthetic and transport proteins such as CER6, CER8, MAH1, CER5, LTPG, among others, may generate plants with more wax or tailored plant wax compositions for biotechnology.

6.6 How does YFP-GPI surface accumulation compare with that of YFP-LTPG?

Whether changes in the extracellular accumulation pattern of YFP-LTPG in the various mutant backgrounds are attributed to the GPI or the LTP domains is unknown. YFP-LTPG accumulated differently at the plant surface when expressed in genotype *ltpg-1* versus *cer5-2, cer6* and *mah1-1* plants. YFP-GPI accumulated extracellularly, appearing indistinguishable from YFP-LTPG. The YFP-GPI construct that I made can be crossed into and expressed in the same mutant backgrounds, *cer5-2, cer6* and *mah1-1*, and the secant and top planes of stem epidermal cells can be examined to determine if the accumulation is similar to YFP-LTPG, *i.e.* fluorescence occurs only over the long walls. If fluorescence of YFP-GPI resembles YFP-LTPG in the various mutant backgrounds, then one might conclude that the change in cuticular lipid flux affects, in some way, the GPI domain. Alternatively, if YFP-GPI does not display accumulation along the long cell walls and resembles YFP-LTPG in *ltpg-1* (wild-type condition), then one may conclude that the non-uniform accumulation is related to the LTP domain and its putative interactions with the pectins of the cuticular layer or the cuticle proper.

6.7 What does cell wall localized YFP-LTPG imply for the cell biology of cuticular lipid deposition?

LTPG is involved in wax export; it would seem that gene duplication has resulted in a number of Arabidopsis proteins (LTPs with significant homology to LTPA1 and/ or LTPG) with tertiary structures sufficient to transport wax. The work of Pyee and Kolattukudy (1995), and that described by Jefferee (2006) details the existence of osmiophilic or lipidic paths in the cell wall

extending into the cuticle. There appears to be a continuum between wax export and cell wall deposition/biosynthesis. My work shows the existence of a cell wall population of LTPG whose final localization is influenced by cuticular lipid flux. Future studies of lipid transfer proteins and wax biosynthesis will benefit from investigating the extent to which cuticular lipid deposition and cell wall assembly are linked.

Works Cited

Aarts M.G.M., Keijzer C.J., Stiekema W.J., and Pereira A. (1995). Molecular characterization of the *CER1* gene of Arabidopsis involved in epicuticular wax biosynthesis and pollen fertility. Plant Cell. **7,** 2115-2127.

Abdelkader A.B. and Mazliak P. (1970). Lipid exchange between mitochondria, microsomes and cytoplasmic supernatant of cells of potatoes and cauliflower. Eur. J. Biochem. **15,** 250-262.

Abrami L., Fivaz M., and van der Goot F.G. (2000). Adventures of a pore-forming toxin at the target cell surface. Trends Microbiol. **8,** 168-172.

Abramoff M., Magelhaes P., and Ram S. (2004). Image processing with ImageJ. Biophoton Int. **11,** 36-42.

Aharoni A., Dixit S., Jetter R., Thoenes E., Van Arkel G., and Pereira A. (2004). The SHINE clade of AP2 domain transcription factors activates wax biosynthesis, alters cuticle properties, and confers drought tolerance when overexpressed in Arabidopsis. Plant Cell. **16,** 2463-2480.

Alberts B., Johnson A., Lewis J., Raff M., Roberts K., and Walter P. Molecular biology of the cell. 2002. 497-510.

Allen E. and Howell M.D. (2010). miRNAs in the biogenesis of trans-acting siRNAs in higher plants. Semin. Cell Dev. Biol. **21,** 798-804.

Aoyama T. and Chua N.H. (1997). A glucocorticoid-mediated transcriptional induction system in transgenic plants. Plant J. **11,** 605-612.

Arondel V., Vergnolle C., Tchang F., and Kader J.C. (1990). Bifunctional lipid-transfer: fatty acid-binding proteins in plants. Mol. Cell. Biochem. **98,** 49-56.

Ausubel F., Brent R., Kingston R., Moore D., Seidman J., Smith J., and Struhl K. (1987). Current protocols in molecular biology. John Wiley & Sons.

Axelrod D., Koppel D., Schlessinger J., Elson E., and Webb W. (1976). Mobility measurement by analysis of fluorescence photobleaching recovery kinetics. Biophys. J. **16,** 1055-1069.

Bach L., Michaelson L.V., Haslam R., Bellec Y., Gissot L., Marion J., Da Costa M., Boutin J.P., Miquel M., and Tellier F. (2008). The very-long-chain hydroxy fatty acyl-CoA dehydratase PASTICCINO2 is essential and limiting for plant development. Proc. Natl. Acad. Sci. U. S. A. **105,** 14727-14731.

Bannai H., Tamada Y., Maruyama O., Nakai K., and Miyano S. (2002). Extensive feature detection of amino-terminal protein sorting signals. Bioinformatics **18,** 298-305.

Baron-Epel O., Gharyal P.K., and Schindler M. (1988). Pectins as mediators of wall porosity in soybean cells. Planta. **175,** 389-395.

Barthlott W. and Neinhuis C. (1997). Purity of the sacred lotus, or escape from contamination in biological surfaces. Planta. **202,** 1-8.

Beamer L.J., Carroll S.F., and Eisenberg D. (1997). Crystal Structure of Human BPI and Two Bound Phospholipids at 2.4 Angstrom Resolution. Science. **276,** 1861-1864.

Beaudoin F., Wu X., Li F., Haslam R.P., Markham J.E., Zheng H., Napier J.A., and Kunst L. (2009). Functional Characterization of the Arabidopsis β-Ketoacyl-Coenzyme A Reductase Candidates of the Fatty Acid Elongase. Plant Physiol. **150,** 1174-1191.

Beisson F., Koo A.J., Ruuska S., Schwender J., Pollard M., Thelen J.J., Paddock T., Salas J.J., Savage L., Milcamps A., Mhaske V.B., Cho Y., and Ohlrogge J.B. (2003). Arabidopsis genes involved in acyl lipid metabolism. A 2003 census of the candidates, a study of the distribution of expressed sequence tags in organs, and a web-based database. Plant Physiol. **132,** 681-697.

Bernhard W.R., Thoma S., Botella J., and Somerville C.R. (1991). Isolation of a cDNA clone for spinach lipid transfer protein and evidence that the protein is synthesized by the secretory pathway. Plant Physiol. **95,** 164-170.

Bhat R.A. and Panstruga R. (2005). Lipid rafts in plants. Planta **223,** 5-19.

Bird D., Beisson F., Brigham A., Shin J., Greer S., Jetter R., Kunst L., Wu X., Yephremov A., and Samuels L. (2007). Characterization of Arabidopsis ABCG11/WBC11, an ATP binding cassette (ABC) transporter that is required for cuticular lipid secretion. Plant J. **52,** 485-498.

Blilou I., Ocampo J.A., and Garcia-Garrido J.M. (2000). Induction of Ltp (lipid transfer protein) and Pal (phenylalanine ammonia-lyase) gene expression in rice roots colonized by the arbuscular mycorrhizal fungus Glomus mosseae. J. Exp. Bot. **51,** 1969-1977.

Böhme K., Li Y., Charlot F., Grierson C., Marrocco K., Okada K., Laloue M., and Nogué F. (2004). The Arabidopsis *COW1* gene encodes a phosphatidylinositol transfer protein essential for root hair tip growth. Plant J. **40,** 686-698.

Bonaventure G., Salas J.J., Pollard M.R., and Ohlrogge J.B. (2003). Disruption of the *FATB* gene in Arabidopsis demonstrates an essential role of saturated fatty acids in plant growth. Plant Cell. **15,** 1020-1033.

Borner G.H.H., Sherrier D.J., Stevens T.J., Arkin I.T., and Dupree P. (2002). Prediction of glycosylphosphatidylinositol-anchored proteins in Arabidopsis. A genomic analysis. Plant Physiol. **129,** 486-499.

Borner G.H., Sherrier D.J., Weimar T., Michaelson L.V., Hawkins N.D., Macaskill A., Napier J.A., Beale M.H., Lilley K.S., and Dupree P. (2005). Analysis of detergent-resistant membranes in Arabidopsis. Evidence for plasma membrane lipid rafts. Plant Physiol. **137,** 104-116.

Borner G.H.H., Lilley K.S., Stevens T.J., and Dupree P. (2003). Identification of Glycosylphosphatidylinositol-Anchored Proteins in Arabidopsis. A Proteomic and Genomic Analysis. Plant Physiol. **132,** 568-577.

Brandizzi F., Frangne N., Marc-Martin S., Hawes C., Neuhaus J.M., and Paris N. (2002). The destination for single-pass membrane proteins is influenced markedly by the length of the hydrophobic domain. Plant Cell **14,** 1077-1092.

Breu V., Guerbette F., Kader J., Kannangara C., Svensson B., and Von Wettstein-Knowles P. (1989). A 10 kD barley basic protein transfers phosphatidylcholine from liposomes to mitochondria. Carlsberg Res. Commun. **54,** 81-84.

Brody J.R. and Kern S.E. (2004). Sodium boric acid: a Tris-free, cooler conductive medium for DNA electrophoresis. BioTechniques **36,** 214-217.

Broun P., Poindexter P., Osborne E., Jiang C.Z., and Riechmann J.L. (2004). WIN1, a transcriptional activator of epidermal wax accumulation in Arabidopsis. Proc. Natl. Acad. Sci. U. S. A. **101,** 4706-4711.

Bruce C., Chouinard R.A., and Tall A.R. (1998). Plasma Lipid Transfer Proteins, High-density Lipoproteins, and Reverse cholesterol transport. Annu. Rev. Nutr. **18,** 297-330.

Brunner G., Metz C., Nguyen H., Gabrilove J., Patel S., Davitz M., Rifkin D., and Wilson E. (1994). An endogenous glycosylphosphatidylinositol-specific phospholipase D releases basic fibroblast growth factor-heparan sulfate proteoglycan complexes from human bone marrow cultures. Blood **83,** 2115-2125.

Buhot N., Gomes E., Milat M.L., Ponchet M., Marion D., Lequeu J., Delrot S., Coutos-Thevenot P., and Blein J.P. (2004). Modulation of the biological activity of a tobacco LTP1 by lipid complexation. Mol. Biol. Cell **15,** 5047-5052.

Caffall K.H. and Mohnen D. (2009). The structure, function, and biosynthesis of plant cell wall pectic polysaccharides. Carbohydr. Res. **344,** 1879-1900.

Caffall K.H., Pattathil S., Phillips S.E., Hahn M.G., and Mohnen D. (2009). Arabidopsis thaliana T-DNA Mutants Implicate *GAUT* Genes in the Biosynthesis of Pectin and Xylan in Cell Walls and Seed Testa. Mol. Plant. **2,** 1000-1014.

Cameron K.D., Moskal W.A., and Smart L.B. (2006a). A second member of the Nicotiana glauca lipid transfer protein gene family, *NgLTP2*, encodes a divergent and differentially expressed protein. **33,** 141-152.

Cameron K.D., Teece M.A., and Smart L.B. (2006b). Increased Accumulation of Cuticular Wax and Expression of Lipid Transfer Protein in Response to Periodic Drying Events in Leaves of Tree Tobacco. Plant Physiol. **140,** 176-183.

Capel J., Jarillo J.A., Salinas J., and Martinez-Zapater J.M. (1997). Two homologous low-temperature-inducible genes from Arabidopsis encode highly hydrophobic proteins. Plant Physiol. **115,** 569.

Caro L., Tettelin H., Vossen J., Ram A., Van Den Ende H., and Klis F. (1997). *In silicio* identification of glycosyl-phosphatidylinositol-anchored plasma-membrane and cell wall proteins of Saccharomyces cerevisiae. Yeast **13,** 1477-1489.

Chae K., Kieslich C.A., Morikis D., Kim S.C., and Lord E.M. (2009). A Gain-of-Function Mutation of Arabidopsis Lipid Transfer Protein 5 Disturbs Pollen Tube Tip Growth and Fertilization. Plant Cell **21,** 3902-3914.

Chapman M.A., Leebens-Mack J.H., and Burke J.M. (2008). Positive Selection and Expression Divergence Following Gene Duplication in the Sunflower *CYCLOIDEA* Gene Family. Molecular Biology and Evolution **25,** 1260-1273.

Champigny, M.J., Shearer, H., Mohammad, A., Haines, K., Neumann, M., Thilmony, R., He, S-H., Fobert, P., Dengler, N. and Cameron R.K. (2011). Localization of DIR1 at the tissue, cellular and subcellular levels during Systemic Acquired Resistance in Arabidopsis using DIR1:GUS and DIR1:EGFP reporters. BMC Plant Biology, **11**:125.

Charvolin D., Douliez J.P., Marion D., Cohen-Addad C., and Pebay-Peyroula E. (1999). The crystal structure of a wheat nonspecific lipid transfer protein (ns-LTP1) complexed with two molecules of phospholipid at 2.1 Å resolution. Eur. J. Biochem. **264,** 562-568.

Chassot C., Nawrath C., and Métraux J.P. (2007). Cuticular defects lead to full immunity to a major plant pathogen. Plant J. **49,** 972-980.

Chen X., Goodwin S.M., Boroff V.L., Liu X., and Jenks M.A. (2003). Cloning and characterization of the *WAX2* gene of Arabidopsis involved in cuticle membrane and wax production. Plant Cell **15,** 1170-1185.

Cheng H., Cheng P., Peng P., Lyu P., and Sun Y. (2004). Lipid binding in rice nonspecific lipid transfer protein-1 complexes from Oryza sativa. Protein Sci. **13,** 2304-2315.

Clark R.M., Schweikert G., Toomajian C., Ossowski S., Zeller G., Shinn P., Warthmann N., Hu T.T., Fu G., Hinds D.A., Chen H., Frazer K.A., Huson D.H., Scholkopf B., Nordborg M., Ratsch G., Ecker J.R., and Weigel D. (2007). Common sequence polymorphisms shaping genetic diversity in *Arabidopsis thaliana*. Science **317,** 338-342.

Clough S.J. and Bent A.F. (1998). Floral dip: a simplified method forAgrobacterium-mediated transformation of*Arabidopsis thaliana*. Plant J. **16,** 735-743.

Coll E.P., Kandt C., Bird D.A., Samuels A.L., and Tieleman D.P. (2007). The distribution and conformation of very long-chain plant wax components in a lipid bilayer. J. Phys. Chem. B. **111,** 8702-8704.

Cosgrove D.J. (2005). Growth of the plant cell wall. Nat. Rev. Mol. Cell. **6,** 850-861.

Coyne C.B. and Bergelson J.M. (2006). Virus-induced Abl and Fyn kinase signals permit coxsackievirus entry through epithelial tight junctions. Cell **124,** 119-131.

Cregg J.M., Vedvick T.S., and Raschke W.C. (1993). Recent advances in the expression of foreign genes in Pichia pastoris. Nat. Biotechnol. **11,** 905-910.

Cregg J.M. (2007). Chapter 1. Distinctions Between Pichia pastoris and Other Expression Systems in Pichia protocols 2nd edition. Methods in Molecular Biology Vol. 389. Cregg J.M., ed (Humana Press Inc). pp. 1-42

Curtis M.D. and Grossniklaus U. (2003). A Gateway Cloning Vector Set for High-Throughput Functional Analysis of Genes in Planta. Plant Physiol. **133,** 462-469.

Cutler S.R., Ehrhardt D.W., Griffitts J.S., and Somerville C.R. (2000). Random GFP::cDNA fusions enable visualization of subcellular structures in cells of Arabidopsis at a high frequency. Proc. Natl. Acad. Sci. U. S. A. **97,** 3718-3723.

Daly R. and Hearn M.T.W. (2005). Expression of heterologous proteins in *Pichia pastoris*: a useful experimental tool in protein engineering and production. J. Mol. Recognit. **18,** 119-138.

de Laat B., Derksen R.H.W.M., van Lummel M., Pennings M.T.T., and de Groot P.G. (2006). Pathogenic anti-beta2-glycoprotein I antibodies recognize domain I of beta2-glycoprotein I only after a conformational change. Blood **107,** 1916-1924.

DeBono A., Yeats T.H., Rose J.K.C., Bird D., Jetter R., Kunst L., and Samuels L. (2009). Arabidopsis LTPG is a glycosylphosphatidylinositol-anchored lipid transfer protein required for export of lipids to the plant surface. Plant Cell **21,** 1230-1238.

Demel R., Wirtz K., Kamp H., Geurts van Kessel W., and Van Deenen L. (1973). Phosphatidylcholine exchange protein from beef liver. Nature **246,** 102-105.

Denic V. and Weissman J.S. (2007). A Molecular Caliper Mechanism for Determining Very Long-Chain Fatty Acid Length. Cell **130,** 663-677.

Dombrowski J.E., Schroeder M.R., Bednarek S.Y., and Raikhel N.V. (1993). Determination of the functional elements within the vacuolar targeting signal of barley lectin. Plant Cell **5,** 587-596.

Douady D., Grosbois M., Guerbette F., and Kader J. (1982). Purification of a basic phospholipid transfer protein from maize seedlings. Biochim. Biophys. Acta. **710,** 143-153.

Ebeneezer T., and Gargamel H. (1972). Inexpensive molecular technique for DNA preparation from bacterial systems. Biochim. Biophys. Acta. **650,** 112-118.

Edidin M., Kuo S.C., and Sheetz M.P. (1991). Lateral movements of membrane glycoproteins restricted by dynamic cytoplasmic barriers. Science **254,** 1379-1382.

Edidin M., Zuniga M.C., and Sheetz M.P. (1994). Truncation mutants define and locate cytoplasmic barriers to lateral mobility of membrane glycoproteins. Proc. Nat. Acad. Sci. U.S.A. **91,** 3378-3382.

Edqvist J., Rönnberg E., Rosenquist S., Blomqvist K., Viitanen L., Salminen T.A., Nylund M., Tuuf J., and Mattjus P. (2004). Plants express a lipid transfer protein with high similarity to mammalian sterol carrier protein-2. J. Biol. Chem. **279,** 53544-53553.

Edstam M.M., Viitanen L., Salminen T.A., and Edqvist J. (2011). Evolutionary History of the Non-Specific Lipid Transfer Proteins. Molecular Plant.doi:10.1093/mp/ssr019

Eisenhaber B., Wildpaner M., Schultz C.J., Borner G.H., Dupree P., and Eisenhaber F. (2003). Glycosylphosphatidylinositol lipid anchoring of plant proteins. Sensitive prediction from sequence- and genome-wide studies for Arabidopsis and rice. Plant Physiol. **133,** 1691-1701.

Ellis M., Egelund J., Schultz C.J., and Bacic A. (2010). Arabinogalactan-Proteins: Key Regulators at the Cell Surface? Plant Physiol. **153,** 403-419.

Elortza F., Nuhse T.S., Foster L.J., Stensballe A., Peck S.C., and Jensen O.N. (2003). Proteomic Analysis of Glycosylphosphatidylinositol-anchored Membrane Proteins. Mol. Cell. Proteomics. **2,** 1261-1270.

Elortza F., Mohammed S., Bunkenborg J., Foster L.J., Nuhse T.S., Brodbeck U., Peck S.C., and Jensen O.N. (2006). Modification-specific proteomics of plasma membrane proteins: identification and characterization of glycosylphosphatidylinositol-anchored proteins released upon phospholipase D treatment. J. Proteome Res. **5,** 935-943.

Estevez J.M., Kieliszewski M.J., Khitrov N., and Somerville C. (2006). Characterization of synthetic hydroxyproline-rich proteoglycans with arabinogalactan protein and extensin motifs in Arabidopsis. Plant Physiol. **142,** 458-470.

Feraru E., Feraru M.I., Kleine-Vehn J., Martinière A., Mouille G., Vanneste S., Vernhettes S., Runions J., and Friml J. (2011). PIN Polarity Maintenance by the Cell Wall in *Arabidopsis*. Curr. Biol. **21,** 338-343.

Fiebig A., Mayfield J.A., Miley N.L., Chau S., Fischer R.L., and Preuss D. (2000). Alterations in *CER6*, a gene identical to *CUT1*, differentially affect long-chain lipid content on the surface of pollen and stems. Plant Cell. **12,** 2001-2008.

Fischer R., Drossard J., Emans N., Commandeur U., and Hellwig S. (1999). Towards molecular farming in the future: *Pichia pastoris*-based production of single-chain antibody fragments. Biotechnol. Appl. Biochem. **30,** 117-120.

Fleming A., Mandel T., Hofmann S., Sterk P., Vries S., and Kuhlemeier C. (1992). Expression pattern of a tobacco lipid transfer protein gene within the shoot apex. Plant J. **2,** 855-862.

Fraering P., Imhof I., Meyer U., Strub J.M., Van Dorsselaer A., Vionnet C., and Conzelmann A. (2001). The GPI transamidase complex of Saccharomyces cerevisiae contains Gaa1p, Gpi8p, and Gpi16p. Mol. Biol. Cell **12,** 3295-3306.

Franke R., Briesen I., Wojciechowski T., Faust A., Yephremov A., Nawrath C., and Schreiber L. (2005). Apoplastic polyesters in Arabidopsis surface tissues-a typical suberin and a particular cutin. Phytochemistry. **66,** 2643-2658.

Frieman M.B. and Cormack B.P. (2003). The ω-site sequence of glycosylphosphatidylinositol-anchored proteins in Saccharomyces cerevisiae can determine distribution between the membrane and the cell wall. Mol. Microbiol. **50,** 883-896.

Frieman M.B. and Cormack B.P. (2004). Multiple sequence signals determine the distribution of glycosylphosphatidylinositol proteins between the plasma membrane and cell wall in Saccharomyces cerevisiae. Microbiology. **150,** 3105-3114.

Fujita M. and Kinoshita T. (2010). Structural remodeling of GPI anchors during biosynthesis and after attachment to proteins. FEBS Lett. **584,** 1670-1677.

Gerber L., Kodukula K., and Udenfriend S. (1992). Phosphatidylinositol glycan (PI-G) anchored membrane proteins. Amino acid requirements adjacent to the site of cleavage and PI-G attachment in the COOH-terminal signal peptide. J. Biol. Chem. **267,** 12168-12173.

Girault, T., Francois, J., Rogniaux, H., Pascal, S., Delrot, S., Coutos-Thevenot, P., and Gomes, E. (2008) Exogenous application of a lipid transfer protein-jasmonic acid complex induces protection of grapevine towards infection by *Botrytis cinerea.* Plant Phys. and Biochem. **146,** 140e-149.

Gomar J., Petit M.C., Sodano P., Sy D., Marion D., Kader J.C., Vovelle F., and Ptak M. (1996). Solution structure and lipid binding of a nonspecific lipid transfer protein extracted from maize seeds. Protein Sci.**5,** 565-577.

Goud G.N., Bottazzi M.E., Zhan B., Mendez S., Deumic V., Plieskatt J., Liu S., Wang Y., Bueno L., Fujiwara R., Samuel A., Ahn S.Y., Solanki M., Asojo O.A., Wang J., Bethony J.M., Loukas A., Roy M., and Hotez P.J. (2005). Expression of the Necator americanus hookworm larval antigen Na-ASP-2 in *Pichia pastoris* and purification of the recombinant protein for use in human clinical trials. Vaccine. **23,** 4754-4764.

Graca J., Schreiber L., Rodrigues J., and Pereira H. (2002). Glycerol and glyceryl esters of omega-hydroxyacids in cutins. Phytochemistry. **61,** 205-215.

Greer S., Wen M., Bird D., Wu X., Samuels L., Kunst L., and Jetter R. (2007). The cytochrome P450 enzyme CYP96A15 is the midchain alkane hydroxylase responsible for formation of secondary alcohols and ketones in stem cuticular wax of Arabidopsis. Plant Physiol. **145,** 653-667.

Griesbeck O., Baird G.S., Campbell R.E., Zacharias D.A., and Tsien R.Y. (2001). Reducing the environmental sensitivity of yellow fluorescent protein. J. Biol. Chem. **276,** 29188-29194.

Gupta R., Jung E., and Brunak S. (2004). NetNGlyc 1.0
Server: http://www.cbs.dtu.dk/services/NetNGlyc

Hadley N. (1981). Cuticular lipids of terrestrial plants and arthropods: a comparison of their structure, composition, and waterproofing function. Biol. Rev. **56,** 23-47.

Hardham A.R. (2001). The cell biology behind Phytophthora pathogenicity. Australas. Plant Pathol. **30,** 91-98.

Hardham A.R. (2007). Cell biology of plant–oomycete interactions. Cell. Microbiol. **9,** 31-39.

Heim R. and Tsien R.Y. (1996). Engineering green fluorescent protein for improved brightness, longer wavelengths and fluorescence resonance energy transfer. Curr. Biol. **6,** 178-182.

Hellens R.P., Edwards E.A., Leyland N.R., Bean S., and Mullineaux P.M. (2000). pGreen: a versatile and flexible binary Ti vector for Agrobacterium-mediated plant transformation. **42,** 819-832.

Hiller K., Grote A., Scheer M., Münch R., and Jahn D. (2004). PrediSi: prediction of signal peptides and their cleavage positions. Nucleic Acids Res. **32,** W375-W379.

Hilson P., Allemeersch J., Altmann T., Aubourg S., Avon A., Beynon J., Bhalerao R.P., Bitton F., Caboche M., and Cannoot B. (2004). Versatile Gene-Specific Sequence Tags for Arabidopsis Functional Genomics: Transcript Profiling and Reverse Genetics Applications. Genome Res. **14,** 2176-2189.

Huuskonen J., Wohlfahrt G., Jauhiainen M., Ehnholm C., Teleman O., and Olkkonen V.M. (1999). Structure and phospholipid transfer activity of human PLTP: analysis by molecular modeling and site-directed mutagenesis. J. Lipid. Res. **40,** 1123-1130.

Isaac Kirubakaran S., Begum S.M., Ulaganathan K., and Sakthivel N. (2008). Characterization of a new antifungal lipid transfer protein from wheat. Plant Physiol Bioch **46,** 918-927.

Jamet E., Boudart G., Borderies G., Charmont S., Lafitte C., Rossignol M., Canut H., and Pont-Lezica R. (2008). Chapter 17. Isolation of plant cell wall proteins in 2D PAGE: Sample Preparation and Fractionation. Methods in Molecular Biology Vol. 425. Posch, A., ed (Humana Press) pp.187-201.

Jayaraj J. and Punja Z. (2007). Combined expression of chitinase and lipid transfer protein genes in transgenic carrot plants enhances resistance to foliar fungal pathogens. Plant Cell Rep. **26,** 1539-1546.

Jeffree C. (2006). Chapter 2. The fine structure of the plant cuticle in The Biology of the Plant Cuticle. Annual Plant Reviews, Vol. 23, Markus Riederer and Caroline Müller, ed (Blackwell Publishing) pp. 11-125.

Jenks M., Tuttle H., Eigenbrode S., and Feldmann K. (1995). Leaf epicuticular waxes of the *eceriferum* mutants in *Arabidopsis*. Plant Physiol. **108,** 369-377.

Jetter R., Kunst L., and Samuels A. (2006). Chapter 4. Composition of plant cuticular waxes in The Biology of the Plant Cuticle. Annual Plant Reviews, Vol. 23, Markus Riederer and Caroline Müller, ed (Blackwell Publishing) pp. 145-215.

Jose-Estanyol M., Gomis-Ruth F.X., and Puigdomenech P. (2004). The eight-cysteine motif, a versatile structure in plant proteins. Plant Physiol. Biochm. **42,** 355-365.

Julenius, K., Johansen, M. B., Zhang, Y., Brunak, S. and Gupta, R.(2009) Prediction of Glycosylation Sites in Proteins, in Bioinformatics for Glycobiology and Glycomics: An Introduction C.-W. von der Lieth, T. Lütteke and M. Frank , ed (John Wiley & Sons) pp. 163-185.

Kader J.C., Julienne M., and Vergnolle C. (1984). Purification and characterization of a spinach-leaf protein capable of transferring phospholipids from liposomes to mitochondria or chloroplasts. Eur. J. Biochem. **139,** 411-416.

Kader J. (1996). Lipid-transfer proteins in plants. Annu. Rev. Plant Physiol. Pant. Mol. Biol. **47,** 627-654.

Kapteyn J.C., Van Den Ende H., and Klis F.M. (1999). The contribution of cell wall proteins to the organization of the yeast cell wall. Biochim Biophys. Acta **1426,** 373-383.

Karplus M. (1963). Vicinal proton coupling in nuclear magnetic resonance. J. Am. Chem. Soc. **85,** 2870-2871.

Kinoshita T., Ohishi K., and Takeda J. (1997). GPI-anchor synthesis in mammalian cells: genes, their products, and a deficiency. J. Biochem. **122,** 251-257.

Kinoshita T., Fujita M., and Maeda Y. (2008). Biosynthesis, Remodelling and Functions of Mammalian GPI-anchored Proteins: Recent Progress. J. Biochem. **144,** 287-294.

Kinoshita T. and Fujita M. (2009). Chapter 1. Overview of GPI Biosynthesis in The Enzymes. Volume 26, Anant K. Menon, Peter Orlean,Taroh Kinoshita and Fuyuhiko Tamanoi, ed (Academic Press) pp. 1-30.

Kolattukudy P.E. (1980). Biopolyester Membranes of Plants: Cutin and Suberin. Science. **208,** 990-1000.

Kolattukudy P. (2001). Polyesters in Higher Plants in Biopolyesters. Vol. 71, Wolfgang Babel and Alexander Steinbüchel, eds (Springer Berlin / Heidelberg) pp. 1-49.

Kolatukudy P.E., Walton T.J., and Kushwaha R.P.S. (1973). Biosynthesis of the C18 family of cutin acid:. ω-Hydroxyoleic acid, ω-hydroxy-9,10-epoxystearic acid, 9,10,18-trihydroxystearic acid, and their Δ-Unsaturated analogs. Biochemistry-US. **12,** 4488-4498.

Kosma D.K., Bourdenx B., Bernard A., Parsons E.P., Lü S., Joubes J., and Jenks M.A. (2009). The impact of water deficiency on leaf cuticle lipids of Arabidopsis. Plant Physiol. **151,** 1918-1929.

Kunst L. and Samuels L. (2009). Plant cuticles shine: advances in wax biosynthesis and export. Curr. Opin. Plant Biol. **12,** 721-727.

Kunst L. and Samuels A.L. (2003). Biosynthesis and secretion of plant cuticular wax. Prog. Lipid Res. **42,** 51-80.

Kunst L., Jetter R., and Samuels A. (2006). Chapter 5. Biosynthesis and transport of plant cuticular waxes in The Biology of the Plant Cuticle. Annual Plant Reviews, Vol. 23, Markus Riederer and Caroline Müller, ed (Blackwell Publishing) pp. 182-215.

Kusumi A., Nakada C., Ritchie K., Murase K., Suzuki K., Murakoshi H., Kasai R.S., Kondo J., and Fujiwara T. (2005). Paradigm shift of the plasma membrane concept from the two-dimensional continuum fluid to the partitioned fluid: high-speed single-molecule tracking of membrane molecules. Annu. Rev. Biophys. Biomol. Struct. **34,** 351-378.

Lai Z., Gross B.L., Yizou, J.A., and Rieseberg, L.H. (2006). Microarray analysis reveals differential gene expression in hybrid sunflower species. Mol. Ecol. **15,** 1213-1227.

Lajoie P., Goetz J.G., Dennis J.W., and Nabi I.R. (2009). Lattices, rafts, and scaffolds: domain regulation of receptor signaling at the plasma membrane. J. Cell Biol. **185,** 381-385.

Landon C., Berthault P., Vovelle F., and Desvaux H. (2001). Magnetization transfer from laser polarized xenon to protons located in the hydrophobic cavity of the wheat nonspecific lipid transfer protein. Protein Sci. **10,** 762-770.

Lardizabal K.D., Metz J.G., Sakamoto T., Hutton W.C., Pollard M.R., and Lassner M.W. (2000). Purification of a Jojoba Embryo Wax Synthase, Cloning of its cDNA, and Production of High Levels of Wax in Seeds of Transgenic Arabidopsis. Plant Physiol. **122,** 645-656.

Lascombe M., Bakan B., Buhot N., Marion D., Blein J., Larue V., Lamb C., and Prangé T. (2008). The structure of “defective in induced resistance” protein of Arabidopsis thaliana, DIR1, reveals a new type of lipid transfer protein. Protein Sci. **17,** 1522-1530.

Lee S.B., Jung S.J., Go Y.S., Kim H.U., Kim J.K., Cho H.J., Park O.K., and Suh M.C. (2009). Two Arabidopsis 3-ketoacyl CoA synthase genes, *KCS20* and *KCS2/DAISY*, are functionally redundant in cuticular wax and root suberin biosynthesis, but differentially controlled by osmotic stress. Plant Physiol. **60,** 462-475.

Lee J., Min K., Cha H., Shin D., Hwang K., and Suh S. (1998). Rice non-specific lipid transfer protein: the 1.6 Å crystal structure in the unliganded state reveals a small hydrophobic cavity. J. Mol. Biol. **276,** 437-448.

Lee S.B., Go Y.S., Bae H., Park J.H., Cho S.H., Cho H.J., Lee D.S., Park O.K., Hwang I., and Suh M.C. (2009). Disruption of Glycosylphosphatidylinositol-Anchored Lipid Transfer Protein Gene Altered Cuticular Lipid Composition, Increased Plastoglobules, and Enhanced Susceptibility to Infection by the Fungal Pathogen *Alternaria brassicicola*. Plant Physiol. **150,** 42-54.

Lerche M.H., Kragelund B.B., Bech L.M., and Poulsen F.M. (1997). Barley lipid-transfer protein complexed with palmitoyl CoA: the structure reveals a hydrophobic binding site that can expand to fit both large and small lipid-like ligands. Structure. **5,** 291-306.

Li J.F., Park E., Von Arnim A.G., and Nebenführ A. (2009). The FAST technique: a simplified Agrobacterium-based transformation method for transient gene expression analysis in seedlings of Arabidopsis and other plant species. Plant Methods. **5,** doi:10.1186/1746-4811-5-6

Li Y., Beisson F., Koo A.J.K., Molina I., Pollard M., and Ohlrogge J. (2007). Identification of acyltransferases required for cutin biosynthesis and production of cutin with suberin-like monomers. Proc. Natl. Acad. Sci. U.S.A. **104,** 18339-18344.

Li Z., Moon B.P., Xing A., Liu Z.B., McCardell R.P., Damude H.G., and Flaco S.C. (2010). Stacking multiple transgenes at a selected genomic site via repeated recombinase mediated DNA cassette exchanges. Plant Physiol. **154,** 622-631.

Li F., Wu X., Lam P., Bird D., Zheng H., Samuels L., Jetter R., and Kunst L. (2008). Identification of the Wax Ester Synthase/Acyl-Coenzyme A:Diacylglycerol Acyltransferase WSD1 Required for Stem Wax Ester Biosynthesis in Arabidopsis. Plant Physiol. **148,** 97-107.

Lin P., Xia L., Wong J.H., Ng T.B., Ye X., Wang S., and Xiangzhu S. (2007). Lipid transfer proteins from *Brassica campestris* and mung bean surpass mung bean chitinase in exploitability. J. Pept. Sci. **13,** 642-648.

Lingwood D. and Simons K. (2010). Lipid Rafts As a Membrane-Organizing Principle. Science **327,** 46-50.

Lu S., Song T., Kosma D.K., Parsons E.P., Rowland O., and Jenks M.A. (2009). Arabidopsis *CER8* encodes LONG-CHAIN ACYL-COA SYNTHETASE 1 (LACS1) that has overlapping functions with LACS2 in plant wax and cutin synthesis. Plant J. **59,** 553-564.

Lu C., Napier J.A., Clemente T.E., and Cahoon E.B. (2011). New frontiers in oilseed biotechnology: meeting the global demand for vegetable oils for food, feed, biofuel, and industrial applications. Curr. Opin. Biotechnol. **22,** 252-259.

Luo B., Xue X.Y., Hu W.L., Wang L.J., and Chen X.Y. (2007). An ABC transporter gene of Arabidopsis thaliana, AtWBC11, is involved in cuticle development and prevention of organ fusion. Plant Cell Physiol. **48,** 1790-1802.

Maldonado A.M., Doerner P., Dixon R.A., Lamb C.J., and Cameron R.K. (2002). A putative lipid transfer protein involved in systemic resistance signalling in Arabidopsis. Nature **419,** 399-403.

Marsh M. and Helenius A. (2006). Virus entry: open sesame. Cell **124,** 729-740.

Martinière A., Gayral P., Hawes C., and Runions J. (2011). Building bridges: Formin1 of Arabidopsis forms a connection between the cell wall and the actin cytoskeleton. Plant J. **66,** 354-365.

Mathur J., Radhamony R., Sinclair A.M., Donoso A., Dunn N., Roach E., and Radford D. (2010). mEosFP-Based Green-to-Red Photoconvertible Subcellular Probes for Plants. Plant Physiol. **154,** 1573-1587.

Maxfield F.R. and Menon A.K. (2006). Intracellular sterol transport and distribution. Curr. Opin. Cell Biol. **18,** 379-385.

Mayor S. and Riezman H. (2004). Sorting GPI-anchored proteins. Nat. Rev. Mol. Cell. Bio. **5,** 110-120.

McFarlane H.E., Shin J.J.H., Bird D.A., and Samuels A.L. (2010). Arabidopsis ABCG Transporters, Which Are Required for Export of Diverse Cuticular Lipids, Dimerize in Different Combinations. Plant Cell. **22,** 3066-3075.

McKinney S.A., Murphy C.S., Hazelwood K.L., Davidson M.W., and Looger L.L. (2009). A bright and photostable photoconvertible fluorescent protein. Nat. Methods **6,** 131-133.

Metz C.N., Brunner G., Choi-Muira N.H., Nguyen H., Gabrilove J., Caras I.W., Altszuler N., Rifkin D.B., Wilson E.L., and Davitz M.A. (1994). Release of GPI-anchored membrane proteins by a cell-associated GPI-specific phospholipase D. EMBO J. **13,** 1741-1751.

Metz J.G., Pollard M.R., Anderson L., Hayes T.R., and Lassner M.W. (2000). Purification of a Jojoba Embryo Fatty Acyl-Coenzyme A Reductase and Expression of Its cDNA in High Erucic Acid Rapeseed. Plant Physiol. **122,** 635-644.

Millar A.A., Clemens S., Zachgo S., Giblin E.M., Taylor D.C., and Kunst L. (1999). CUT1, an Arabidopsis gene required for cuticular wax biosynthesis and pollen fertility, encodes a very-long-chain fatty acid condensing enzyme. Plant Cell **11,** 825-838.

Millar A.A., Wrischer M., and Kunst L. (1998). Accumulation of very-long-chain fatty acids in membrane glycerolipids is associated with dramatic alterations in plant morphology. Plant Cell **10,** 1889-1902

Molina A. and Garcia-Olmedo F. (1997). Enhanced tolerance to bacterial pathogens caused by the transgenic expression of barley lipid transfer protein LTP2. Plant J. **12,** 669-675.

Molina A., Segura A., and Garcia-Olmedo F. (1993). Lipid transfer proteins (nsLTPs) from barley and maize leaves are potent inhibitors of bacterial and fungal plant pathogens. FEBS. Lett. **316,** 119-122.

Moran P. and Caras I.W. (1991a). A nonfunctional sequence converted to a signal for glycophosphatidylinositol membrane anchor attachment. J. Cell Biol. **115,** 329-336.

Moran P. and Caras I.W. (1991b). Fusion of sequence elements from non-anchored proteins to generate a fully functional signal for glycophosphatidylinositol membrane anchor attachment. J. Cell Biol. **115,** 1595-1600.

Motose H., Sugiyama M., and Fukuda H. (2004). A proteoglycan mediates inductive interaction during plant vascular development. Nature **429,** 873-878.

Nemhauser J., Hong F., and Chory J. (2006). Different plant hormones regulate similar processes through largely nonoverlapping transcriptional responses. Cell **126,** 467-475.

Nielsen K., Nielsen J., Madrid S., and Mikkelsen J. (1996). New antifungal proteins from sugar beet (Beta vulgaris L.) showing homology to non-specific lipid transfer proteins. Plant Mol. Biol. **31,** 539-552.

Nieuwland J., Feron R., Huisman B.A.H., Fasolino A., Hilbers C.W., Derksen J., and Mariani C. (2005). Lipid Transfer Proteins Enhance Cell Wall Extension in Tobacco. Plant Cell **17,** 2009-2019.

Oparka K., Prior D., and Crawford J. (1994). Behaviour of plasma membrane, cortical ER and plasmodesmata during plasmolysis of onion epidermal cells. Plant, Cell Environ. **17,** 163-171.

Orlean P. and Menon A. (2007). Thematic review series: lipid posttranslational modifications. GPI anchoring of protein in yeast and mammalian cells, or: how we learned to stop worrying and love glycophospholipids. J. Lipid Res. **48,** 993-1011.

Oxley D. and Bacic A. (1999). Structure of the glycosylphosphatidylinositol anchor of an arabinogalactan protein from Pyrus communis suspension-cultured cells. Proc. Natl. Acad. Sci. U.S.A. **96,** 14246-14251.

Panikashvili D., Savaldi-Goldstein S., Mandel T., Yifhar T., Franke R.B., Hofer R., Schreiber L., Chory J., and Aharoni A. (2007). The Arabidopsis DESPERADO/AtWBC11 transporter is required for cutin and wax secretion. Plant Physiol. **145,** 1345-1360.

Partikian A., Ölveczky B., Swaminathan R., Li Y., and Verkman A. (1998). Rapid diffusion of green fluorescent protein in the mitochondrial matrix. J. Cell Biol. **140,** 821-829.

Pelengaris S., Khan M., and Evan G. (2002). c-MYC: more than just a matter of life and death. Nat Rev. Cancer **2,** 764-776.

Pietraszewska-Bogiel A. and Gadella T.W.J. (2011). FRET microscopy: from principle to routine technology in cell biology. J. Microsc. **241,** 111-118.

Pighin J.A., Zheng H., Balakshin L.J., Goodman I.P., Western T.L., Jetter R., Kunst L., and Samuels A.L. (2004). Plant Cuticular Lipid Export Requires an ABC Transporter. Science **306,** 702-704.

Pollard M., Beisson F., Li Y., and Ohlrogge J.B. (2008). Building lipid barriers: biosynthesis of cutin and suberin. Trends Plant Sci. **13,** 236-246.

Pollard M., McKeon T., Gupta L., and Stumpf P. (1979). Studies on biosynthesis of waxes by developing jojoba seed. II. The demonstration of wax biosynthesis by cell-free homogenates. Lipids **14,** 651-662.

Post-Beittenmiller D. (1996). Biochemistry and molecular biology of wax production in plants. Annu. Rev. Plant Physiol. Plant Mol. Biol. **47,** 405-430.

Pyee J., Yu H., and Kolattukudy P. (1994). Identification of a lipid transfer protein as the major protein in the surface wax of broccoli (Brassica oleracea) leaves. Arch. Biochem. Biophys. **311,** 460-468.

Pyee J. and Kolattukudy P. (1995). The gene for the major cuticular wax-associated protein and three homologous genes from broccoli (Brassica oleracea) and their expression patterns. Plant J. **7,** 49-59.

Qiu X., Mistry A., Ammirati M.J., Chrunyk B.A., Clark R.W., Cong Y., Culp J.S., Danley D.E., Freeman T.B., Geoghegan K.F., Griffor M.C., Hawrylik S.J., Hayward C.M., Hensley P., Hoth L.R., Karam G.A., Lira M.E., Lloyd D.B., McGrath K.M., Stutzman-Engwall K.J., Subashi A.K., Subashi T.A., Thompson J.F., Wang I., Zhao H., and Seddon A.P. (2007).

Crystal structure of cholesteryl ester transfer protein reveals a long tunnel and four bound lipid molecules. Nat. Struct. Mol. Biol. **14,** 106-113.

Raffaele S., Vailleau F., Leger A., Joubes J., Miersch O., Huard C., Blee E., Mongrand S., Domergue F., and Roby D. (2008). A MYB transcription factor regulates very-long-chain fatty acid biosynthesis for activation of the hypersensitive cell death response in Arabidopsis. Plant Cell. **20,** 752-767.

Raffaele S., Bayer E., Lafarge D., Cluzet S., German Retana S., Boubekeur T., Leborgne-Castel N., Carde J., Lherminier J., Noirot E., Satiat-Jeunemaitre B., Laroche-Traineau J., Moreau P., Ott T., Maule A.J., Reymond P., Simon-Plas F., Farmer E.E., Bessoule J., and Mongrand S. (2009). Remorin, a Solanaceae Protein Resident in Membrane Rafts and Plasmodesmata, Impairs Potato virus X Movement. Plant Cell **21,** 1541-1555.

Rashotte A.M., Jenks M.A., Ross A.S., and Feldmann K.A. (2004). Novel eceriferum mutants in Arabidopsis thaliana. Planta **219,** 5-13.

Raven J. (1984). Physiological correlates of the morphology of early vascular plants. Bot. J. Linn. Soc. **88,** 105-126.

Regente M.C. and De La Canal L. (2000). Purification, characterization and antifungal properties of a lipid-transfer protein from sunflower (Helianthus annuus) seeds. Physiol. Plantarum **110,** 158-163.

Riederer M. and Muller C. (2006). Chapter 1. Introduction: biology of the plant cuticle In The Biology of the Plant Cuticle. Annual Plant Reviews, Vol. 23, Markus Riederer and Caroline Müller, ed (Blackwell Publishing) pp. 1-10.

Rose J.K.C., Cosgrove D.J., Albersheim P., Darvill A.G., and Bennett A.B. (2000). Detection of expansin proteins and activity during tomato fruit ontogeny. Plant Physiol. **123,** 1583.

Roudier F., Fernandez A.G., Fujita M., Himmelspach R., Borner G.H., Schindelman G., Song S., Baskin T.I., Dupree P., Wasteneys G.O., and Benfey P.N. (2005). COBRA, an Arabidopsis extracellular glycosyl-phosphatidyl inositol-anchored protein, specifically controls highly anisotropic expansion through its involvement in cellulose microfibril orientation. Plant Cell **17,** 1749-1763.

Rowland O., Zheng H., Hepworth S., Lam P., Jetter R., and Kunst L. (2006). CER4 encodes an alcohol-forming fatty acyl-coenzyme A reductase involved in cuticular wax production in Arabidopsis. Plant Physiol. **142,** 866-877.

Rowland O., Lee R., Franke R., Schreiber L., and Kunst L. (2007). The CER3 wax biosynthetic gene from Arabidopsis thaliana is allelic to WAX2/YRE/FLP1. FEBS. Lett. **581,** 3538-3544.

Rydberg E.H., Sidhu G., Vo H.C., Hewitt J., Ct H.C.F., Wang Y., Numao S., Macgillivray R.T.A., Overall C.M., and Brayer G.D. (1999). Cloning, mutagenesis, and structural analysis of human pancreatic α-amylase expressed in Pichia pastoris. Prot. Sci. **8,** 635-643.

Saalbach G., Rosso M., and Schumann U. (1996). The vacuolar targeting signal of the 2S albumin from Brazil nut resides at the C terminus and involves the C-terminal propeptide as an essential element. Plant Physiol. **112,** 975-985.

Samuels L., Kunst L., and Jetter R. (2008). Sealing Plant Surfaces: Cuticular Wax Formation by Epidermal Cells. Annu. Rev. Plant Biol. **59,** 683–707.

Sardar H.S., Yang J., and Showalter A.M. (2006). Molecular interactions of arabinogalactan proteins with cortical microtubules and F-actin in Bright Yellow-2 tobacco cultured cells. Plant Physiol. **142,** 1469-1479.

Sawano Y., Hatano K., Miyakawa T., Komagata H., Miyauchi Y., Yamazaki H., and Tanokura M. (2008). Proteinase inhibitor from Ginkgo seeds is a member of the plant nonspecific lipid transfer protein gene family. Plant Physiol. **146,** 1909-1919.

Scallon B.J., Fung W., Tsang T.C., Li S., Kado-Fong H., Huang K.S., and Kochan J.P. (1991). Primary structure and functional activity of a phosphatidylinositol-glycan-specific phospholipase D. Science **252,** 446-448.

Schnurr J., Shockey J., and Browse J. (2004). The acyl-CoA synthetase encoded by LACS2 is essential for normal cuticle development in Arabidopsis. Plant Cell **16,** 629-642.

Schwab R., Ossowski S., Riester M., Warthmann N., and Weigel D. (2006). Highly Specific Gene Silencing by Artificial MicroRNAs in Arabidopsis. Plant Cell **18,** 1121-1133.

Sedbrook J.C., Carroll K.L., Hung K.F., Masson P.H., and Somerville C.R. (2002). The Arabidopsis SKU5 gene encodes an extracellular glycosyl phosphatidylinositol–anchored glycoprotein involved in directional root growth. Plant Cell **14,** 1635-1648.

Seifert G.J. and Roberts K. (2007). The biology of arabinogalactan proteins. Annu. Rev. Plant Biol. **58,** 137-161.

Shaner N.C., Steinbach P.A., and Tsien R.Y. (2005). A guide to choosing fluorescent proteins. Nat. Methods **2,** 905-909.

Sherrier D.J., Prime T.A., and Dupree P. (1999). Glycosylphosphatidylinositol-anchored cell-surface proteins from Arabidopsis. Electrophoresis **20,** 2027-2035.

Shieh J.T.C. and Bergelson J.M. (2002). Interaction with decay-accelerating factor facilitates coxsackievirus B infection of polarized epithelial cells. J. Virol. **76,** 9474-9780.

Shin D., Lee J., Hwang K., Kyu Kim K., and Suh S. (1995). High-resolution crystal structure of the non-specific lipid-transfer protein from maize seedlings. Curr. Biol. **3,** 189-199.

Shockey J., Fulda M., and JA B. (2002). Arabidopsis contains nine long-chain acyl-coenzyme A synthetase genes that participate in fatty acid and glycerolipid metabolism. Plant Physiol. **129,** 1710-1722.

Signorell A. and Menon A.K. (2009). Chapter 7. Attachment of a GPI Anchor to Protein In The Enzymes Vol. 26, Anant K. Menon, Peter Orlean,Taroh Kinoshita and Fuyuhiko Tamanoi, ed (Academic Press) pp. 133-149.

Somerville C., Browse J., Jaworski J.G., and Ohlrogge J.B. (2000). Chapter 10. Lipids in Biochemistry & Molecular Biology of Plants. Bob B. Buchanan, Wilhelm Gruissem, Russel L. Jones, ed (American Society of Plant Physiologists) pp. 488-490.

Sossountzov L., Ruizavila L., Vignols F., Jolliot A., Arondel V., Tchang F., Grosbois M., Guerbette F., Miginiac E., Delseny M., Puigdomenech P., and Kader J.C. (1991). Spatial and Temporal Expression of a Maize Lipid Transfer Protein Gene. Plant Cell **3,** 923-933.

Sottosanto J., Gelli A., and Blumwald E. (2004). DNA array analyses of Arabidopsis thaliana lacking a vacuolar Na+/H+ antiporter: impact of AtNHX1 on gene expression. Plant J. **40,** 752-771.

Sprague B.L. and McNally J.G. (2005). FRAP analysis of binding: proper and fitting. Trends Cell Biol. **15,** 84-91.

Staehelin L.A., and Newcomb, E.H. (2000). Chapter 1. Membrane Structure and Membranous Organelles in Biochemistry & Molecular Biology of Plants. Bob B. Buchanan, Wilhelm Gruissem, Russel L. Jones, ed (American Society of Plant Physiologists) pp. 10-11.

Stark R. and Tian S. (2006). Chapter 3. The cutin biopolymer matrix in The Biology of the Plant Cuticle. Annual Plant Reviews, Vol. 23, Markus Riederer and Caroline Müller, ed (Blackwell Publishing) pp. 126-144.

Sterk P., Booij H., Schellekens G., Van Kammen A., and De Vries S. (1991). Cell-specific expression of the carrot EP2 lipid transfer protein gene. Plant Cell **3,** 907-921.

Sterling J., Atmodjo M., Inwood S., Kolli V., Quigley H., Hahn M., and Mohnen D. (2006). Functional identification of an Arabidopsis pectin biosynthetic homogalacturonan galacturonosyltransferase. Proc. Natl. Acad. Sci. U.S.A. **103,** 5236-5241.

Storch J. and Thumser A.E.A. (2000). The fatty acid transport function of fatty acid-binding proteins. Biochim. Biophys. Acta. **1486,** 28-44.

Suh M.C., Samuels A.L., Jetter R., Kunst L., Pollard M., Ohlrogge J., and Beisson F. (2005). Cuticular Lipid Composition, Surface Structure, and Gene Expression in Arabidopsis Stem Epidermis. Plant Physiol. **139,** 1649-1665.

Sun W., Xu J., Yang J., Kieliszewski M.J., and Showalter A.M. (2005). The lysine-rich arabinogalactan-protein subfamily in Arabidopsis: gene expression, glycoprotein purification and biochemical characterization. Plant Cell Physiol. **46,** 975-984.

Svetek J., Yadav M.P., and Nothnagel E.A. (1999). Presence of a Glycosylphosphatidylinositol Lipid Anchor on Rose Arabinogalactan Proteins. J. Biol. Chem. **274,** 14724-14733.

Takao D. and Kamimura S. (2008). FRAP analysis of molecular diffusion inside sea-urchin spermatozoa. J. Exp. Biol. **211,** 3594-3600.

Takishima K., Watanabe S., Yamada M., and Mamiya G. (1986). The amino-acid sequence of the nonspecific lipid transfer protein from germinated castor bean endosperms. BBA-Protein Struct. M.. **870,** 248-255.

Tall A.R. (1986). Plasma lipid transfer proteins. J. Lipid Res. **24,** 361-367.

Tanaka T., Tanaka H., Machida C., Watanabe M., and Machida Y. (2004). A new method for rapid visualization of defects in leaf cuticle reveals five intrinsic patterns of surface defects in Arabidopsis. Plant J. **37,** 139-146.

Tassin Moindrot S., Caille A., Douliez J., Marion D., and Vovelle F. (2000). The wide binding properties of a wheat nonspecific lipid transfer protein. Eur. J. Biochem. **267,** 1117-1124.

Tepeer M. and Taylor I.E.P. (1981). The Permeability of Plant Cell Walls as Measured by Gel Filtration Chromatography. Science **213,** 761-763.

Thoma S., Kaneko Y., and Somerville C. (1993). A non-specific lipid transfer protein from Arabidopsis is a cell wall protein. Plant J. **3,** 427-436.

Thoma S., Hecht U., Kippers A., Botella J., De Vries S., and Somerville C. (1994). Tissue-Specific Expression of a Gene Encoding a Cell Wall-Localized Lipid Transfer Protein from Arabidopsis. Plant Physiol. **105,** 35-45.

Thoma S., Kaneko Y., and Somerville C. (1993). A Nonspecific Lipid Transfer Protein from Arabidopsis Is a Cell-Wall Protein. Plant Physiol. **3,** 427-436.

Titapiwatanakun B., Blakeslee J.J., Bandyopadhyay A., Yang H., Mravec J., Sauer M., Cheng Y., Adamec J., Nagashima A., Geisler M., Sakai T., Friml J., Peer W.A., and Murphy A.S. (2009). ABCB19/PGP19 stabilises PIN1 in membrane microdomains in Arabidopsis. Plant J. **57,** 27-44.

Tjellström H., Hellgren L.I., Wieslander Å., and Sandelius A.S. (2010). Lipid asymmetry in plant plasma membranes: phosphate deficiency-induced phospholipid replacement is restricted to the cytosolic leaflet. FASEB J. **24,** 1128-1138.

Tsuji A., Kawasaki K., Ohnishi S., Merkle H., and Kusumi A. (1988). Regulation of band 3 mobilities in erythrocyte ghost membranes by protein association and cytoskeletal meshwork. Biochemistry **27,** 7447-7452.

Van Tol A. (2002). Phospholipid transfer protein. Curr. Opin. Lipidol. **13,** 135-139.

Verkman A.S. (2002). Solute and macromolecule diffusion in cellular aqueous compartments. Trends Biochem. Sci. **27,** 27-33.

Verrier P.J., Bird D., Burla B., Dassa E., Forestier C., Geisler M., Klein M., Kolukisaoglu Ã., Lee Y., Martinoia E., Murphy A., Rea P.A., Samuels L., Schulz B., Spalding E.P., Yazaki K., and Theodoulou F.L. (2008). Plant ABC proteins - a unified nomenclature and updated inventory. Trends Plant Sci. **13,** 151-159.

Vink M., Simonetta M., Transidico P., Ferrari K., Mapelli M., De Antoni A., Massimiliano L., Ciliberto A., Faretta M., and Salmon E.D. (2006). In vitro FRAP identifies the minimal requirements for Mad2 kinetochore dynamics. Curr Biol. **16,** 755-766.

Wang J.L. and Edelman G.M. (1971). Fluorescent Probes for Conformational States of Proteins. J. Biol Chem. **246,** 1185-1191.

Wang X.Q., Ullah H., Jones A.M., and Assmann S.M. (2001). G protein regulation of ion channels and abscisic acid signaling in Arabidopsis guard cells. Science **292,** 2070-2072.

Weise F., Stierhof Y.D., Kuhn C., Wiese M., and Overath P. (2000). Distribution of GPI-anchored proteins in the protozoan parasite Leishmania, based on an improved ultrastructural description using high-pressure frozen cells. J. Cell. Sci. **113,** 4587-4603.

Wellman C.H. and Gray J. (2000). The microfossil record of early land plants. Philos. Trans. R. Soc. Lond. B. Biol. Sci. **355,** 717-732.

Wenzel C.L., Hester Q., and Mattsson J. (2008). Identification of genes expressed in vascular tissues using NPA-induced vascular overgrowth in Arabidopsis. Plant Cell Physiol. **49,** 457-468.

West G., Viitanen L., Alm C., Mattjus P., Salminen T.A., and Edqvist J. (2008). Identification of a glycosphingolipid transfer protein GLTP1 in Arabidopsis thaliana. FEBS J. **275,** 3421-3437.

Wiese M., Berger O., Stierhof Y.D., Wolfram M., Fuchs M., and Overath P. (1996). Gene cloning and cellular localization of a membrane-bound acid phosphatase of Leishmania mexicana. Mol. Biochem. Parasitol. **82,** 153-165.

Wirtz K. and Zilversmit D. (1968). Exchange of phospholipids between liver mitochondria and microsomes in vitro. J. Biol. Chem. **243,** 3596-3602.

Wu G., Truksa M., Datla N., Vrinten P., Bauer J., Zank T., Cirpus P., Heinz E., and Qiu X. (2005). Stepwise engineering to produce high yields of very long-chain polyunsaturated fatty acids in plants. Nat Biotech. **23,** 1013-1017.

Xu Q., Buckley D., Guan C., and Guo H.C. (1999). Structural insights into the mechanism of intramolecular proteolysis. Cell **98,** 651-661.

Xu X., Dietrich C.R., Lessire R., Nikolau B.J., and Schnable P.S. (2002). The endoplasmic reticulum-associated maize GL8 protein is a component of the acyl-coenzyme A elongase involved in the production of cuticular waxes. Plant Physiol. **128,** 924-934.

Yang J. and Showalter A.M. (2007). Expression and localization of AtAGP18, a lysine-rich arabinogalactan-protein in Arabidopsis. Planta **226,** 169-179.

Yeats T.H. and Rose J.K.C. (2008). The biochemistry and biology of extracellular plant lipid-transfer proteins (LTPs). Prot. Sci. **17,** 191-198.

You W., Choi W., Koh Y., Shin H., Jang Y., and Chung K. (2004). Functional characterization of recombinant batroxobin, a snake venom thrombin-like enzyme, expressed from Pichia pastoris. FEBS Lett. **571,** 67-73.

Zachowski A., Guerbette F., Grosbois M., Jolliot-Croquin A., and Kader J.C. (1998). Characterisation of acyl binding by a plant lipid-transfer protein. Eur. J. Biochem. **257,** 443-448.

Zagyansky Y. and Edidin M. (1976). Lateral diffusion of concanavalin a receptors in the plasma membrane of mouse fibroblasts. Biochim. Biophys. Acta. **433,** 209-214.

Zhang J.Y., Broeckling C.D., Blancaflor E.B., Sledge M.K., Sumner L.W., and Wang Z.Y. (2005). Overexpression of WXP1, a putative Medicago truncatula AP2 domain-containing

transcription factor gene, increases cuticular wax accumulation and enhances drought tolerance in transgenic alfalfa (Medicago sativa). Plant J. **42,** 689-707.

Zhao Z.D., Tan L., Showalter A.M., Lamport D.T.A., and Kieliszewski M.J. (2002). Tomato LeAGP-1 arabinogalactanprotein purified from transgenic tobacco corroborates the Hyp contiguity hypothesis. Plant J. **31,** 431-444.

Zheng H., Rowland O., and Kunst L. (2005). Disruptions of the Arabidopsis enoyl-CoA reductase gene reveal an essential role for very-long-chain fatty acid synthesis in cell expansion during plant morphogenesis. Plant Cell **17,** 1467-1481.

Appendices

Appendix A: Reagents and solutions

Genomic DNA extraction

FTA wash solution

10 mM Tris Cl pH 8.3; 2 mM EDTA; 0.1 % Tween 20 (v/v); dH_2O

TE-1 solution

10 mM Tris Cl pH 8.0; 0.1 M EDTA; dH_2O

Lysis Buffer

10 mM Tris-HCl pH 8.0; 1 mM EDTA pH 8.0; 0.1% SDS; 0.1M NaCl; 1% PVP ; 100 µg Rnase; 9 mM DTT

Protein precipitation buffer

3 M potassium / 5 M acetate

Create a mixture of the following: 60 mL, 5 M potassium acetate; 11.5 mL, glacial acetic acid; 28.5 mL, dH_2O

DNA binding buffer

Buffer AP3/E – “Binding buffer”

1 M Guanidine Hydrochloride in 95% Ethanol

Ethanol wash

70% Ethanol in dH_2O

DNA electrophoresis

Sodium borate buffer

20X or 100 mM: 77g sodium borate decahydrate dissolved in 2000 mL dH_2O

Mini-plasmid preparation

Cell resuspension solution

50 mM Tris-Cl pH 7.5; 10 mM EDTA; 25-100 μg/mL RNaseA

Alkaline lysis solution

0.2 M NaOH; 1% w/v SDS in dH_2O

Neutralization solution

4.09 M guanidine hydrochloride; 759 mM potassium acetate in dH_2O and made to pH 4.2 with glacial acetic acid. Note: Measured pH must be below 5.0.

Column wash solution

80% ethanol in dH_2O

Buffered Methanol-complex Medium (BMMY)

1% yeast extract; 2% peptone; 100 mM potassium phosphate, pH 6.0; 1.34% Yeast nitrogen base; 4×10^{-5} % biotin; 0.5% methanol; dH_2O q.s. 1 L

Western Transfer Buffer

112.6 g glycine; 20% Methanol dH_2O q.s. 1 L

Tris buffered saline with Tween (TBST)

50 mM Tris; 150 mM NaCl; 0.05% Tween 20. pH to 7.6 with HCl in dH_2O

Alkaline phosphatase buffer

100 mM Tris-Cl pH 9.5; 100 mM NaCl; 5 mM $MgCl_2$ in dH_2O

Appendix B: Microscopes settings.

Confocal laser scanning microscopy

YFP at Zeiss Pascal (p)/ Zeiss Meta 510 (m)

Objectives: 63X oil and 63X water

Main Beam splitter: HFT 458/514

Dichroic beam splitter: NFT 545

Emission filter: 530-600 nm

Laser intensity: 514 nm at 10-20%

Pinhole: 106 μm for conservative imaging. 300 μm for non-conservative imaging. Non-conservative imaging is defined as settings that generate an image quickly but this image is coarse or grainy.

Alternatively YFP was imaged with 488 nm laser with identical settings except for a 488 nm capable beam splitter.

Red dyes (FM4-64, propidium iodide) at Zeiss Pascal/Zeiss Meta

Objectives: 63X oil and 63X water

Main Beam splitters: HFT 543 or HFT 488/561

Dichroic beam splitter: NFT 565

Laser intensity: 543 nm and 561 nm (m) 30-60%

Emission Filter: LP560

Spectral detection range: 595-560 nm (m)

Pinhole 106-136 μm (p, z)

Laser module output was increased as the laser module aged. Laser output was set to 25% in 2007-2010. The laser output was set to 40% in years 2010-2011.

Spinning disk confocal microscopy

YFP at Quorum or Perkin Elmer UltraView Vox

Objectives: 63X oil, glycerol, water

Dichroic used: 405/440/514/640

Emission Filters used: 528/38 nm or 540/30 (PE)

Sensitivity/Gain: 100-255. As number increases image becomes coarser.

Lasers diodes: 491 nm or 514 nm (PE) with intensity 4-9%

Red dyes FM4-64 and Propidium iodide at Quorum

Objectives: 63X oil, 63X glycerol, 63X water

Dichroic used: 405/488/561/640

Emission Filter used: 527/55

Sensitivity: 88-150

Laser diode: 561 nm – intensity 100%

Appendix C: Primers used in this study.

All primers are written from 5' to 3'.

P01	ACTTTGTGTTTGGACTTTGCG
P02	AGGGACAAAAACAAAAGCACC
P03	CGAGGGGTACCCGTCAAAGACAAAGCGCAAAGA
P04	CGAGGTACCCGAGGTGGGACTGGA AAAAGGT
P05	GCATTACTACTCGAGGTTCATCAGCCAGAGCTCCTCCGG G
P06	CATAATCGTCTAGACGATGAATGCAACCAGGAT
P07	CCGTATACACTGCAGGGACTGGAAAAAGGTATAGAG
P08	GCATCCATGCTCGAGTTCCTGGAGGTGGAGGTGGAG CTGTGAGCAAG
P09	CTATGCATTCTAGAGGCGCAGCAGCACCAG CAGGATCCTTGTACAG
P10	gtacgatcagaattcTTGGGAGCTCTCCGG
P11	gtatagcccctcgaggccatcctttgctg
P12	AACAAGCGAAGACAGGAGGA
P13	CTAGAGCAACGACTGCGTGA
P14	CCAGAAGGATGCATATGTTGGTGA
P15	GAGGAGCCTCGGTAAGAAGA
P25	gagatcccagGGTACCggtattttaggtcctttgtctaacctttgttttgagtcatcta
P26	GagatcccagGaattcccGCTCAGAGCCGCCTTTGCTGT
P27	Gagatcccaggaattct CCT GGA GGT GGAGGTGGAGCTGT
P28	cttgacaatctgcagccGGCGCAGCAGCACCAGCAGGATCCTT
P29	cttgacaatctgcagccTGTGGCGAAGTTAACAGCAATTTGAAACC

P30 cttgacaatGGATCCACATATGTACGTGTTGCACTTGGTGTTGAACC

P31 cttgacaatggatccCCGGCAACTCCAGCTACGTCCACGGAT

P32 cttgtcaaaACTAGTGGACTGGAAAAAGGTATAGAGATGTTAGATATAT
TCATCAGCTGTGAGATGCG

P35 cttgtcaaaTCTAGAcCCGGCAACTCCAGCTACGTC

P36 gagatcccagACTAGTattctggacttgaagctgagagttacccattaaattc

P37 tatcagtttttctttctttgttcaattactcttttgcttgttgaagatcttgtttg

P38 ATGGCTGGTCTTATGAAGTTAGGATGCTTGGTCTTTGTCTTCGTG

P41 gcaatttaaGAATTCcgtcaaagacaaagcgcaaagacgaaaattcc

P44 ctaacgtcgACTAGTatcAGGCGCAGCAGCACCAGCAGGATC

P45 ATGGTTCCTGGAGGTGGAGGTGGAGCTGTG

P51 CGTGTGCCAGGTGCCCACGGAATAGT

P52 GTTCATTGC GAATTC ATG AAG GGT CTT CAT CTC CAC

P53 GTT CAT TGC TCT AGA CC CTT ATC CGT GGA CGT AGC tg

P55 TTGTAGAGATCATGTGGATGTGG

P56 ATGCATGACCATTGTCTGTTG

P57 CTTATTTTGTACCAGCGAGGC

P58 TTGTGTACGGACTGTGGAGAAG

P59 GGGTCGATCGACATTTTAATTG

P60 GCCTTGGGTTCTCGACTTAAC

P61 AAAAATCCAAAATTTCAGAATGC

P62 TGTGTGAAATTTTTGAAAATTAATCC

P63 TCGATGCATAATCAAATCGTG

P64 GTTCAAACACAATGGCTTTCG

LBa1 TGGTTCACGTAGTGGGCCATCG

AGR51 CAACCACGTCTTCAAAGCAA

AGR56 CTGGGGTACCGAATTCCTC

AGR64 CTTGCGCTGCAGTTATCATC

AGR69 AGGCGTCTCGCATATCTCAT

Appendix D: Constructs engineered for this study

proLTPG::YFP-LTPG

proLTPG::secreted-YFP

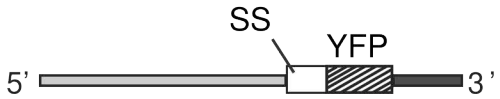

proLTPG::cytoplasmic-YFP

proLTPG::YFP-GPI

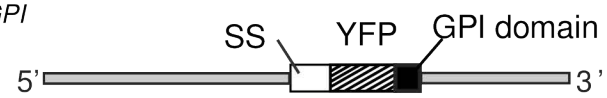

Constructs engineered for this study. The construct proLTPG::YFP-LTPG was engineered to include genomic DNA spanning (5') -1800 from the start translation site to 800 bp downstream from the predicted translation stop site (3'). YFP (hatched box) was introduced downstream of the amino terminal signal sequence (SS). The grey segment linking open boxes represents the LTPG intron. Exon two (open box proximal to the 3' terminus) shows the GPI domain as a grey box. Constructs secreted-YFP, cytoplasmic-YFP and YFP-GPI are shown. Each construct is based on the YFP-LTPG construct with various domains deleted. Note that all constructs are driven with the *LTPG* promoter. *Secreted-YFP* and *cytoplasmic-YFP* use the *nopaline synthase* (*NOS*) transcription termination signal (dark grey, proximal the 3' terminus), taken from vector pMDC32. *YFP-GPI* uses the native *LTPG* transcription terminator.

Appendix E: LTPG expression analysis by RT-PCR

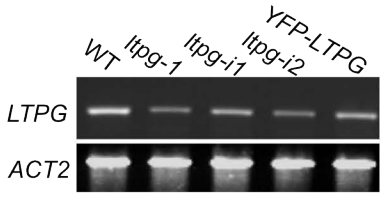

LTPG expression analysis RT-PCR in primary inflorescence stems of Arabidopsis, comparing wild type (WT, Columbia-0) with the mutant *(ltpg-1)* and transgenic lines harboring RNAi constructs *(ltpgi-1* and *ltpg-i2),* and the *proLTPG::YFP-LTPG fusion. ACTIN* wasused as an amplification and loading control.